



SCUOLA DI DOTTORATO  
UNIVERSITÀ DEGLI STUDI DI MILANO-BICOCCA

Department of Material Science

PhD program  
Material Science and Nanotechnology

Cycle XXXI

# **NOVEL COLLOIDAL APPROACH TO PREPARE HIGHLY-LOADED SILICA-BASED ELASTOMERIC NANOCOMPOSITES**

Irene Tagliaro

Registration number: 736430

Tutor: Dr. Barbara Di Credico

Supervisor: Dr. Luca Giannini

Coordinator: Prof. Marco Bernasconi

**ACADEMIC YEAR 2017/2018**



To my grandmothers Liliana and Elsa,  
being women in their century was way different.



# Index

<b>1</b>	<b>Introduction and aims</b>	<b>2</b>
1.1	Rubber nanocomposites	4
1.2	Characteristics of rubber nanocomposites	6
1.2.1	Silica-based nanofillers	6
1.2.2	Nanocomposite morphology and filler networking	9
1.2.3	Nanocomposite properties	10
1.3	Rubber-clay nanocomposites	13
1.3.1	Layered clay nanofillers	14
1.3.2	Preparation of rubber-clay nanocomposites	16
1.3.3	Properties of rubber-clay nanocomposites	19
1.4	Colloids in rubber nanocomposites	20
1.4.1	Theory about colloids: colloidal stability	20
1.5	Aim of the thesis	32
1.5.1	Structure of the thesis	33
1.6	Bibliography	34
<b>2</b>	<b>Materials and Methods</b>	<b>40</b>
2.1	Materials of tyre compounding	42
2.1.1	Rubber	42
2.1.2	Silica-based fillers	45
2.1.3	Coupling agents	49
2.1.4	Curing agents and additives	50
2.2	Procedures	51
2.2.1	Latex compounding technique	51
2.2.2	In situ Pickering emulsion polymerization	53
2.2.3	Preparation of composite materials for tyre application	54
2.3	Bibliography	56
<b>3</b>	<b>Latex compounding technique for preparing silica-based natural rubber masterbatches</b>	<b>58</b>
3.1	Characterization of colloidal dispersions	60
3.1.1	NRL	60
3.1.2	SiO <sub>2</sub> dispersion	61
3.1.3	SepS9 and SepB5 dispersions	63
3.2	Thermal, spectroscopic and morphological characterization of filler/NR masterbatches	68
3.2.1	SiO <sub>2</sub> /NR masterbatch	68
3.2.2	SepX/NR masterbatch	72

3.3	Dynamic-mechanical properties of MB-SepX/NR	79
3.4	Discussions on flocculation mechanisms	81
3.5	Conclusions	84
3.6	Bibliography	85
4	<b>Nanocomposite materials for tyre applications</b>	87
4.1	Mechanical properties of nanocomposite materials	90
4.1.1	Dynamic-mechanical analysis of cured and uncured nanocomposites prepared by MB-SiO <sub>2</sub> /NR	90
4.1.2	Dynamic-mechanical analysis of cured and uncured nanocomposites prepared by MB-SepX/NR	93
4.1.3	More-in-depth analysis of composite materials: the oxidation process of NC(MB-SepX/NR)	95
4.2	Conclusions	100
4.3	Bibliography	101
5	<b>Pickering emulsion polymerization for preparing silica-based waterborne latexes</b>	104
5.1	Waterborne silica-based polymer nanocomposites by Pickering emulsion polymerization	106
5.2	SiO <sub>2</sub> /polyisoprene latex nanocomposite	107
5.2.1	Pickering emulsion polymerization mechanism for L-SiO <sub>2</sub> /PI	115
5.3	SepS9/PI latex nanocomposites	118
5.3.1	Pickering emulsion polymerization mechanism for L-SepS9/PI	122
5.4	Conclusions	123
5.5	Bibliography	124
	Conclusions	127
	Appendix	131



## Abstract

Worldwide, sustainability has become a major field of industrial interest, leading to increased attention to the ecological impact and to the utilization of renewable materials. For the scientific community the main challenge lies in the identification of green synthetic approaches and new alternatives to petroleum-based materials. In the case of the tyre industry, the final goal is to identify new feasible design strategies and alternatives to reduce the environmental impact throughout the life cycle of tyres, based on the use of environmentally friendly materials and on the development of innovative products, showing reduced energy consumption and CO<sub>2</sub> emissions.

In this context, the present PhD thesis is focused on the preparation of eco-friendly silica-based nanocomposites by using a colloidal approach to increase the dispersion of hydrophilic fillers in line with the new requirements of sustainability of the EU policies.

The colloidal approach aims at compounding the nanocomposites through aqueous dispersions of hydrophilic fillers, *i.e.* silica or clays, whose efficient dispersion through traditional melt mixing still remains a challenging issue, due to their poor compatibility with the organic matrix. The proposed technique aims at increasing the filler dispersion without any expensive surface modification. The colloidal approach adopted in the present work represents an economic and eco-friendly alternative to the commonly employed melt mixing technique, because of the elimination of the volatile components released during the traditional melt mixing, with significant benefits for the environment and the workplace safety.

In this PhD thesis, two different colloidal approaches have been applied: i) latex compounding technique (LCT) and ii) Pickering emulsion polymerization to prepare highly-loaded nanocomposite rubber materials containing silica-based fillers, such as silica and sepiolite (Sep) clay, which are considered promising filler candidates for the polymer strengthening due to the fibrous structure and high particle aspect ratio (AR).

The concentration, the charge and the shape of silica-based nanofillers have been studied as relevant parameters on stabilization of natural and synthetic polyisoprene (PI) latexes and thus in the subsequent coagulation process.

An effective LCT procedure was established to produce eco-friendly composites, namely masterbatches (MBs), by incorporating silica or Sep into natural rubber latex (NRL), emulsion in water of *cis*-1,4-polyisoprene, through the flocculation (*i.e.* aggregation resulting from the bridging of polymer particles) of the silica-based nanofillers/rubber mixed aqueous system. In particular, Sep fibers having different surface charges, have been selected: pristine Sep, from Spanish landfill (SepS9) and a commercial Sep organically modified with a benzyl ammonium salt (SepB5). In addition, the LCT procedure was also applied to produce



nanocomposites enclosing spherical nanoparticles of silica, in order to highlight the role of the Sep anisotropy.

LCT showed to favour a homogeneous dispersion of hydrophilic Sep fibers in the rubber matrix, allowing the production of high-loaded Sep rubber composites. The main physicochemical parameters which control aggregation processes in the aqueous medium, i.e. pH,  $\zeta$ -potential, concentration, as well as the morphological features of the final Sep-natural rubber (NR) MB, were comprehensively investigated to figure out the Sep-NR interactions and to propose a flocculation mechanism, based on electrostatic and depletion attraction forces, remarkably connected to both the high content (50 wt.%) and the peculiar anisotropy of the Sep fibers.

Concerning the mechanical properties, the uniform Sep distribution in the rubber matrix, characteristic of the proposed LCT approach and the percolative filler network have improved the performances of Sep/NR MBs in comparison to those of analogous materials prepared by conventional melt mixing.

Furthermore, the MBs with high filler loadings were used to produce environmentally friendly composites, by combining LCT and melt mixing. This combined approach takes advantage of the good filler distribution of high-loaded rubber composites and prevents dust from floating in the air during processing, in line with the increasing legislative restrictions about emissions.

By employing a controlled drying process to avoid possible oxidation reactions, elastomeric composites were obtained showing satisfactory mechanical properties, in line with the reference materials prepared directly by melt mixing. Therefore, this combined LCT and melt mixing technique can be considered a suitable approach to prepare rubber nanocomposites with environmental benefits, without affecting the properties of the final material.

In a further phase of the work, Pickering emulsion polymerization, an in situ polymerization technique, was evaluated as an alternative colloidal approach to produce eco-friendly nanocomposites. Isoprene was polymerized in the presence of silica-based nanofillers, which provide stabilizing effects acting like a surfactant by occupying the interface between the two phases, thus lowering the interfacial tension and stabilizing the emulsion.

Pickering emulsions of isoprene, stabilized by employing silica or SepS9, have been polymerized to produce nanobeads of polyisoprene covered by the reinforcing filler nanoparticles. The formation of polyisoprene (core)-silica-based (shell) structured composite particles was evaluated considering the physicochemical parameters affecting the colloidal stability, and particularly pH,  $\zeta$ -potential and concentration.

On the basis of these results, a possible mechanism for emulsion polymerizations stabilized by solid particles was proposed. In detail, in the case of silica, the inorganic particles are driven towards the interface as a result of a hetero-coagulation event in the water phase with a growing oligoradical. In the case of Sep fibers, the suggested mechanism is based on particle-particle interactions

leading to the formation of a three-dimensional network of particles in the continuous phase.

Although versatile, our Pickering emulsion polymerizations do show some limitations, in particular, an excess of solid stabilizers remaining in the continuous phase after polymerization.

In conclusion, the colloidal approach, based on both LCT and Pickering emulsion polymerization, can be considered as green, simple and effective method suitable for high-performance technological applications. The outcomes indicate the suitability of the adopted strategies as a sustainable procedure for the production of highly-loaded silica based-rubber nanocomposites.

## Riassunto

La sostenibilità è recentemente diventata un ambito di grande interesse industriale, portando ad una aumentata attenzione verso l'impatto ecologico e verso l'utilizzo di materiali rinnovabili. Una sfida per la comunità scientifica è l'identificazione di approcci sostenibili e nuove alternative ai materiali derivati del petrolio. L'industria degli pneumatici si prefigge di indagare possibili strategie di sintesi per ridurre l'impatto ambientale durante l'intero ciclo di vita dello pneumatico, attraverso l'uso di materiali sostenibili e lo sviluppo di tecniche innovative che riducano il consumo di energia e le emissioni di CO<sub>2</sub>.

In questo contesto, questo progetto di dottorato è focalizzato sulla preparazione di nanocompositi eco-sostenibili attraverso l'uso di un approccio colloidale per aumentare la dispersione di filler idrofilici, in linea con i nuovi requisiti di sostenibilità richiesti dalle politiche europee.

L'approccio colloidale punta a produrre nanocompositi con filler idrofilici, la cui efficiente dispersione attraverso tecniche di miscelazione tradizionali rimane difficoltosa a causa della scarsa compatibilità con la matrice organica. Questa tecnica ha lo scopo di incrementare la dispersione di filler senza alcuna modifica superficiale, consentendo l'eliminazione delle polveri prodotte durante il mescolamento con significativi benefici per l'ambiente e i lavoratori.

Due diversi approcci colloidali sono stati utilizzati: i) una tecnica di miscelazione in lattice e ii) una polimerizzazione *in situ* in emulsione per la produzione di nanocompositi altamente carichi contenenti filler come silice e sepiolite (Sep). Questi ultimi sono considerati filler promettenti nell'ambito del rinforzo dei polimeri grazie alla loro struttura fibrosa e all'elevato rapporto di forma.

La concentrazione, la carica, la forma dei nanofiller a base silicea sono stati studiati come parametri rilevanti per la stabilizzazione e destabilizzazione di lattici a base di poliisoprene naturale e sintetico.

Una efficiente procedura di miscelazione in lattice è stata messa a punto per produrre compositi eco-sostenibili, chiamati masterbatches (MBs), attraverso l'incorporazione di silice o Sep nel lattice di gomma naturale (emulsione in acqua di *cis*-1,4-poliisoprene), attraverso la flocculazione (aggregazione risultante dalla coesione di particelle di polimero) di una miscela acquosa di nanofiller a base silicea e gomma. In particolare, fibre di Sep con diversa carica superficiale sono state selezionate: Sep tal quale (SepS9) e Sep organicamente modificata con un sale ammonio benzilico (SepB5). La tecnica di miscelazione in lattice è stata, inoltre, applicata per la produzione di nanocompositi contenenti silice al fine di mettere in luce il ruolo della anisotropia della Sep.

La tecnica di miscelazione in lattice ha dimostrato di favorire una omogenea dispersione di fibre di sepiolite idrofilica in matrice di gomma. Le principali caratteristiche fisico-chimiche che controllano i processi di aggregazione in acqua come il pH, il potenziale  $\zeta$ , la concentrazione, assieme alle caratteristiche

morfologiche del MB Sep-gomma naturale, sono state prese in considerazione allo scopo di investigare le interazioni Sep-gomma naturale. E' stato proposto un meccanismo di flocculazione basato su attrazioni elettrostatiche e depletive, connesso all'elevato contenuto di filler (50% in peso) e alla peculiare anisotropia delle particelle di Sep.

Inoltre, i MBs sono stati utilizzati per preparare compositi sostenibili attraverso la combinazione di miscelazione in lattice e mescolazione meccanica. Questo approccio combinato sfrutta la buona distribuzione del filler e previene il rilascio di polveri durante il processo.

Attraverso l'utilizzo di un processo di asciugatura controllato al fine di evitare fenomeni ossidativi, sono stati ottenuti nanocompositi che hanno dimostrato proprietà meccaniche soddisfacenti, in linea con i materiali di riferimento, assemblati mediante la tecnica tradizionale di mescolamento. Questo approccio combinato si è, quindi, dimostrato valido per la produzione di nanocompositi a basso impatto ambientale, mantenendo inalterate le proprietà meccaniche dei materiali finali.

Una polimerizzazione Pickering in situ è stata considerata come alternativa per la produzione di nanocompositi eco-sostenibili. Particelle poliisoprene/filler a base silicea sono state sintetizzate sfruttando l'effetto stabilizzante di filler inorganici che possono agire come tensioattivi, riducendo la tensione superficiale e stabilizzando l'emulsione.

La formazione di particelle poliisoprene (core)-filler a base silicea (shell) è stata studiata in base ai parametri fisico-chimici che influiscono sulla stabilità colloidale, quali pH, potenziale  $\zeta$  e concentrazione. Sulla base dei risultati ottenuti, viene suggerito un possibile meccanismo di polimerizzazione in emulsione stabilizzata da particelle solide. In dettaglio, nel caso della silice, le particelle inorganiche vengono attratte verso l'interfaccia in seguito ad eventi di etero-coagulazione con un oligoradicale in acqua. Nel caso delle fibre di Sep, il meccanismo suggerito si basa sulla interazione particelle-particella che porta alla formazione di un network tridimensionale di particelle nella fase continua.

Sebbene versatile, il nostro approccio di polimerizzazione in emulsione Pickering ha qualche limitazione. In particolare, un eccesso di particelle solide rimane nella fase continua dopo la polimerizzazione.

In conclusione, l'approccio colloidale, basato su miscelazione in lattice e polimerizzazione Pickering in situ, può essere considerato un metodo sostenibile, semplice ed efficace adatto per applicazioni tecnologiche altamente performanti. I risultati indicano che le strategie utilizzate sono adatte per produrre nanocompositi altamente caricati di filler a base silicea.



## Glossary

ADS	Air-Dried Sheets
AFM	Atomic Force Microscopy
AR	Aspect Ratio
ATR-FTIR	Attenuated Total Reflection-Fourier Transform Infrared Spectroscopy
BR	Butadiene Rubber
BSE	Backscattered Electrons
CBS	N-cyclohexyl-2-benzothiazole sulfenamide
CE	Capillary Electrophoresis
DLS	Dynamic Light Scattering
EDX	Energy Dispersive X-ray Analysis
HA	High Ammonia
ICP-OES	Inductively Coupled Plasma Optical Emission Spectrometry
IEP	Isoelectric Point
IR	Isoprene Rubber
L-SiO <sub>2</sub> /PI	Latex SiO <sub>2</sub> /PI
L-SepX/PI	Latex SepX/PI
LCT	Latex Compounding Technique
LA	Low Ammonia
MA	Medium Ammonia
MB	Masterbatch
MB-SiO <sub>2</sub> /NR	Masterbatch SiO <sub>2</sub> /NR
MB-SepX/NR	Masterbatch SepX/NR
MMT	Montmorillonite
NC(MB-SiO <sub>2</sub> /NR)	Nanocomposite(MB-SiO <sub>2</sub> /NR)
NC(MB-SepX/NR)	Nanocomposite(MB-SepX/NR)
NMR	Nuclear Magnetic Resonance
NR	Natural Rubber
NRL	Natural Rubber Latex
pdi	potential-determining ions
PI	Polyisoprene
RPA	Rubber Process Analyzer
rpm	rounds per minute
RSS	Rubber Smoked Sheets

SBR	Styrene Butadiene Rubber
phr	parts per hundred rubber
SAXS	Small-angle X-ray Scattering
SE	Secondary Electrons
SEM	Scanning Electron Microscopy
Sep	Sepiolite
SepX	SepS9 or SepB5
TEM	Transmission Electron Microscopy
TESPT	Bis(3triethoxysilylpropyl)tetrasulfide
$T_g$	Glass Transition Temperature
TGA	Thermogravimetric analysis
NMR	Nuclear Magnetic Resonance
XRD	X-Ray Diffraction





## Chapter 1.

### Introduction and aims



## 1.1 Rubber nanocomposites

Nanocomposites are composite materials containing nano-sized particles (at least with one dimension from 1 to 100 nm) dispersed in a continuous matrix. The composite materials, produced by the introduction of nanometric particles, gain novel interesting features with respect to the starting materials, ranging from mechanical to electrical to thermal properties. Nanocomposites are a relatively new category of materials, relevant for several application fields such as energy storage,<sup>1</sup> catalysis,<sup>2,3</sup> transportation,<sup>4</sup> constructions.<sup>5</sup>

Among nanocomposites, elastomeric nanocomposites represent a class of materials where the polymer component (continuous matrix) typically has structural functions and may tune the processability of the final material, whereas the nano-sized inorganic component (dispersed particles) can introduce specific functionalities (catalytic activity, luminescence, magnetism *etc.*) and/or reinforce the mechanical and thermal properties of the polymer.<sup>6,7</sup> Because of the high amount of exposed surface of the nano-sized particles, a huge interfacial area is present in elastomeric nanocomposites, resulting in an extended interphase which determines properties that differ from the single bulk materials. A representation of the increase of surface area with the decrease of the particles dimension is given in *Figure 1-1*.

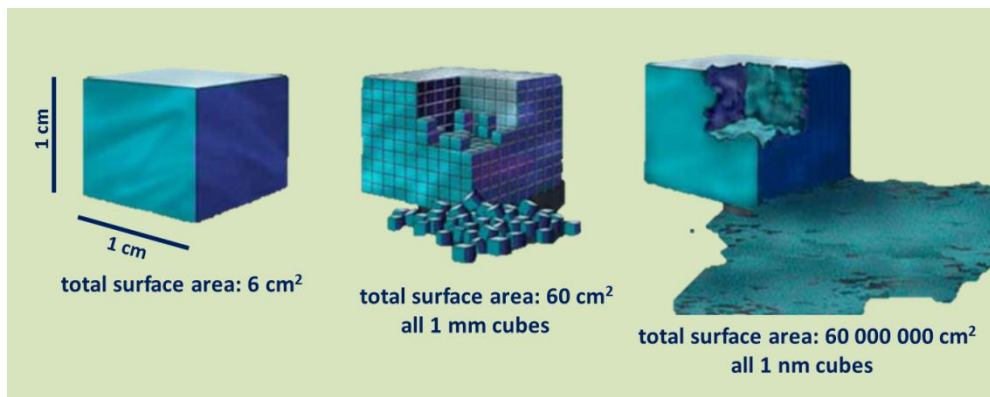


*Figure 1-1. Increase of the surface area with dimension decrease.*

Rubber nanocomposites are relevant in the field of automotive industry, particularly for the production of tyres. Dispersed nano-sized particles (fillers) are important for rubber reinforcement, as discovered in the first half of the 20<sup>th</sup> century.

Rubber properties are improved by the introduction of nanofillers in terms of abrasion, tear, cutting and rupture resistance, and in stiffness and hardness of vulcanized compounds. Rubber-filler nanocomposites acquire non-linear mechanical properties such as high hysteresis, stress softening and strain

dependent dynamic modulus (see Paragraph 2.3). Those characteristics depend on specific filler properties, i.e. particle size, shape and aspect ratio (AR, length/diameter ratio), surface chemistry. Also important are the chemical nature, the flexibility and the intrinsic modulus of the polymer.<sup>8</sup>

Carbon black and amorphous precipitated silica are the most commonly used fillers. However, recently, novel filler systems have received attention, such as polyhedral oligomeric silsesquioxane (POSS), carbon-nanotubes, graphene, layered double hydroxides, clays (*Figure 1-2*). In particular, clay fillers are interesting because they are highly anisotropic, environmentally friendly, naturally occurring and readily available in large quantities at low cost.

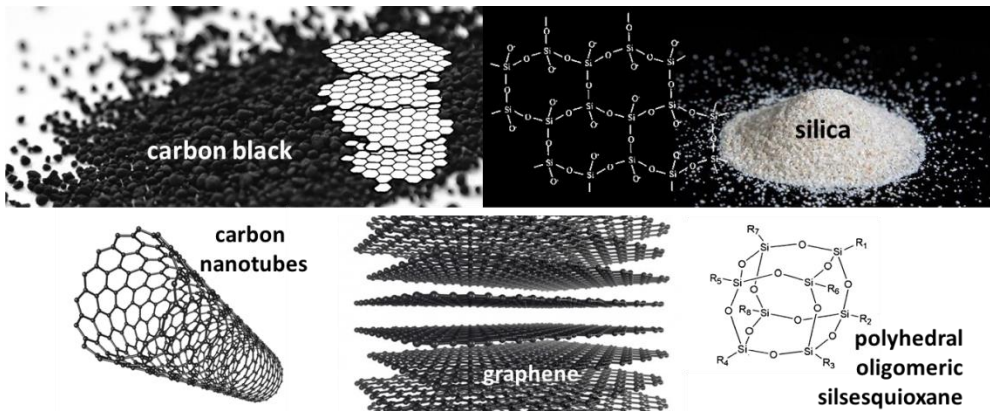


*Figure 1-2. Examples of fillers.*

Despite of the impressive advances of the technology in the nanocomposite production, a complete understanding of the complex mechanisms by which fillers modify the rubber macro-scale mechanical properties remains largely unclear. Among the different contributions which are known to impart rubber reinforcement (i.e. hydrodynamic effect, polymer network, inter-particle filler-filler and interface filler-rubber interactions), the filler dispersion and networking through the polymer matrix is known to be of crucial importance. The good filler dispersion depends on several factors regarding the filler nature and filler rubber interactions, i.e. filler compatibility with the matrix, filler-filler interaction and therefore aggregation and agglomeration state. Also different kinds of compounding and processing techniques can influence the final product properties.<sup>9</sup> Growing knowledge on the structural-mechanical relationship of nanocomposite materials is of huge importance in the aim of achieving good mechanical properties.

Moreover, an increased attention for ecological safety and utilization of renewable materials became a field of great interest in the rubber industry. Thanks to the EU policies, aimed at reducing the CO<sub>2</sub> emission and pollution, the development of more efficient and safe materials is a main purpose of industrial

and academic research.<sup>10</sup> Low energy compounding techniques can be considered an alternative way to produce advanced rubber materials with a low environmental impact. The use of advanced material composites is, however, inhibited by their high manufacturing costs. The improving of the manufacturing techniques will enable the production of composite materials at lower cost, with the possibility of a much wider exploitation.<sup>11</sup>

In this frame, colloidal chemistry has been proposed with the aim of producing organic/inorganic nanocomposites relevant for several applications besides tyres, ranging from cosmetics and pharmaceuticals to adhesives and coatings.<sup>12</sup> The main advantage of a colloidal approach for compounding nanocomposites ingredients is the fine control of the nanoparticle dispersion and its organization in the matrix. Colloidal chemistry, in principle, offers the possibility of imparting a nano-, meso-, and even macroscopic order to the nanocomposite, i.e. it enables simultaneously the synthesis of particles (nano-scale order), their assembling by tuning particle-particle interface and interactions (meso-scale order) and as well the production of films or 3D objects of defined characteristics (macro-scale order).<sup>13</sup> In respect to this, colloidal chemistry offers a possibility to tailor rubber nanocomposite morphology, thus tuning the mechanical properties.

## 1.2 Characteristics of rubber nanocomposites

### 1.2.1 Silica-based nanofillers

The introduction of fillers in the rubber matrix imparts several improvements to the composite mechanical properties, such as hardness, toughness and wear resistance.<sup>14</sup>

Carbon black is the most commonly used filler.<sup>14</sup> It imparts high reinforcement, but also carries strong hysteresis to the materials. In tyres, the dissipation of energy is connected to the increase of the rolling resistance (i.e. force resisting the motion when a body rolls on a surface), which determines fuel consumption, associated to polluting emissions and costs.

A partial substitution of carbon black with silica in tyres began in the 1980's, thanks to the introduction of coupling agents as modifiers of the silica surface. The use of silica and the so-called *white fillers* marked the beginning of the era of the "Green Tyres",<sup>15</sup> showing good performances in terms of rolling resistance, good abrasion resistance and reduction of the heat build-up.<sup>16</sup>

More recently, clays have received particular attention as promising new fillers that allow a further improvement in the balance between hysteresis and reinforcement of materials.

Several features of silica-based fillers have to be considered in order to improve mechanical properties of rubber nanocomposites: particle size and shape, chemical structure, surface chemistry, aggregation, agglomeration, and filler networking.

### 1.2.1.1 Particle size, aggregation and agglomeration

Non-nanometric fillers, like calcium carbonate were employed in tyre production just to reduce the cost of the material, since they did not exert reinforcing effects. Only later, indeed, the size of the filler was found to have high impact on the rubber reinforcement. In particular, it was found that the decrease of the particles size is related to the increase of the elastic modulus.<sup>17</sup> This effect is related to the increase of surface energy connected to the decrease of the particles size, which determines higher agglomeration and increase of the modulus. On the other hand, when compatibilized, high surface area allows the possibility of obtaining high dispersion and, thus, higher interactions between filler and polymer, resulting also in an increase of the modulus.

Amorphous precipitated silica is a nanometric reinforcing filler whose primary particle dimensions range from 5 to 45 nm. The primary particles form aggregates of 100-500 nm, because of dehydration which takes place with the particles synthesis. Aggregates between primary particles are linked by covalent bonds of siloxane. The networking structure of aggregates determine the formation of agglomerates, from 1 to 40  $\mu\text{m}$ , where hydrogen bonding and Van der Waals forces connect the aggregates (*Figure 1-3*). The aggregates are defined like non-dispersible clusters of nanoparticles, while the agglomerate can be redispersed by shearing forces. In rubber nanocomposites, the existence of excessive agglomeration and aggregation lead to insufficient homogeneity, rigidity and low impact strength.

Anyway, in a given range of particle loading, the reinforcement is believed to be related to the formation of complex interconnected structures, through both direct particle interactions and their bridging by polymer chains. Interfacial interaction between filler and polymer was found to reduce the chain mobility by increasing the fraction of the polymer rigid phase.<sup>18</sup>

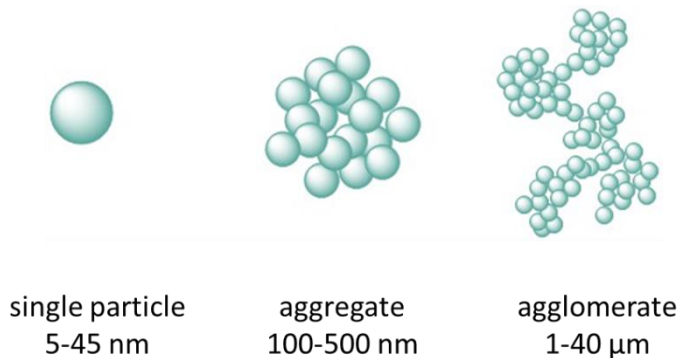


*Figure 1-3. Representation of single silica particles, aggregate and agglomerates.*

### 1.2.1.2 Surface chemistry

The surface chemistry of the filler determines both the filler-filler and the filler-rubber interactions. Those interactions are also affected by the surface energy which, together with the surface chemistry defines aggregation and dispersion. Silica is a polar and hydrophilic filler because of the presence of siloxane and silanols on its surface. So, it requires a surface modification to improve composite material features, otherwise, silica itself tends to the formation of big aggregates, leading to the production of materials with high hysteresis.<sup>10</sup> Consequently, silica is modified by the reaction with coupling agents which increase its affinity for the rubber matrix. Sulfurated silanes are used to create covalent bonds between silica and rubber with the creation of a filler-rubber network. This reaction will be explained in detail in Chapter 2 Paragraph 1.3.

Beyond the use of coupling agents, the silica-rubber interactions may be enhanced by the *in situ* generation of silica by means of sol-gel synthesis via hydrolysis and condensation of silica alkoxides, like tetraethoxysilanes (TEOS).<sup>19,20</sup> The reaction is carried out in the presence of a monomer or a polymer leading to the formation of filler-rubber hybrid structures. The *in situ* synthesis of silica determines the formation of compatibilized silica which has intimate contact with the polymer, providing homogeneous filler distribution inside the rubber matrix. Mechanical properties, i.e. elastic modulus, are improved by the *in situ* synthesis with respect to the corresponding composite materials prepared with the conventional mechanical mixing.<sup>21</sup>

### 1.2.1.3 Particle shape

The particle shape has high impact on the mechanical properties of the nanocomposite. Generally, the higher the anisotropy (which impacts on the surface area) the higher the reinforcement. In addition, highly anisotropic particles also reduce the gas permeability and the solvent diffusion more efficiently than spherical particles.

The influence of the silica particle shape on the dynamic-mechanical behaviour was studied in styrene butadiene rubber (SBR) nanocomposites. Tadiello et al. synthesized silica with AR ranging from 1 to 7.<sup>22</sup> By transmission electron microscopy (TEM) and Atomic force microscopy (AFM) analysis, it was found that the spherical shape determines lower contact zones with rubber, while anisotropic particles (AR >1 up to 7) formed domains of rods preferentially aligned along the main axis with high filler-rubber contact. The higher reinforcement in nanocomposites with higher AR was related to the self-alignment of the anisotropic silica particles with the formation of domains where rubber is immobilized. These results suggest the possibility of tuning the formation of the filler network improving the filler-rubber interaction by using high AR fillers, like clays.

Among clays, montmorillonite (MMT), a plate-like silicate, is the most widely used as filler in rubber nanocomposites because it imparts good mechanical properties thanks to its high cation exchange capacity, large surface area and surface adsorptive properties, beyond the anisotropy. MMT is made of tetrahedral coordinated silicon atoms fused to an edge-shared octahedral sheet of either aluminium or magnesium hydroxide making 1 nm thick layers, with plate dimensions between 100 and 1000 nm (AR = 100 and 1000 respectively). MMT layers are stacked being held together by van der Waals forces. To obtain good mechanical reinforcement with MMT particles, it is required to produce intercalated clay/rubber structures, which implies the expansion of the interlayer distance because of the penetration of the polymer chain inside the lamellar structure. Deeper explanation of this concept is given in Paragraph 3.1.

### 1.2.2 Nanocomposite morphology and filler networking

The compounding of filler and polymer should result in a homogeneously distributed nanocomposite, where filler-filler interactions provide a certain degree of aggregation and low tendency of agglomeration. When the filler volume fraction is relatively high, the tendency of the filler is to form agglomerates, especially in the case of hydrophilic fillers dispersed in a hydrophobic matrix because of the lack of affinity.

With the aim of better defining the concept of homogeneous nanocomposite, a distinction must be done between dispersion and distribution. Dispersion is a term related more specifically to the inter-particle distances, while distribution defines the aggregate and agglomerate spreading inside the matrix. A visual clarification of these concepts is given in *Figure 1-4*.

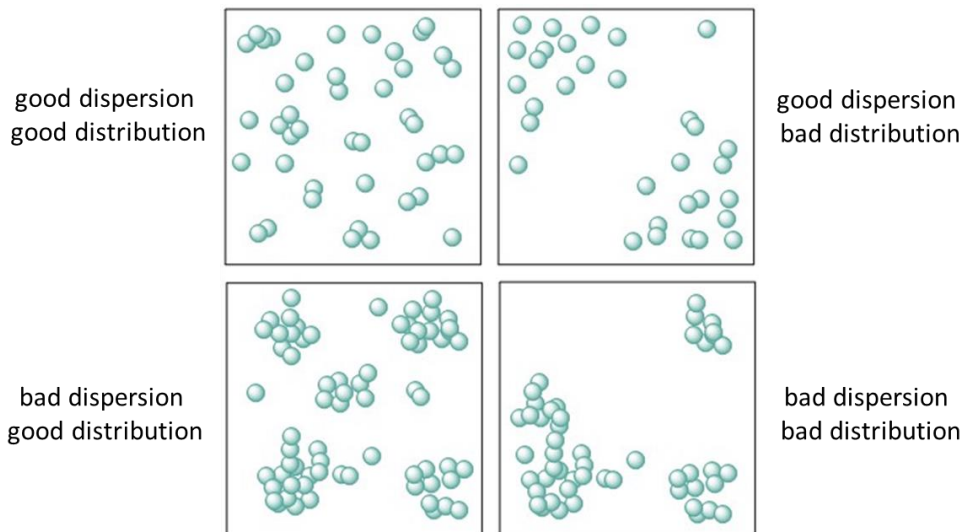


*Figure 1-4. Representation of filler dispersion and distribution.*



The increase of the filler content defines a threshold attained at the formation of a percolative network. The percolation threshold is, indeed, defined as the volume fraction at which all the isolated, aggregated and agglomerated particles are interconnected. Referring to the definition of nanocomposites based on continuous and dispersed phase, given in Paragraph 1.1, at the percolative threshold, the discontinuous phase becomes an actual continuous phase where the matrix fills the void spaces. Based on geometrical considerations, in a nanocomposite made of spheres of equal radius closely packed (dispersed phase), the 74% of the volume is occupied by the particles while only the 26% corresponds to the matrix phase (continuous phase).<sup>23</sup> This theoretical percolation threshold is much higher than the real one because the reinforcement effect of nanoparticles is not just based on geometrical considerations. The real percolation threshold is indeed influenced by filler-filler and filler-rubber interactions as well as by the formation of interphase which allows the obtainment of a reinforcing filler network without an actual close packing of nanoparticles.

The percolation threshold is defined by the drastic change of a property at the increase of the volume fraction of the discontinuous phase. This dramatic change is due to the interconnected filler network where a continuous path can be drawn. This is true also for electric properties: when an electrically conductive particulate (graphite, carbon nanotube, metal nanoparticles) is dispersed in a non-conductive matrix (like most of the polymers), the resulting composite is not significantly conductive until the reaching of the percolation threshold.

In the same way, the elastic modulus increases of about one order of magnitude at the formation of a percolative network (see Paragraph 2.3). The morphological features of nanoparticles affect the percolation threshold. In particular, the higher the AR the lower the percolation threshold. For this reason anisotropic nanofillers have higher reinforcement effect at lower filler content. Clays, naturally anisotropic nanoparticles, have a lower percolation threshold in comparison to silica-based spherical particles.

Moreover, it is expected that the compounding of particles of different shape (spherical and anisotropic nanoparticles) create an interconnected network with high reinforcing properties. Little is known about the network involved in mixed-filler systems. Bokobza demonstrated that composites materials filled with mixtures of pyrogenic silica and clays developed improved reinforcement with regard to single filler materials.<sup>24</sup>

### 1.2.3 Nanocomposite properties

Composite materials containing filler and rubber typically acquire a viscoelastic non-linear behaviour.<sup>25</sup> The term viscoelastic refers to the fact that the characteristics of the material are intermediate between an elastic solid and a viscous liquid. So, under the application of a force, a fraction of the energy is partially elastically stored and partially dissipated as heat in a hysteretic manner.

To determine in which way the composite material responds under certain stress, dynamic-mechanical tests are performed. Dynamic-mechanical analysis gives information about the deformation (strain) obtained in a certain sample undergoing an applied force (stress). The stress is defined in terms of force applied to the sample normalised to the section of the sample itself yielding dimensionally a pressure (measured in Pa).

To characterize the viscoelastic behaviour of a composite material the sample undergoes oscillatory dynamic mechanical test. According to the model of Maxwell,<sup>25</sup> when a sinusoidal shear strain ( $\gamma$ ) of angular frequency ( $\omega$ ) is applied to a viscoelastic material, the response in stress ( $\sigma$ ) results out of phase by an angle of  $\delta$  as expressed by the equation (where  $t$  is time and  $\gamma_0$  and  $\sigma_0$  are strain and stress of the initial position):

$$\gamma(t) = \gamma_0 \sin(\omega t) \quad (\text{Eq. 1.1})$$

$$\sigma(t) = \sigma_0 \sin(\omega t + \delta) \quad (\text{Eq. 1.2})$$

So:

$$\sigma(t) = \sigma_0 [\sin(\omega t) \cos(\delta) + \cos(\omega t) \sin(\delta)] \quad (\text{Eq. 1.3})$$

For deformations of small entities,  $G'$  and  $G''$ , respectively the storage and the loss modulus, are independent from the initial position but dependent on the frequency ( $\omega$ ). In these conditions the behaviour of the composite material is considered linear:

$$G' = (\sigma_0 / \gamma_0) \cos(\delta) \quad (\text{Eq. 1.4})$$

$$G'' = (\sigma_0 / \gamma_0) \sin(\delta) \quad (\text{Eq. 1.5})$$

A linear viscoelastic behaviour is typical of rubber without filler. In this case, the modulus is dependent on the temperature and on the frequency but not on the deformation. A viscoelastic non-linear behaviour is typical of composite materials and of vulcanized rubber and is dependent on the amplitude of deformation.

Tan $\delta$  (loss factor) is defined as:

$$\tan \delta = G'' / G' \quad (\text{Eq. 1.6})$$

At different working temperatures, a correlation was found between tan $\delta$  measured at "standard conditions" of about 1 Hz and important properties of a tyre (Figure 1-5).<sup>26</sup>

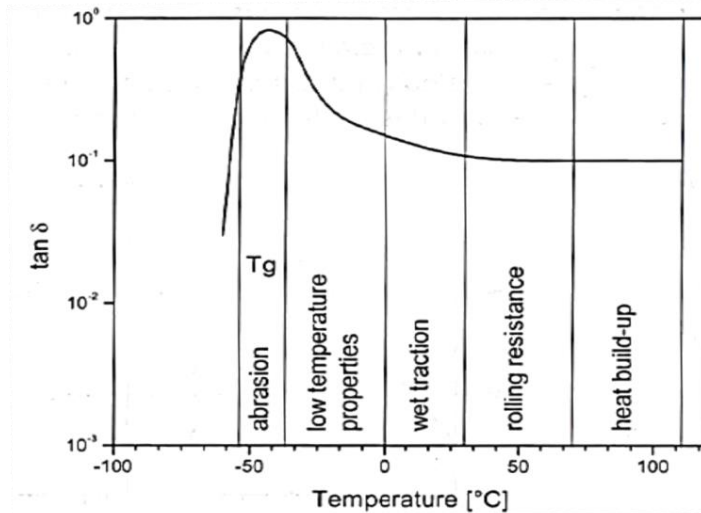


Figure 1-5. Variation of  $\tan\delta$  in function of temperature.

As shown in Figure 1-5,  $\tan\delta$  at 50 °C provides informations on rolling resistance (i.e. force resisting the motion when a body rolls on a surface): the lower the  $\tan\delta$  at 50 °C the lower the energy loss. In the region of the wet traction, evaluated from 0 to around 20 °C, since a higher dissipation is needed to provide a useful friction, the higher the  $\tan\delta$  the better the wet traction.

Indications on the energy storage are given by the Payne effect.<sup>10</sup> The elastic modulus was observed to decrease in function of the strain. The Payne effect is defined as:

$$\Delta G = G'_0 - G'_\infty \quad (\text{Eq. 1.7})$$

This effect was found to be dependent on the filler-filler network developed in the rubber matrix. The filler network, under high deformation, breaks down gradually because of the rupture of bonds between aggregates. Thus, the higher the filler content, the higher the filler-filler network, the higher the Payne effect (Figure 1-6). This effect is known to be independent from the other factors which determine the degree of the  $G'$ : the in-rubber structure (i.e. which is determined by the formation of occluded rubber by the filler structure), hydrodynamic effects (i.e. relative to the volume occupied by the filler) and polymer network (i.e. network deriving from vulcanization).

Silica, thanks to the formation of hydrogen bonds, has high filler-filler interactions and is known to have high Payne effect, which is lowered by the silanization.

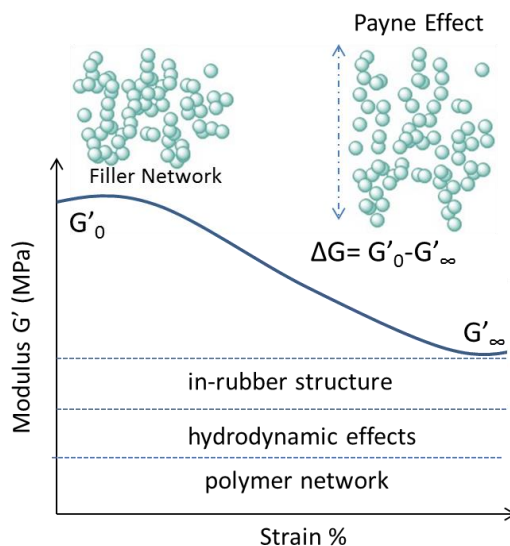


Figure 1-6. Storage modulus vs strain and Payne effect.

### 1.3 Rubber-clay nanocomposites

Rubber–clay nanocomposites have been recently investigated for their unique properties.<sup>27</sup> Clay minerals, normally crystalline fillers, are hydrous aluminium phyllosilicates with variable amounts of iron, magnesium, alkali metals, alkaline earths and other cations. Clays are available as inexpensive natural silicates which are considered to be safe and, therefore, were also applied in bio-devices.

The use of clay in nanocomposites is linked to the obtainment of novel properties which derive mainly from the particle shape. Nanometric clay size, high AR and high surface area improve rubber composite physical properties, such as tensile strength and modulus, gas permeability, lower coefficient of thermal expansion.<sup>28</sup> In particular, high AR of clay particles was studied to provide a significant rubber reinforcement. This reinforcement, beside the filler-filler interaction, was related to the inner organization of particles that provide a higher percentage of filler-rubber interface.

The industrial application of clays still shows certain difficulties which are associated to processing. Achieving high clay dispersion with a filler loading above 5-7 parts per hundred rubber (phr) is challenging because, beyond that concentration, clay nanoparticles tend to form agglomerates.<sup>29</sup> Polymers and inorganic materials, indeed, do not necessarily make a nanocomposite, since separation of the phases may occur, leading to bad mechanical properties. Being natural products, clays are naturally agglomerated. For this reason, a modification of the filler surface is usually made to favour the filler-rubber interactions. A common strategy is the modification of the clay by organic molecules (typically

cationic surfactants), via ion exchange reaction or by grafting reaction with silane-based coupling agents.

### 1.3.1 Layered clay nanofillers

Layered clays are constituted of plate-shaped nanosized particles which form structures of dimensions in the microscale. 2:1 phyllosilicates are the most common layered clays used in nanocomposites applications. Their crystal structure (Figure 1-7) is made of two-dimensional layers where a central octahedral sheet of alumina or magnesia is in the middle of two silica tetrahedral sheets. The thickness of the layers is around 1 nm linked by Van der Waals forces, while the dimension of the layers range from 300 Å to several μm. These structures make layered clays highly porous materials.

MMT, hectorite, saponite, vermiculite, laponite, sepiolite, and bentonite are the most commonly used 2:1 clays. The general formula is  $(Ca,Na,H)(Al,Mg,Fe,Zn)_2(Si,Al)_4O_{10}(OH)_{2-x}H_2O$ , but they differ in chemical content and in particles dimensions.<sup>30</sup>

Because of their hydrophilic nature and their natural tendency to make aggregates and agglomerates, clays are usually organically modified to enhance their compatibility and dispersion in rubber. Depending on the crystalline structure of clays, polymer chains could have access to the filler galleries in between the layers. If the galleries are accessible the clay may be intercalated (i.e. separation of the layers around 20-30 Å) or exfoliated (i.e. separation of the layers of 80-100 Å and more) (Figure 1-7). Highly exfoliated structures, where each individual nanolayer has been separated from its initial stack and dispersed uniformly throughout the polymer matrix, were proved to enhance various physical properties.<sup>31</sup>

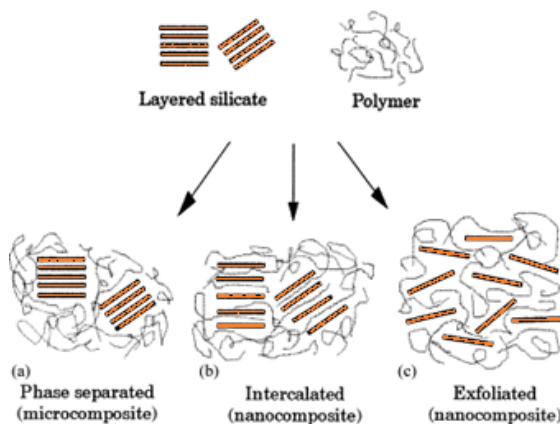


Figure 1-7. Schematic representation of layered silicates: a) phase separated, b) intercalated, c) exfoliated.

The main strategy to obtain organo-modified clays is by exchanging the cations with various cationic surfactants including primary, secondary, tertiary, and quaternary alkylammonium or alkylphosphonium cations. This modification allows a lowering of the surface energy of the inorganic host and an improvement in the wetting characteristics of the polymer matrix.<sup>32</sup>

### 1.3.1.1 Sepiolite

Among phyllosilicates, pristine sepiolite (Sep) is a natural magnesium layered silicate which is extracted from mines. Thanks to the high surface area and the high amount of micropores, Sep has remarkable adsorptive properties and therefore has been used in preparation of polymer nanocomposites with improving processability, mechanical strength and thermal resistance.

Sep, with chemical formula  $\text{Mg}_8\text{Si}_{12}\text{O}_{30}(\text{OH})_4(\text{H}_2\text{O})_4 \cdot 8\text{H}_2\text{O}$ , presents a periodic structural interval along the *b*-axis and micropores along the *c*-axis (Figure 1-8 b and c). It is classified as 2:1 clay, meaning that it has two silica tetrahedral sheets including one central magnesium octahedral sheet. Each sheets is 1.34 nm long and share the edge producing an interesting chessboard structure that cannot be exfoliated (Figure 1-8).<sup>33</sup> The silica layer at regular intervals in the *b*-axis undergoes an inversion of the tetrahedral sheets, which results in the exposure of  $\text{Mg}^{2+}$  ions to the external surface.<sup>28</sup> Around the 33% of the total amount of  $\text{Mg}^{2+}$  ions is estimated to be exposed to the external surface, where the total amount of  $\text{Mg}^{2+}$  ions is the 10-15% in weight of Sep.<sup>34</sup>

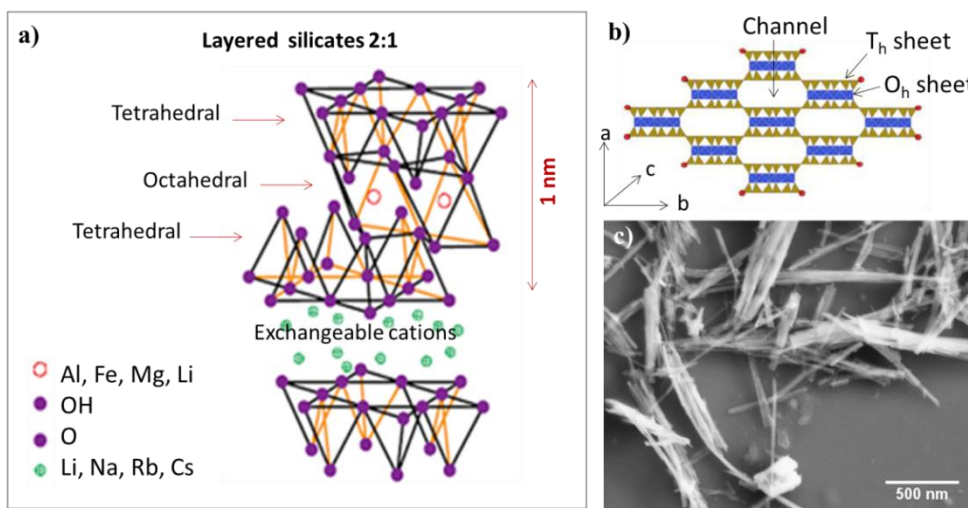


Figure 1-8. Schematic structure of a) layered silicates 2:1 and b) Sep chessboard structure with (c) its SEM micrograph.

The Sep particles are fibers of width 40-150 nm and length 1-10  $\mu\text{m}$ . Fibers are stuck together in bundles having 0.1 to 1  $\mu\text{m}$  diameter, which, furthermore, form randomly-oriented aggregates having size ranging 10-100  $\mu\text{m}$ . The breaking down of these almost tightly packed aggregates is still a challenge but is crucial for designing nanostructured materials. Moreover, the low value in cation exchange capacity of Sep limits the possibility to functionalization with traditional methods.<sup>35</sup>

In rubber nanocomposites, the use of pristine Sep is limited due to its hydrophilic surface and to the consequent low affinity toward organic polymers. Pristine Sep is frequently organically-modified with alkyl ammonium groups, resulting in increased dispersion of the filler. The higher dispersion typically does not result in increased polymer-filler interaction, which remains poor because of the hydrophilic silanol groups on the Sep surface.<sup>36</sup>

Different treatments have been proposed to functionalize and disperse Sep fibers to prepare Sep nanocomposites.<sup>37,38</sup> Di Credico et al.<sup>39</sup> performed a controlled acid treatment and contemporary silanization on Sep, producing Sep-modified nanofillers which were used to prepare SBR nanocomposites. The authors suggest that the increased amount of silanols and the reduction of the particles size, produced by the acid treatment, favor self-organization of Sep in rubber-filler domains and therefore improve reinforcing and reduced hysteresis.

### 1.3.2 Preparation of rubber-clay nanocomposites

The preparation of rubber-clay nanocomposites is based on different dry or solution methods. Rubber compounding is a complex procedure where incorporation of ingredients and chemical reactions take place. In this process, besides reinforcing filler, also accelerators (initiators of the vulcanization process), zinc oxide (vulcanization activator), antioxidants (to prevent aging), softeners (to facilitate processing of the rubber), coupling agents (for the compatibilization of silica-based fillers) and sulfur (vulcanizing agents) are added.<sup>40</sup> A deeper explanation of rubber composite ingredients and of their compounding is reported in Chapter 2.

The preparation of rubber-clay nanocomposites includes the aspects of incorporation, distribution and dispersion of inorganic fillers into organic matrices to produce homogeneous products. After the compounding, the nanocomposite is vulcanized to obtain the desired properties.

At present, there are four principal methods of producing polymer-clay nanocomposites: melt mixing, latex compounding, *in situ* polymerization and solution mixing techniques. Melt mixing is the common compounding technique suitable for industrial purpose, while all the other techniques are based on wet-processing which deals with the use of colloids (see Paragraph 1.4).

Solution mixing is a process where dry rubber is dissolved in a suitable solvent along with clays, followed by solvent evaporation.<sup>41,42</sup> Latex compounding and *in*

*situ* polymerization take advantage of aqueous dispersions of fillers to produce nanocomposites. These two methods are largely discussed in Paragraph 4.

The common point of both wet and dry methods is to provide homogeneous particle dispersion and distribution. Indeed, the ultimate result of poor dispersion is the presence of weak polymer/particles interactions, which usually make poorer the mechanical properties of the nanocomposite.

From an industrial standpoint, the melt mixing is the most direct and simple method to synthesize clay-rubber nanocomposites. It involves equipment like internal mixers and open mills. In the first case (*Figure 1-9*), materials are sheared between the internal rollers inside the chamber, while in the latter the material is passed between two heavy metal rollers mounted horizontally.

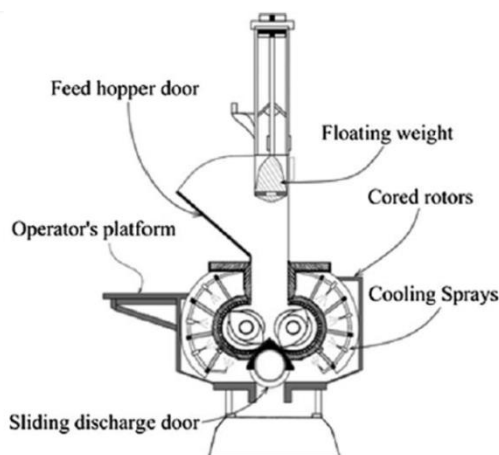


*Figure 1-9. Schematic representation of internal mixer.*

Melt mixing is of particular practical interest because it presents significant advantages, first of all the minimization of capital costs because of its compatibility with industrial existing processes. Melt processing allows nanocomposites to be formulated directly using ordinary compounding devices. At the same time, melt processing does not require the use of any solvents avoiding the complex dealing with clay–solvent and polymer–solvent interactions.

Although the several advantages for industrial application, in the case of fillers like clays, melt mixing can induce significant production of dust, which is environmentally impacting and potentially harmful for operators, and does not provide by itself good dispersion of clay lamellae.<sup>43</sup> Moreover, internal mixers require efficient cooling systems to provide a careful control of the temperature. This is provided by channels in the walls of the mixing chamber, where water passes to control the mixing temperature (*Figure 1-9*).

The first effort to compound NR–MMT nanocomposites using a melt mixing technique was made by Varghese et al.<sup>44</sup> An impressive amount of examples are



given in the literature for the compounding of clays to many kinds of polymers by melt mixing.<sup>28</sup> Efforts were made in the aim of dispersing clay fillers and lowering the dimensions of the filler aggregates by physical and chemical methods.<sup>43</sup> Surface modification strategies involving the addition of coupling agents were indeed applied to increase the compatibility and enhance dispersion by melt mixing approach.<sup>45</sup>

The preparation of the final materials ends with the vulcanization. This process modifies the structure of the polymer, inducing changing of the mechanical properties. In particular, the vulcanized rubber is more elastic, has a higher tensile strength and increased resistance to oxidation. Vulcanization, moreover, is able to suppress undesired properties of uncured rubber, such as stickiness and abrasion.<sup>46</sup> The reactions involved in the vulcanization make use of sulphur, accelerants and activants and bring to the saturation of double bounds of the rubber chain by the formation of sulphur bridges. Thus, vulcanization determines the formation of a tridimensional network of crosslinked polymer having desired characteristics of elasticity and hardness.

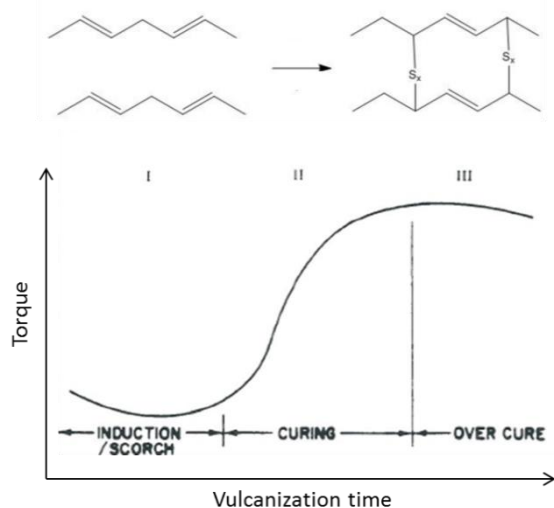


Figure 1-10. Schematic representation of the vulcanization curve and of the formation of a crosslinked polymer.

The changing of the mechanical properties can be appreciated during vulcanization by monitoring the torque or the elastic modulus over the time of curing. The region I (Figure 1-10), called induction time or scorch delay, is the period when the reactions of the accelerants take place. The exact intermediates involved in these reactions are still not completely understood.<sup>47</sup> In region II (curing), vulcanization reaches its maximum thanks to the formation of mono- and multi-sulphur bonds, as explained in Figure 1-10. In the region III, the decrease of torque reflects mechanisms of degradation of the sulphur bonds.<sup>48</sup>

### 1.3.3 Properties of rubber-clay nanocomposites

Rubber-clay nanocomposites are interesting materials from both an academic and an industrial point of view. Improved performances in particular with regards to mechanical properties are obtained by use of clay nano-fillers in rubber matrices. Improvements in thermal stability and fire retardancy are also studied in clay nanocomposites.<sup>49</sup> These materials were found to be relevant for their superior barrier properties against gas and vapor permeability.<sup>50</sup>

As explained in Paragraph 2.3, rubbers filled with nanoparticles act as viscoelastic materials in response to external stimuli. The mechanical properties are mainly given by the formation of a filler-filler and filler-rubber network, which is linked to the organic-inorganic compatibilization and to the vulcanization process.<sup>48</sup>

Clays are being applied as substitutes for the conventional reinforcing fillers like carbon black and silica. Arroyo et al.<sup>51</sup> found that the mechanical properties of natural rubber (NR) filled with 10 phr of modified MMT were comparable to NR filled with 40 phr of carbon black. MMT demonstrated to improve the strength of the nanocomposite with an increment of 350% without an effective reduction in the elasticity of the material. This was related to the higher number of cross-links. The high reinforcement effect implies strong interactions between matrix and clay, thanks to the uniform dispersion of fillers, which is not always achieved in clay nanocomposites.

Gatos et al.<sup>52</sup> demonstrated that different filler dispersion produces very different mechanical properties at high deformation. Since the effective filler volume depends on the dispersion grade, the immobilized rubber content varies with the dispersion quality. According to this model, a higher modulus is expected with a better filler dispersion.

The improvement of tensile strength was also unexpectedly found in rubber clay nanocomposites. The explanation of this phenomena is associable to filler orientation and chain slippage, able to release the tension caused by stretching.<sup>46</sup>

At high clay filler loading, a deterioration of the mechanical performances was observed in some papers.<sup>53,54</sup> The formation of big aggregates was shown to favour the initiation of catastrophic failure.

Differently, Lu et al.<sup>55</sup> found that the dispersion homogeneity in highly-filled clay nanocomposites improved consistently the modulus. The authors claim that this is due to the formation of a strong network between the clay layers. When platelet-platelet distance is very small, the clay layers can interact by hydrogen bonding between silanols located on the edge of the clay layers, so that rubber chains may have access and being constrained in silicate galleries.

## 1.4 Colloids in rubber nanocomposites

In recent times, colloidal chemistry has been exploited with the aim of producing elastomeric nanocomposites. Latex compounding technique (LCT) and *in situ* polymerization have been proposed as alternative ways to incorporate hydrophilic fillers in polymer matrices. These approaches take advantage of aqueous dispersions of fillers and seem particularly appropriate for hydrophilic clay fillers, whose efficient dispersion through melt mixing still is an open issue. Moreover, unlike melt mixing, a colloidal approach does not require the use of heat for processing polymers with  $T_g$  (glass transition temperature) lower than ambient temperature with benefits in terms of energy saving.<sup>56</sup>

In LCT, hydrophilic fillers are directly incorporated into polymer latexes by mixing filler and polymer colloid, while *in situ* polymerization provides the synthesis of waterborne polymer latexes in a dispersion of clay particles. In both cases, the separation of a solid product is performed by simple casting or by coagulation (see Paragraph 4.1.4).

The application of LCT and *in situ* polymerization seem particularly interesting in the case of clays also because the use of wet-processing would decrease drastically the production of dust with improvements in terms of particulate release. Since clays are highly hydrophilic particles, water can act as a swelling agent, providing clay dispersion by simple stirring. On these grounds, with the aim of avoiding surface chemical modification of clay nanoparticles, a colloidal wet-approach appears as an effective solution.

### 1.4.1 Theory about colloids: colloidal stability

Colloids or colloidal dispersions are systems where a phase is homogeneously dispersed in another one. We can define as “dispersed phase” the one where the component is discontinuously represented and a “continuous phase” the one in which the component is present without interruption of continuity<sup>57</sup>. This definition extends to all the physical states of matter as explained in *Figure 1-11*.

Although there is not a clear distinction between a solution and a colloidal dispersion, it is possible to make a classification based on the particle dimensions of the dispersed phase. When the diameter ranges below 10 Å the dispersion is a solution (molecular dispersion) and up to 0.5 μm the dispersion is a colloid. Over 0.5 μm the particles are visible to the optical microscope.









		Continuous Phase		
		Gas	Liquid	Solid
Dispersed Phase	Gas	None	(Foam) Hair mousse, Shave foam 	(Xerogel) Sponge, Styrofoam, Silica gel 
	Liquid	(Aerosol) Hair spray 	(Emulsion) Cream, Lotion 	(Gel) Pomade, Food gelatin, 
	Solid	(Aerosol) Powdery Spray 	(Suspension) Nail enamel, Foundation 	(Solid colloid) Colored glass 

Figure 1-11. Table of different colloidal dispersions.<sup>57</sup>

The presence of two phases determines the presence of a region of interphase.

We can think that the colloid itself is mainly made by interphase, since colloids are constituted by drops of immiscible phases which generate a surface stress. In liquids, it is usually described as the “solvophobic effect”, since the system tends to decrease the interphase surface extent. From the thermodynamic point of view surface stress ( $\gamma$ ) can be defined as the change in free surface energy ( $G$ ) per increase in surface area ( $A$ ):

$$\gamma = \frac{dG}{dA} \quad (\text{Eq. 1.8})$$

A colloidal dispersion is a metastable system, because of the high amount of surface that is generated, which implies that the colloid is not the most stable state of that matter, but, depending on its thermodynamic characteristics, it will last for a limited period of time (*Figure 1-12*). This is because, following the foundation principles of thermodynamics, the system tends to stay in the most stable state of energy, thus lowering the amount of surface/interphase of the system. Practically, what is defined as a “stable” colloidal dispersion is a dispersion where the number and the dimension of the dispersed phase does not change for a reasonably long period of time.

As  $G$  of the system diminishes, the system becomes more stable; equilibrium is reached when  $\Delta G = 0$ . This can be achieved either by a reduction in  $\gamma$  or by a decrease in the area of the interface. The latter determines the definitive separation of the two phases. The interfacial tension depends on the affinity of the two phases and may be reduced by a repulsive force or a potential threshold or by the addition of a tensioactive compound. Thus, the system remains in its metastable state.<sup>23</sup>

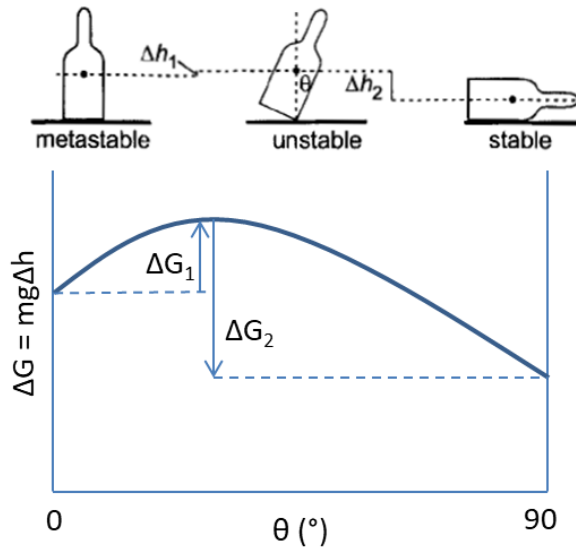


Figure 1-12. Variation of potential energy with the angle  $\vartheta$  of rotation of the bottle. Adapted from Ref.<sup>23</sup>

Some theories describe the particle stability, considering factors of attraction and repulsion. The simple model of Figure 1-13 describes the energy of two entities approaching. This function is true for molecules as well as for droplets in dispersions or solid particles. There are always two components which define a minimum of energy at a certain distance, which respond to the sum of opposite forces of attraction and repulsion.

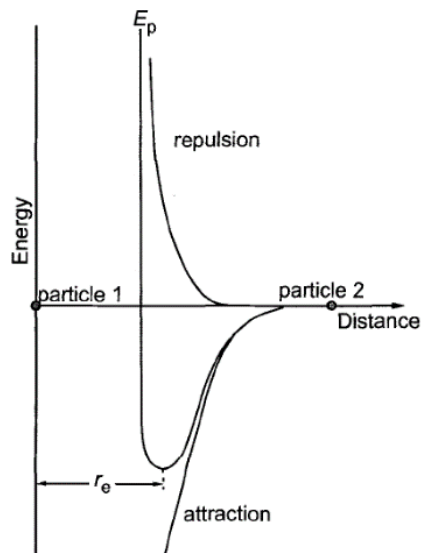


Figure 1-13. Energy as a function of the distance between two entities.<sup>23</sup>

The stability of colloidal dispersions is defined by a balance between attractive and repulsive forces, which may be quantitatively described by the DLVO theory (named after Boris Derjaguin and Lev Landau, Evert Verwey and Theodor Overbeek). This theory explains the forces between charged surfaces interacting through a liquid medium.<sup>58</sup> The total potential energy ( $V_T$ ) of a system defined by DLVO theory is:

$$V_T = V_A + V_R + V_S \quad (\text{Eq. 1.9})$$

$V_A$  = potential energy for attractive contribution

$V_R$  = potential energy for repulsive contribution

$V_S$  = potential energy of the solvent

The component of attraction ( $V_A$ ) is usually defined through Van der Waals forces, which become relevant only when the two entities are very close. These attractive forces are mainly due to phenomena of dipole polarization, depending on the nature of the particles. Van der Waals forces between atoms or molecules are independent of scale, so this means that the attraction between colloidal particles is the same whether the radius is 50 nm or 1  $\mu\text{m}$ . They are greater than  $kT$  ( $k$  Boltzmann constant) at distances slightly less than the particle size. Van der Waals forces in the presence of a liquid medium decrease, but they act over long distances.

The repulsion between two entities ( $V_R$ ) is linked to the formation of an electric double layer which is formed at any interface. Depending on the nature of the two surfaces the formation of the electric double layer is due to phenomena of charge separation whose direction is normal to the geometrical plane of contact. The double layer refers to two parallel layers of charges surrounding the object. Depending on the surface charge, which can be either positive or negative, ions will be adsorbed onto the object due to chemical interactions. Another layer of ions, attracted to the surface charge via the Coulomb force, will electrically screen the first layer. Those ions are loosely associated to the attractive surface and are more free to move, making the so-called "diffuse layer".

The definition of the electric double layer changed in time from the definition given by Helmholtz who described it like a plane condenser where the electrostatic interactions between ions and the surface decrease linearly with the distance, to the model of Gouy-Chapman, which introduced the idea of the diffuse layer, to Stern which basically proposed a model combination of the previous two. The Gouy-Chapman-Stern-Grahame model, then, overcame the Stern limitations due to the assumption of only a single plane for chemisorbed and physisorbed ions. This theory models also the presence of a hydration shell. The model, as summarised in *Figure 1-14*, defines two new localized planes: the IHP (Inner Helmholtz plane) which is related to the chemisorbed ions and also determines the position of the hydration shell for repulsive reasons and the OHP (Outer Helmholtz plane), the

hydration shell, that is defined by the ions of opposite charge which are closer to the surface in the order of crystallographic radius.<sup>59</sup>

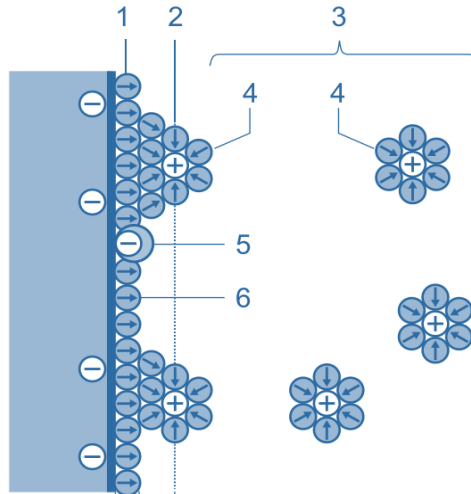


Figure 1-14. Schematic representation of a double layer for the Gouy-Chapman-Stern-Grahame model with 1. Inner Helmholtz plane, (IHP), 2. Outer Helmholtz plane (OHP), 3. Diffuse layer, 4. Solvated ions (cations) 5. Specifically adsorbed ions, 6. Molecules of the electrolyte solvent.

The overall charge of the electric double layer is called  $\zeta$ -potential and it is measured by  $\zeta$ -metry (see Appendix).

Other relevant forces in the stability of colloids that are worth of mention are hydrophilic interactions, also called structural forces. These forces are relevant in the presence of highly hydrophilic surfaces (i.e. proteins, silica, clays) that cause molecular order in the adjacent neighbouring water molecules (acting as dipoles). This effect leads to repulsion between particles.<sup>60,61</sup>

#### 1.4.1.1 Liquid-liquid interface: emulsions

A liquid phase dispersed in a continuous liquid phase is an emulsion and is thermodynamically unstable since the system tends to reach the most stable state in which the two phases (e.g. oil and water) are separated. The term emulsion is referred to the system where the oil is dispersed in water (o/w emulsion) and to the reverse case (w/o emulsion). Upon mixing of the two phases, we can create an emulsion which is thermodynamically unstable and phase separates in a very short time after the mixing is stopped. To extend the time of metastability of the system and to make it useful in chemical applications, the use of an emulsifier is needed. The emulsifier is a species which tends to occupy the region at the interface and thus to lower the interfacial tension between the phases. Surfactants are amphiphilic molecules, which have an hydrophilic and an hydrophobic part and for

this reason are soluble in both water and oil. Common amphiphilic substances are soaps, detergents and lipoproteins. Their ability of emulsification is due to their tendency to orient themselves normal to the interface, with the polar sites towards the water phase and the apolar moieties to the oil phase. This molecule disposition is associated with a decrease in free energy. To choose an efficient emulsifier there is a general rule (Bancroft's rule) which states that the phase in which the emulsifier is more soluble is the outer phase.<sup>62</sup>

#### 1.4.1.2 Latex

The latex is an aqueous emulsion of rubber polymer particles in the submicron-micron range. The term latex applies not only to natural rubber, but also to emulsions of synthetic rubbers. Anyway, not all the kinds of rubber exist in their own latex form and some latex compounds require stabilizers to ensure adequate processing stability.

Natural rubber latex (NRL) is a natural emulsion of poly-isoprene (PI) which has widely been applied in nanocomposite synthesis for a very broad range of applications.

NRL is the sap of *Hevea brasiliensis* and is one of the few commercial rubbers from a natural source. The biosynthesis of the tree produces poly(1,4-*cis*-isoprene) (IR) whose polymeric chain starts and ends with different groups (*Figure 1-15*):

- $\omega$ - terminal, a peptide or unidentified functional group which is bound to two trans-1,4-PI units, which is associated with proteins to form crosslinks via hydrogen bonding,
- $\alpha$ -terminal, mono- and diphosphate groups linked with phospholipids by hydrogen or ionic bonds.<sup>63</sup>

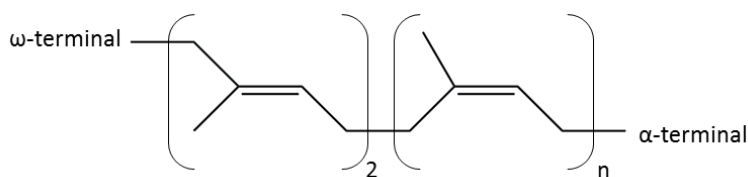


*Figure 1-15. Chemical structure of NR.*

The rubber phase is emulsified by the presence of phospholipids and proteins deriving from the bio-synthesis and adsorbed on the surface of particles having size ranging from 0.02 to 3  $\mu\text{m}$ . Phospholipids and proteins form a shell with a thickness of around 20 nm (*Figure 1-16*). The shell is linked to the terminal ends of the rubber chains, thus increasing the stability of the emulsion.<sup>64</sup> The proteins act as emulsifiers in the rubber latex and are responsible for dispersing the insoluble fraction of natural rubber (NR) in the water medium.



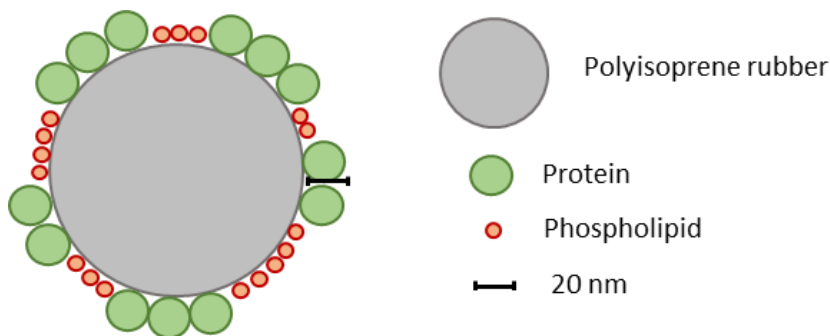


Figure 1-16. Proposed model of the NR latex particle surrounded by a layer of proteins and phospholipids with IR rubber as core.

The non-rubber phase deriving from the bio-synthesis is organized in other particle structures, mainly lutoids and Frey-Wyssing particles.<sup>65</sup> The lutoids are single membrane-bound vacuoles of around 2-5  $\mu\text{m}$  containing water soluble substances such as acid minerals and sugars, which may have destabilizing properties for the emulsion. The Frey-Wyssing particles are complex organelles of lipid globules, carotenoids bounded by a double layer membrane which may be the possible site of rubber biosynthesis, taking place on the surface of the rubber particles.<sup>66</sup>

NRL has been extensively applied in LCT for the compounding of different kinds of fillers like carbon black,<sup>67</sup> silica,<sup>68</sup> cellulose,<sup>69</sup> and others.<sup>70</sup>

Also clay-rubber nanocomposites have been compounded with NRL by LCT. The advantages of the application of LCT on clay-rubber nanocomposites are several: i) absence of organic solvents; ii) use of renewable natural raw materials; iii) no need of expensive surface modification for hydrophilic fillers by taking advantage of water as an excellent swelling and exfoliating agent; iv) reduced dust release during compounding.

Tan et al.<sup>71</sup> produced NR/Ca-MMT nanocomposites by LCT with the obtainment of intercalated and exfoliated structures of fillers which showed good mechanical performances, thermal stability and aging resistance. Other examples take advantage of the NRL raw material to incorporate different clays, i.e. Na-MMT,<sup>72</sup> paligorskite,<sup>73</sup> kaolinite.<sup>33</sup> Varghese<sup>74</sup> et al. reported an all-ingredient latex compounding approach by incorporation of sodium bentonite and sodium fluorohectorite in NRL. Alternatively, synthetic polymer latex, such as SBR latex, were applied to prepare nanocomposites with hectorite.<sup>75</sup> NR/butadiene latex blends were studied by Varamesh for the preparation of cloisite nanocomposites.<sup>76</sup> These studies demonstrate the LCT is a suitable method for preparing clay-polymer nanocomposites with good mechanical properties.

On the other hand, the literature reports the preparation of nanocomposite by LCT with a low clay loading. Just few examples study nanocomposites highly loaded.<sup>45</sup>

Furthermore, these promising results are not really supported by a more in depth study of the physico-chemical parameters which affect the nanocomposite preparation and the coagulation process (i.e. the separation of a solid nanocomposite from an aqueous liquid dispersion of filler and polymer particles). Although there is a global agreement in stating that the process of destabilization of the phases is crucial in obtaining of good dispersion of the clay filler, the impact of the features of multi-component system aqueous dispersions on the stability of colloids are far from been completely understood.

#### 1.4.1.3 Pickering emulsions

Already at the beginning of 1900, Ramsden and Pickering discovered another way of stabilizing droplets of two immiscible liquids by using solid particles as emulsifiers.<sup>77</sup> More recently, the stabilization properties of solid particles were exploited to create particle-stabilized emulsions (i.e. Pickering emulsions) and attracted much interest especially in the field of material science and nanomedicine.<sup>78</sup> As in the case of surfactants, the driving force for the displacement of particles at the interface between two phases is the reduction of free energy at the interface. Also in this case, the wettability of the solid particles is what matters for an efficient emulsification. Hydrophilic particles with higher affinity for the water phase would more likely induce the formation of o/w emulsions, while w/o emulsions would be stabilized by hydrophobic particles. Depending on the organic-inorganic interactions the arrangement of inorganic particles on the surface may highly differ from low coverage, to the formation of a monolayer, to multilayer 3D structures of aggregated particles (*Figure 1-17*).<sup>79</sup>

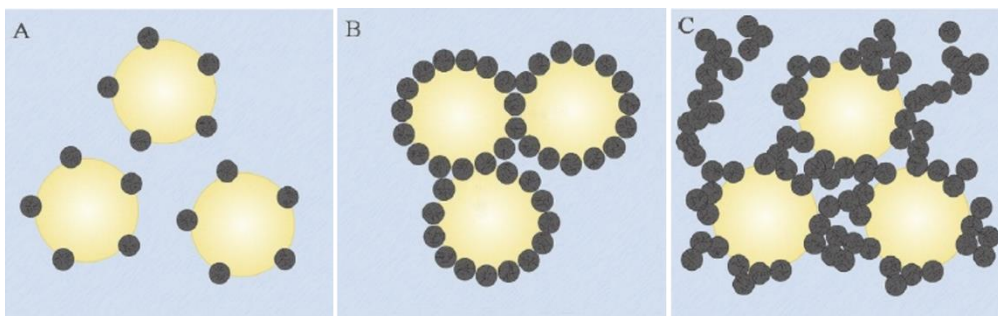


*Figure 1-17. Schematic representation of Pickering particles: A) low surface coverage; B) monolayer surface; C) multilayer coverage and 3D network of aggregated particles in the continuous phase.*

If only solid particles are present as emulsion stabilizers, the system requires higher mixing energy to create droplets and to allow the particles to accumulate at the phase boundary. The stabilization provided by solid particles is affected by  $\zeta$ -potential of the surfaces and also by the geometrical hindrance. The solid particles must, indeed, be considerably smaller than the dispersed phase to induce stabilization.<sup>23</sup>

The stabilization provided by solid particles has been exploited for the *in situ* synthesis of polymers in emulsion.

Emulsion polymerization is a synthetic approach for the radical polymerization of vinyl monomers, carried out in a heterogeneous medium where water is the continuous medium and the monomer is the non-soluble phase. The characteristics of emulsion polymerization are:

- the emulsified monomer creates drops ranging from 0.05 to 5  $\mu\text{m}$
- the initiator is soluble in the continuous phase
- production of a latex of stable emulsified polymer in water
- the use of water allows the polymerization to take place at low temperature, keeping low the viscosity of the reaction matrix.<sup>80</sup>

*In situ* emulsion polymerization has been applied to synthesize organic-inorganic structures commonly made of polystyrene or acrylate polymers in the presence of silica.<sup>81,82</sup> For example, Zhang *et al.*<sup>83</sup> synthesized polystyrene-SiO<sub>2</sub> nanocomposites particles via Pickering emulsion polymerization, with the formation of an armored shell of silica particles surrounding the polymeric core in a raspberry-like structure.

Only few examples of *in situ* emulsion polymerization in the presence of clay particles are available. *In situ* polymerization was reported by Negrete-Herrera in the presence of laponite to synthesize styrene and butyl acrylate (co)polymer particles.<sup>84</sup> The emulsion polymerization was carried out in the presence of the modified organoclay which played the role of a solid initiator. Laponite-armored poly(vinylidene chloride-co-methyl acrylate) latexes were synthesized to study the impact of the clay on particle stabilization during the polymer synthesis.<sup>85</sup> *In situ* emulsion polymerization of acrylamide was performed in the presence of MMT and it was demonstrated that stabilization was provided by clay particles.<sup>86</sup>

The *in situ* polymerization in the presence of clay particles has mainly been applied for the synthesis of styrene or polyacrylate polymers, while no examples are present for the synthesis of PI. Anyway, emulsion polymerization of PI has already been studied in the presence of surfactans.<sup>87</sup>

As a matter of fact, emulsion polymerization deals with complex reactions which remain poorly understood. The complexity of emulsion polymerization is due to the fact that the reaction occurs in both the aqueous phase and the monomer-swollen particles. Moreover, the primary locus of polymerization has been assessed to take place in the latex particles for emulsion polymerization,<sup>88</sup> but

there is no scientific agreement in the case of *in situ* polymerization, where inorganic particles are present. The investigation of how the latex particles are formed and how they grow are still crucial issues in the study of emulsion polymerization.

#### 1.4.1.4 Colloidal destabilization mechanisms

As metastable systems, colloids are going to phase separate spontaneously (*Figure 1-18*). The particles of the dispersed phase are going to coagulate, when the attraction forces become more relevant than the repulsive forces. When the rupture of the film layer stabilizing the droplet happens, whatever the type of emulsification system, particles coalesce because of spontaneous collisions until they reach a size which determines precipitation and the macroscopic phase separation of the system.<sup>89</sup>

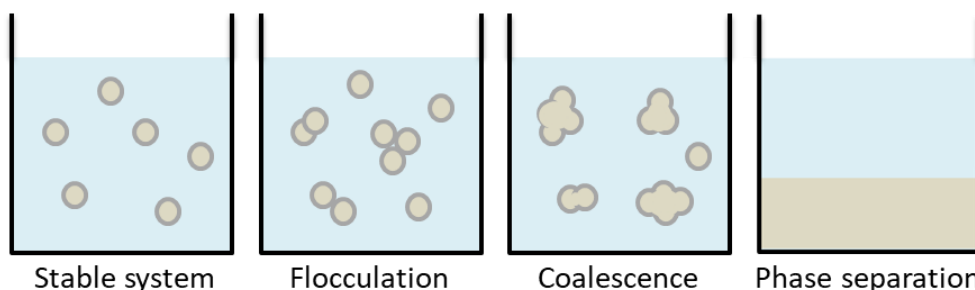


*Figure 1-18. Schematic representation of phase separation of a generic colloid. Grey droplets represent the discontinuous phase, light blue the continuous phase.*

Generally, the so-called *coagulation* is the irreversible aggregation of particles, while *flocculation* is a particle aggregation resulting from the bridging of several particles by a polymer. Creaming is another destabilization mechanism where droplet buoyancy occurs because of density differences. A coagulated aggregate separates out by sedimentation if it is denser than the medium, or creams and rises to the surface if its density is less than that of the dispersion medium.<sup>90</sup>

In order to make colloids useful tools for scientific and technological purposes, it is mandatory a careful control of phase separation phenomena. There are several methods to induce phase separation in emulsions and colloidal dispersions which include physical methods such as intensive ultracentrifugation, variation of pressure and temperature, solvent evaporation, or chemical methods which requires the addition of inorganic salts, or anti-solvents, or chemicals that change the pH of the medium. It is, however, worth noting that both physical and chemical methods imply disadvantages including high energy consumption and significant changes in system composition.<sup>91</sup>

Chemical methods involve changing in the electric double layer of the particles. The addition of acids is known to destabilize colloids by changing the pH and thus bringing the particles to the isoelectric point (IEP), where they have no charge and the  $\zeta$ -potential is close to zero (*Figure 1-19*). Otherwise, the use of electrolytes containing ions with a high charge/radius ratio is an alternative approach which ends in screening the electric double layer until the attractive forces between particles overcome the repulsive forces.<sup>92</sup> In this case, inorganic salts and acids are named coagulating agents.

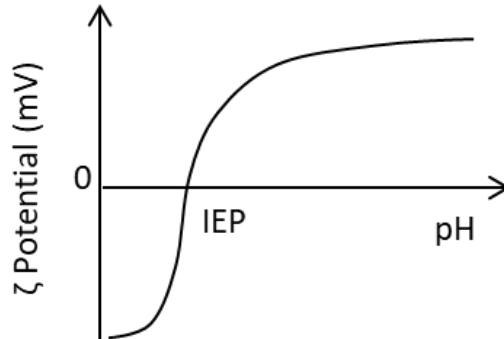


*Figure 1-19. Example of the variation of the  $\zeta$ -potential changing the pH with identification of the IEP.*

Colloidal systems made by a dispersion of solid particles and polymers may undergo different stabilization/destabilization mechanisms, depending on the polymer-particle interactions (*Figure 1-20*). Flocculation process can occur, due to different destabilization mechanisms which may involve or not the neutralization of the charge.<sup>93</sup> A mechanism simply based on charge neutralization occurs in the presence of an attractive potential among the particles and polymers, which can collide due to their Brownian motion. The progressive adsorption of polymer segments on particle surface, lowers the free energy of interaction among the particles, decreasing their distance and leading to flocculation. Otherwise, under constrained equilibrium, the adsorbed polymer may enhance the stability of the suspension because of steric repulsion due to the overlapping of the polymer layers.

In the case of non-adsorbing polymer, a depletion interaction may take place depending on geometrical aspects.<sup>94</sup> Depletion forces are defined as the osmotic forces which arise in colloids of two components, when the size of the radius of gyration of the polymer is larger than the separation between two surfaces of particles. In other words, if the colloidal particles are very close the polymer is geometrically excluded from the area between them and this creates a zone inaccessible for the polymer. The decrease in osmotic pressure in that region generates attractive forces. In this case, the flocculation is influenced by the

molecular mass and the relative concentrations.<sup>23</sup> Depletion flocculation was explained in thermodynamic aspects by Asakura and Oosawa.<sup>95</sup> Since depletion flocculation depends on geometrical exclusion, the effect was found particularly important in the presence of anisotropic particles.<sup>96</sup>

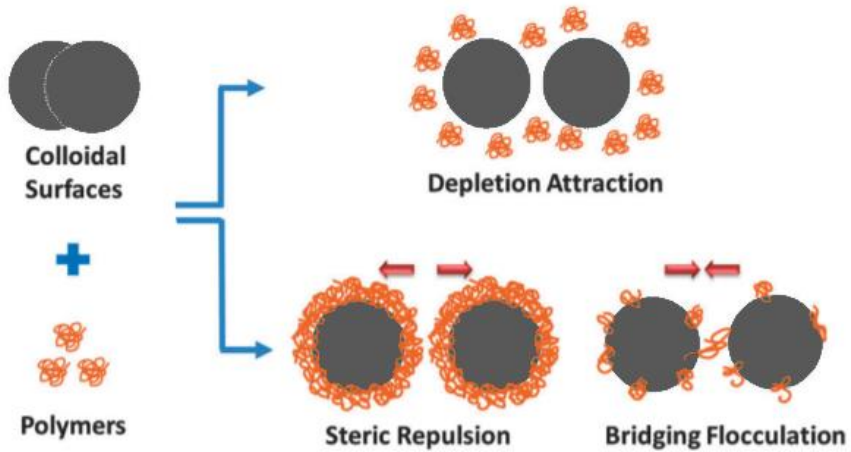


*Figure 1-20. Polymer and colloidal surfaces interactions.*

## 1.5 Aim of the thesis

The aim of this PhD thesis is to investigate novel colloidal approaches for the preparation of rubber nanocomposites for potential application in tyre field. Colloidal approach aims at compounding through aqueous dispersions of the nanocomposite ingredients, in particular rubber and filler. This approach seems particularly appropriate for the compounding of hydrophilic fillers, i.e. silica or clays, whose dispersion through the melt mixing method still remains a challenging issue. This technique allows to increase the filler dispersion without any chemical modification and to avoid the use of other chemical ingredients which increase the cost of the materials in terms of price and environmental impact.

Moreover, it represents an economic and eco-friendly alternative to the commonly employed melt mixing technique thanks to the elimination of the volatile component released during mixing, with significant benefits for environment and workers.

Two different colloidal approaches have been applied: i) LCT and ii) Pickering emulsion polymerization to prepare highly-loaded nanocomposite rubber materials containing silica-based fillers, such as silica and Sep clay. The latter are considered promising filler candidates for the polymer strengthening, due to their fibrous structure and high particle AR.

The concentration, the charge and the shape of silica-based nanofillers have been studied as relevant parameters on stabilization and destabilization of natural and synthetic PI latexes.

LCT has been employed to produce eco-friendly composites, namely masterbatches (MBs), by incorporating silica or Sep into NRL, through the flocculation of the silica-based nanofillers/rubber mixed aqueous system. In particular, Sep fibers having different surface charges have been applied in LCT: pristine Sep, from Spanish landfill (SepS9), and a commercial Sep organically modified with a benzyl ammonium salt (SepB5).

The main physicochemical parameters which control aggregation processes in the aqueous medium, i.e. pH,  $\zeta$ -potential, concentration of particles (aspects that are strongly interconnected), as well as the morphological features of the final Sep-NR MB, were comprehensively investigated. This helped to figure out the Sep-NR interactions and to propose a flocculation mechanism, based on electrostatic and depletion attraction forces, remarkably connected to both the high content (50 wt.%) and the peculiar anisotropy of the Sep fibers.

MBs with high filler loadings have been applied to produce environmentally friendly composites, by combining LCT and melt mixing with the aim of i) taking advantage of the good filler distribution and also ii) preventing dust from floating in the air during processing, in line with the increasing legislative restrictions about emissions.

Pickering emulsion polymerization, an *in situ* polymerization technique, was evaluated as an alternative colloidal approach to produce eco-friendly nanocomposites. Isoprene was polymerized in the presence of silica-based nanofillers, which provide stabilizing effects acting like a surfactant by occupying the interface between the two phases, thus lowering the interfacial tension and stabilizing the emulsion. A possible mechanism for emulsion polymerization stabilized by solid particles has been proposed.

The colloidal approach, based on both LCT and Pickering emulsion polymerization, has been investigated as green, simple and effective method suitable for high-performance technological applications.

### 1.5.1 Structure of the thesis

The research employs a colloidal approach for preparing silica-based elastomeric nanocomposites. The dissertation is organized as follows:

Chapter 2 aims at presenting the materials, synthetic and compounding strategies that have been applied in this thesis.

Chapter 3 describes the preparation of highly-loaded homogeneous SiO<sub>2</sub> and Sep MBs by applying LCT approach with NRL. The main physicochemical parameters which control aggregation processes in the aqueous medium have been comprehensively investigated to highlight the filler-NR interactions and to propose a flocculation mechanism.

Filler/NR MBs were fully characterized and used to prepare composites by conventional melt mixing.

Chapter 4 is focused on rubber nanocomposite materials, compounded with MBs prepared by LCT approach. Dynamic-mechanical analysis of composite materials has been performed in order to investigate filler-filler and filler-rubber interactions, in comparison with the reference composite materials obtained by conventional melt mixing procedure.

The Chapter 5 describes the preliminary study on the preparation of silica-based latex nanocomposites by applying the Pickering emulsion polymerization. In such approach, the production of composite materials is based on the polymerization of the organic isoprene monomer in aqueous emulsion, in the presence of silica-based inorganic colloidal particles, such as silica and Sep, as emulsion stabilizer.

Conclusions sum up the main results and findings of the investigation.



## 1.6 Bibliography

- 1 A. K. Cuentas-Gallegos, M. Lira-Cantú, N. Casañ-Pastor and P. Gómez-Romero, *Adv. Funct. Mater.*, 2005, **15**, 1125–1133.
- 2 B. Di Credico, M. Redaelli, M. Bellardita, M. Calamante, C. Cepek, E. Cobani, M. D’Arienzo, C. Evangelisti, M. Marelli, M. Moret, L. Palmisano and R. Scotti, *Catalysts*, 2018, **8**, 353.
- 3 M. T. Uddin, O. Babot, L. Thomas, C. Olivier, M. Redaelli, M. D’Arienzo, F. Morazzoni, W. Jaegermann, N. Rockstroh, H. Junge and T. Toupance, *J. Phys. Chem. C*, 2015, **119**, 7006–7015.
- 4 J. B. Ferguson, I. Aguirre, H. Lopez, B. F. Schultz, K. Cho and P. K. Rohatgi, *Mater. Sci. Eng. A*, 2014, **611**, 326–332.
- 5 M. R. Nyden, S. L. Manzello and R. H. Harris Jr, in *Recent Advances in Flame Retardancy of Polymeric Materials*, 2017.
- 6 M. D’Arienzo, S. Diré, V. Masneri, D. Rovera, B. Di Credico, E. Callone, S. Mascotto, A. Pegoretti, F. Ziarelli and R. Scotti, *ACS Appl. Nano Mater.*, 2018, **1**, 3817–3828.
- 7 T. Tanaka, G. C. Montanari and R. Mulhaupt, *IEEE Trans. Dielectr. Electr. Insul.*, 2004, **11**, 763–784.
- 8 R. Scotti, M. D’Arienzo, B. Di Credico, L. Giannini and F. Morazzoni, *Hybrid Org. Interfaces*, 2017.
- 9 H. Takino and S. Iwama, *Rubber Chem. ...*, 1997, 5–7.
- 10 P. Zhang, M. Morris and D. Doshi, *Rubber Chem. Technol.*, 2016, **89**, 79–116.
- 11 A. B. Nair and R. Joseph, *Eco-friendly bio-composites using natural rubber (NR) matrices and natural fiber reinforcements*, 2014.
- 12 J. Fendler, *Korean J. Chem. Eng.*, 2001, **18**, 1–13.
- 13 M. J. Solomon, *Langmuir*, 2018, **34**, 11205–11219.
- 14 L. Mullins, *Engineering with Rubber*, Carl Hanser Verlag GmbH & Co. KG, Third Edit., 1986, vol. 59.
- 15 J. W. ten Brinke, S. C. Debnath, L. A. E. M. Reuvekamp and J. W. M. Noordermeer, *Compos. Sci. Technol.*, 2003, **63**, 1165–1174.
- 16 B. Schwaiger and A. Blume, *Rubber World*, 2000, **222**, 32–38.
- 17 J. Móczó and B. Pukánszky, *J. Ind. Eng. Chem.*, 2008, **14**, 535–563.
- 18 B. Di Credico, E. Cobani, E. Callone, L. Conzatti, D. Cristofori, M. D’Arienzo, S. Diré, L. Giannini, T. Hanel, R. Scotti, P. Stagnaro, L. Tadiello and F. Morazzoni, *Appl. Clay Sci.*, 2018, **152**, 51–64.
- 19 L. Wahba, M. D’Arienzo, R. Donetti, T. Hanel, R. Scotti, L. Tadiello and F. Morazzoni, *RSC Adv.*, 2013, **3**, 5832.
- 20 M. Castellano, E. Marsano, A. Turturro, L. Conzatti and G. Busca, *Adsorption*, 2012, **18**, 307–320.
- 21 C. J. Brinker and G. W. Scherer, *Sol-gel science: the physics and chemistry of*

- sol-gel processing*, Academic press, 2013.
- 22 L. Tadiello, M. D'Arienzo, B. Di Credico, T. Hanel, L. Matejka, M. Mauri, F. Morazzoni, R. Simonutti, M. Spirkova and R. Scotti, *Soft Matter*, 2015, **11**, 4022–4033.
- 23 H. Mollet and A. Grubenmann, *Formulation Technology*, WILEY-VCH, Weinheim, 2001.
- 24 L. Bokobza, E. Leroy and V. Lalanne, *Eur. Polym. J.*, 2009, **45**, 996–1001.
- 25 M. T. Shaw and W. J. MacKnight, *Introduction to polymer viscoelasticity*, John Wiley & Sons, 2018.
- 26 K. H. Nordsiek, *Kautschuk und Gummi, Kunststoffe*, 1985, **38**, 178–185.
- 27 M. Galimberti, *Rubber-clay nanocomposites: science, technology, and applications*, Hoboken, 2011.
- 28 M. Kotal and A. K. Bhowmick, *Prog. Polym. Sci.*, 2015, **51**, 127–187.
- 29 S. Rooj, A. Das, K. W. Sto and G. Heinrich, 2014, **1**, 220–246.
- 30 M. Maiti, M. Bhattacharya and A. K. Bhowmick, *Rubber Chem. Technol.*, 2008, **81**, 384–469.
- 31 Q. H. Zeng, A. B. Yu, G. Q. Lu and D. R. Paul, *J. Nanosci. Nanotechnol.*, 2005, **5**, 1574–1592.
- 32 S. Sinha Ray and M. Okamoto, *Prog. Polym. Sci.*, 2003, **28**, 1539–1641.
- 33 J. Ruamcharoen, S. Chotisuwan and P. Ruamcharoen, *Adv. Mater. Res.*, 2012, **489**, 701–705.
- 34 A. Esteban-Cubillo, R. Pina-Zapardiel, J. S. Moya, M. F. Barba and C. Pecharromán, *J. Eur. Ceram. Soc.*, 2008, **28**, 1763–1768.
- 35 E. Galan, 1996, 443–453.
- 36 L. G. Hernández, L. M. Ibarra Rueda and C. C. Antón, *Rubber Chem. Technol.*, 1987, **60**, 606–617.
- 37 A. Singer and E. Galan, *Developments in palygorskite-sepiolite research*, Elsevier, 2011.
- 38 A. J. Aznar, J. Sanz and E. Ruiz-Hitzky, *Colloid Polym. Sci.*, 1992, **270**, 165–176.
- 39 B. Di Credico, E. Cobani, E. Callone, L. Conzatti, D. Cristofori, M. D'Arienzo, S. Dirè, L. Giannini, T. Hanel, R. Scotti, P. Stagnaro, L. Tadiello and F. Morazzoni, *Appl. Clay Sci.*, 2018, **152**, 51–64.
- 40 M. S. Evans, *Tyre compounding for improved performance*, iSmithers Rapra Publishing, 2002, vol. 12.
- 41 S. Sadhu and A. K. Bhowmick, *J. Appl. Polym. Sci.*, 2004, **92**, 698–709.
- 42 M. A. Lopez-Manchado, B. Herrero and M. Arroyo, *Polym. Int.*, 2004, **53**, 1766–1772.
- 43 W. Wang and A. Wang, *Appl. Clay Sci.*, 2016, **119**, 18–30.
- 44 K. N. Madhusoodanan and S. Varghese, *J. Appl. Polym. Sci.*, 2006, **102**, 2537–2543.
- 45 Y. Gui, J. Zheng, X. Ye, D. Han, M. Xi and L. Zhang, *Compos. Part B Eng.*, 2016, **85**, 130–139.

- 46 Y. Wu, Y. Ma, Y. Wang and L. Zhang, *Macromol. Mater. Eng.*, 2004, **289**, 890–894.
- 47 A. Susanna, M. D’Arienzo, B. Di Credico, L. Giannini, T. Hanel, R. Grandori, F. Morazzoni, S. Mostoni, C. Santambrogio and R. Scotti, *Eur. Polym. J.*, 2017, **93**, 63–74.
- 48 A. Y. Coran, *J. Appl. Polym. Sci.*, 2003, **87**, 24–30.
- 49 A. B. Morgan, *Polym. Adv. Technol.*, 2006, **17**, 206–217.
- 50 J. Kim, T. Oh and D. Lee, *Polym. Int.*, 2004, **53**, 406–411.
- 51 M. Arroyo, M. A. López-Manchado and B. Herrero, *Polymer (Guildf.)*, 2003, **44**, 2447–2453.
- 52 K. G. Gatos, N. S. Sawanis, A. A. Apostolov, R. Thomann and J. Karger-Kocsis, *Macromol. Mater. Eng.*, 2004, **289**, 1079–1086.
- 53 A. Mousa and J. Karger-Kocsis, *Macromol. Mater. Eng.*, 2001, **286**, 260–266.
- 54 Y. Chang, Y. Yang, S. Ryu and C. Nah, *Polym. Int.*, 2002, **51**, 319–324.
- 55 Y.-L. Lu, Z. Li, Z.-Z. Yu, M. Tian, L.-Q. Zhang and Y.-W. Mai, *Compos. Sci. Technol.*, 2007, **67**, 2903–2913.
- 56 T. Wang and J. L. Keddie, *Adv. Colloid Interface Sci.*, 2009, **147–148**, 319–332.
- 57 Y. Yamashita, in *Liquid Crystals - Recent Advancements in Fundamental and Device Technologies*, InTech, 2018, pp. 243–261.
- 58 A. Puertas and de las Nieves FJ, *J. Colloid Interface Sci.*, 1999, **216**, 221–229.
- 59 M. Nakamura, N. Sato, N. Hoshi and O. Sakata, *ChemPhysChem*, 2011, **12**, 1430–1434.
- 60 D. Quemada and C. Berli, *Energy of interaction in colloids and its implications in rheological modeling*, 2002, vol. 98.
- 61 E. A. Vogler, *Adv. Colloid Interface Sci.*, 1998, **74**, 69–117.
- 62 H. T. Davis, *Colloids Surfaces A Physicochem. Eng. Asp.*, 1994, **91**, 9–24.
- 63 L. Tarachiwin, J. Sakdapipanich, K. Ute, T. Kitayama and Y. Tanaka, *Biomacromolecules*, 2005, **6**, 1858–1863.
- 64 K. Nawamawat, J. T. Sakdapipanich, C. C. Ho, Y. Ma, J. Song and J. G. Vancso, *Colloids Surfaces A Physicochem. Eng. Asp.*, 2011, **390**, 157–166.
- 65 W. A. Southorn, *Nature*, 1960, **188**, 165.
- 66 J. B. Gomez and H. Samsidar, *J. Nat. Rubber Res.*, 1989, **4**, 75–85.
- 67 M. J. Wang, T. Wang, Y. L. Wong, J. Shell and K. Mahmud, *KGK-Kautschuk und Gummi Kunststoffe*, 2002, **55**, 388–396.
- 68 J. M. Lightsey, J.W., Kneiling, D.J., Long, *Rubber world*, 1998, **218**, 35–40.
- 69 P. Yu, H. He and A. Dufresne, *Mater. Lett.*, 2017, **205**, 202–205.
- 70 P. Yu, H. He, Y. Luo, D. Jia and A. Dufresne, *Macromolecules*, 2017, **50**, 7211–7221.
- 71 J. Tan, X. Wang, Y. Luo and D. Jia, *Mater. Des.*, 2012, **34**, 825–831.
- 72 L. F. Valadares, C. A. P. Leite and F. Galembeck, *Polymer (Guildf.)*, 2006, **47**, 672–678.
- 73 N. Othman, S. N. A. Muttalib and N. I. Ismail, *Macromol. Symp.*, 2017, **371**,

- 35–43.
- 74 S. Varghese and J. Karger-Kocsis, *Polymer (Guildf.)*, 2003, **44**, 4921–4927.
- 75 Y. Wang, H. Zhang, Y. Wu, J. Yang and L. Zhang, *J. Appl. Polym. Sci.*, 2005, **96**, 324–328.
- 76 A. Varamesh, M. Abdollahi and H. H. Khanli, *Polym. Sci. Ser. A*, 2013, **55**, 115–120.
- 77 S. U. Pickering, *J. Chem. Soc. Trans.*, 1907, **91**, 2001–2021.
- 78 J. Wu and G. Ma, *Small*, 2016, 4633–4648.
- 79 A. Schröder, J. Sprakel, K. Schroën, J. N. Spaen and C. C. Berton-Carabin, *J. Food Eng.*, 2018, **234**, 63–72.
- 80 E. Princi, *Sintesi di Polimeri*, Rome, Edizioni N., 2012.
- 81 K. Zhang, W. Wu, H. Meng, K. Guo and J. F. Chen, *Powder Technol.*, 2009, **190**, 393–400.
- 82 J. Frelichowska, M. A. Bolzinger and Y. Chevalier, *J. Colloid Interface Sci.*, 2010, **351**, 348–356.
- 83 X. Zhang, Y. Sun, Y. Mao, K. Chen, Z. Cao and D. Qi, *RSC Adv.*, 2018, **8**, 3910–3918.
- 84 N. Negrete-Herrera, J. L. Putaux, L. David and E. Bourgeat-Lami, *Macromolecules*, 2006, **39**, 9177–9184.
- 85 L. Delafresnaye, P. Y. Dugas, P. E. Dufils, I. Chaduc, J. Vinas, M. Lansalot and E. Bourgeat-Lami, *Polym. Chem.*, 2017, **8**, 6217–6232.
- 86 D. J. Voorn, W. Ming and A. M. Van Herk, *Macromolecules*, 2006, **39**, 2137–2143.
- 87 I. W. Cheong, C. M. Fellows and R. G. Gilbert, *Polymer (Guildf.)*, 2004, **45**, 769–781.
- 88 D. H. Napper and R. G. Gilbert, in *An Introduction to Polymer Colloids*, Springer, 1990, pp. 159–185.
- 89 Y. Chevalier, C. Pichot and C. Graillat, *Colloid Polym. Sci.*, 1992, **821**, 806–821.
- 90 Y. Adachi, *Adv. Colloid Interface Sci.*, 1995, **56**, 1–31.
- 91 O. Myakonkaya and J. Eastoe, *Adv. Colloid Interface Sci.*, 2009, **149**, 39–46.
- 92 H. Xu, W. Jiang, F. Xiao and D. S. Wang, *Colloids Surfaces A Physicochem. Eng. Asp.*, 2014, **452**, 181–188.
- 93 A. J. Chan, K. Steenkeste, A. Canette, M. Eloy, D. Brosseau, F. Gaboriaud and M. P. Fontaine-Aupart, *Langmuir*, 2015, **31**, 12437–12446.
- 94 X. Gong, Z. Wang and T. Ngai, *Chem. Commun.*, 2014, **50**, 6556–6570.
- 95 S. Asakura and F. Oosawa, *J. Polym. Sci. Part A Polym. Chem.*, 1958, **33**, 183–192.
- 96 S. Isci, in *Surface modification of nanoparticle and natural fiber fillers*, 2015, pp. 151–169.





## Chapter 2.

### Materials and Methods

Chapter 2 aims at presenting the materials, synthetic and compounding strategies applied in this thesis.





## 2.1 Materials of tyre compounding

Tyres are complex materials whose generic composition is given in *Table 2-1*.

*Table 2-1. Generic tyre formulation.*

Compound	phr
rubber	100
filler	50
coupling agents	1
softeners	5
antioxidants	1
stearic acid	1
zinc oxide	5
accelerator	1
sluphur	2

The main structural ingredients are rubber and filler which compounded together in an elastomeric nanocomposite material give rise to viscoelastic properties (see Chapter 1 Paragraph 2.3). Silica-based fillers are compatibilized to rubber with coupling agents (see Chapter 2 Paragraph 1.3). Softeners include petroleum oils, resins and waxes and are used mainly as processing aids to improve tack or stickiness of uncured compounds. Antioxidants are added to rubber compounds to protect tyres by the oxygen degradation.<sup>1</sup>

### 2.1.1 Rubber

Rubbers are high molecular weight amorphous polymers which have a low  $T_g$  and high viscosity. In tyre application, the main polymers used are the following: natural rubber (NR) and its synthetic version isoprene rubber (IR); styrene-butadiene rubber (SBR); butadiene rubber (BR); their blends. The use of the polymers is linked to their  $T_g$ , which determines the specific application.

NR is the most widely used polymer in tyre application (around 70% of all tyres).<sup>2</sup> It is exuded from the rubber tree in the form of a colloidal suspension of NRL. When exuded fresh latex is composed by 55-60 wt. % of water, 30-40 wt. % of rubber, while the remnant percentage includes proteins, resins, mineral matter and carbohydrates. The amount of rubber obtained on each tapping (every 4-5 days) depends on clones, ages, soils and climatic conditions.

Fresh latex can be coagulated with the use of coagulants (usually formic acid), pressed between rollers and air- or smoke-dried to produce different types of NR, respectively air-dried sheets (ADS) or rubber smoked sheets (RSS). RSS is usually classified on the base of a visual scale of impurities.

Moreover, fresh latex can be commercialized as centrifuged latex, obtained by high speed centrifugation, allowing to separate the majority of the non-rubber components from the rubber phase. Centrifuged latex is applied in the production of different commercial goods such as footwear, medical supplies and adhesives. To enhance the stability over time of the centrifuged latex, ammonia at different concentration is added depending on the application (High Ammonia (HA), Medium Ammonia (MA), Low Ammonia (LA)), as reported in *Table 2-2*. In fact,  $\text{NH}_4^+$  ions increase the particle electric double layer and promote the partial hydrolysis of phospholipids and proteins.

Also centrifuged latex and NR still retain small amounts of non-rubber components as explicated in *Table 2-2*.

*Table 2-2. Percentage of components in fresh latex, centrifuged latex and dried NR.*

	Fresh latex (%)	Centrifuged latex (%)	NR (%)
<b>Rubber content</b>	30-40	60	93-97
<b>Proteinaceous substances</b>	1-1.5	1	2-3
<b>Ammonia</b>	-	0.6-0.7% HA 0.4-0.5% MA 0.2-0.3% LA	-
<b>Sugar, resins and salts</b>	2.5	1	1
<b>Water</b>	60-70	40	0.5

*Cis*-1,4-polyisoprene with a stereoregularity of around 97% is produced by the biosynthesis from the tree.<sup>3</sup> The structure of NR (2-methyl-1,3-butadiene) has been revealed by nuclear magnetic resonance (NMR) studies as a long sequence of around 20000 *cis*-1,4-polyisoprene units. Its mechanical properties are particularly interesting. In detail, the vulcanized NR provides:

- excellent tensile and tear strength,
- low hysteresis and high fatigue resistance,
- high abrasion resistance,
- good rebound and compression set,
- excellent adhesion to metal and fabrics
- good dielectric strength and electrical insulation.<sup>2</sup>

Drawbacks of NR are poor heat aging and resistance to ozone, oxygen, sunlight, oils and solvents. Addition of fillers, antiozonants and waxes to NR increases its resistance to UV and ozone. The degradation profile of NR STR20, used for this thesis work is given in *Figure 2-1*.

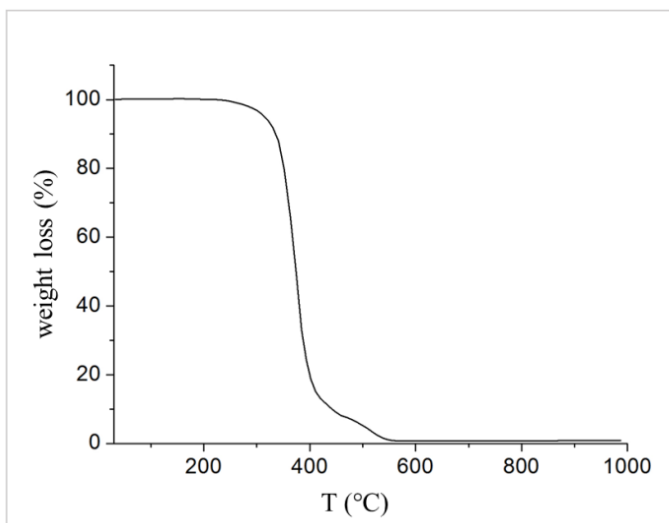


Figure 2-1. Thermogravimetric analysis (TGA) of NR.

Although the synthesis of IR in the presence of Ziegler-Natta catalysts has marked structural resemblance to NR with a stereoregularity of 98.5 %, <sup>4</sup> it shows considerable differences in properties like lower tensile and tear strength and hardness. The main differences between NR and IR, beyond the microstructure, derive from the molecular weight distribution, gel content and amount of non-rubber components. Furthermore, the rise of awareness of environmental issues contributes to maintain a high interest in this renewable source of rubber in comparison to synthetic rubbers which are obtained from non-renewable oil-based resources.

Proteins and phospholipids are probably the origin of branching and gel formation in NR. <sup>5</sup> The influence of these secondary structures were found to have a significant role in the singular effect of the crystallization of unvulcanized and vulcanized NR under strain, which is one of the important characteristics which make unique the mechanical properties of NR. <sup>6</sup> Proteins were also demonstrated to act as reinforcing fillers at low concentration (3-4 wt.%) and to influence the vulcanization process. <sup>7</sup> Anyway, the fact that the elastic modulus increases because of the presence of non-rubber components raised controversies. <sup>8</sup>

Tarachiwin applied Fourier Transform Infrared Spectroscopy (FTIR) for studying intramolecular interactions caused by hydrogen bonding in NR, since the vibrational modes are sensitive also to weak interactions. <sup>9</sup> In *Figure 2-2* FTIR spectroscopy of NR STR20 used in this thesis work is shown with the assignment of the principal vibrations modes (*Table 2-3*). <sup>10</sup>

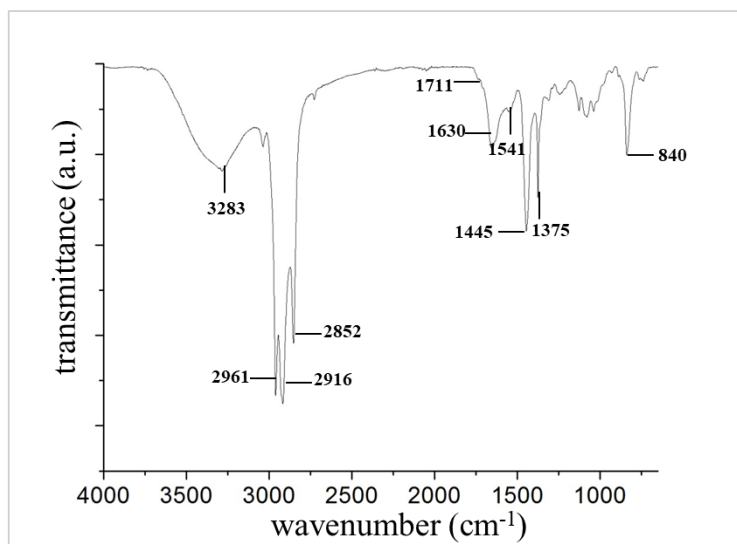


Figure 2-2. FTIR of NR.

Table 2-3. Assignment of the NR principal vibrations.

Wavenumber (cm <sup>-1</sup> )	assignment
<b>Isoprene chain</b>	
2961	$\nu$ CH <sub>3</sub> asymmetric
2916	$\nu$ CH <sub>3</sub> asymmetric
2852	$\nu$ CH <sub>2</sub> symmetric
1445	$\delta$ CH <sub>2</sub> and $\rho$ CH <sub>3</sub>
840	$\gamma$ C-H out of plane bending ( <i>cis</i> -1,4 addition)
<b>Proteins and lipids</b>	
3283	$\nu$ N-H
1711	$\nu$ C=O
1630	$\nu$ R <sub>1</sub> -(C=O)-NH-R <sub>2</sub> (amide I)
1541	$\beta$ N-H and $\nu$ C-N (amide II)

In this thesis, NRL MA, (60% w/w) and poly(1,4-*cis*-isoprene) STR20 (NR) were produced by Von Bundit.

### 2.1.2 Silica-based fillers

Silica and silicates are used as reinforcing fillers in tyre application. The silica surface is highly hydrophilic because of the presence of silanols (*Figure 2-3*), which are classified according to the number of bonds with Si and to their vicinity. Thus, silica-based fillers usually require compatibilization to be dispersed in a rubber matrix.

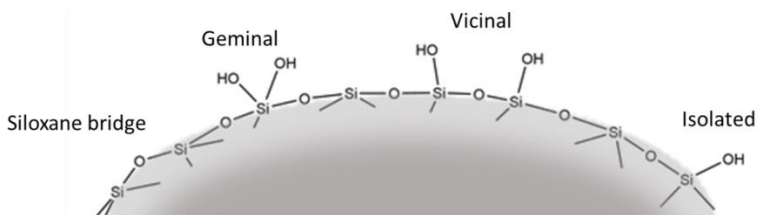


Figure 2-3. Silanols and siloxanes on the silica surface.

Silanol and siloxane groups are detectable by FTIR (Figure 2-4). Table 2-4 summarizes the main vibration modes and the relative assignments for  $\text{SiO}_2$ .

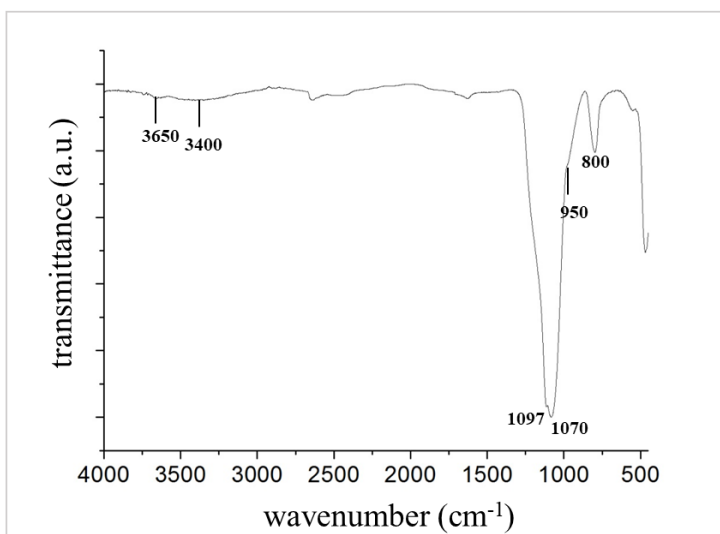


Figure 2-4. FTIR of  $\text{SiO}_2$ .

Table 2-4. FTIR peaks assignment of  $\text{SiO}_2$ .

Wavenumber ( $\text{cm}^{-1}$ )	assignment
3650	$\nu$ Si-OH isolated
3400	$\nu$ OH hydrogen bond
1097	$\nu$ Si-O
1070	$\nu$ Si-O
950	$\nu$ Si-OH
800	$\nu$ Si-O

Depending on the synthesis (fumed, precipitated, sol-gel, etc) silica particles may differ in terms of primary particle size, porosity and silanol surface density. These properties affect the surface chemistry and thus the aggregation and

agglomeration which are relevant characteristics in the frame of nanocomposite reinforcement (see Chapter 1 Paragraph 2.1.1). In this PhD thesis, precipitated nanosilica Zeosil MP1165 (20 nm primary particle size, surface area  $160 \text{ m}^2\text{g}^{-1}$ ) was purchased by Solvay.

The aggregation of silica also affects the stability in a water suspension. LUDOX® AS40 (22 nm primary particles,  $140 \text{ m}^2\text{g}^{-1}$ ) synthesized via sol-gel method by Sigma Aldrich was applied to produce MBs and in the Pickering emulsion of polyisoprene. Analysis of the silica dispersion in water are given in Chapter 3 Paragraph 1.2.

Besides silica, naturally occurring sepiolite nanofibers have been utilized as filler in the present work.

Pristine sepiolite is a natural magnesium layered silicate which is extracted from mines. It has the chemical formula of  $\text{Mg}_8\text{Si}_{12}\text{O}_{30}(\text{OH})_4(\text{H}_2\text{O})_4 \cdot 8\text{H}_2\text{O}$  as reported in Chapter 1 Paragraph 3.1.1.

The crystalline structure produces a fiber shape with a very high AR, with a surface area of  $300 \text{ m}^2\text{g}^{-1}$ . The evaluation of the Sep dimension is given in *Table 2-5* and was calculated as average of the dimensions of 100 fibers in 20 different Scanning Electron Microscopy (SEM) micrographs (*Figure 2-5*).<sup>11</sup>

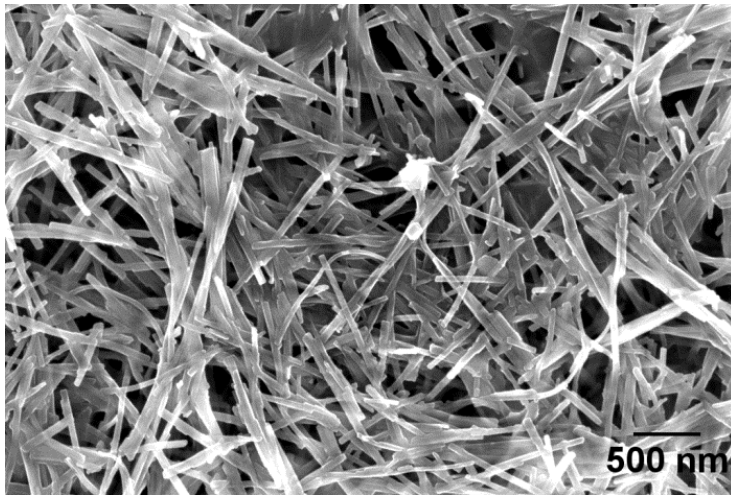


*Figure 2-5. SEM micrograph of Sep.*

*Table 2-5. Dimensions of Sep fibers, obtained by SEM analysis.*

	<i>Length (nm)</i>	<i>Cross-section (nm)</i>	<i>AR</i>
<i>SepB5</i>	1398 ( $\pm 567$ )	67 ( $\pm 15$ )	21 ( $\pm 10$ )
<i>SepS9</i>	1781 ( $\pm 1004$ )	80 ( $\pm 21$ )	22 ( $\pm 11$ )

Sep fibers aggregate along the main axis and form bundles of 10-100  $\mu\text{m}$ .

In detail, two different sepiolite fibers have been utilized in this thesis: Sepiolite Pangel S9 (SepS9), i.e. pristine sepiolite extracted from mines; Sepiolite Pangel B5 (SepB5), from organic modification of sepiolite S9 with N,N-didodecyl-N-methyl-ammonium (DDMA), in order to increase the dispersion and compatibility with polymers.

The diffraction pattern of SepS9 and SepB5 is reported in *Figure 2-6*.

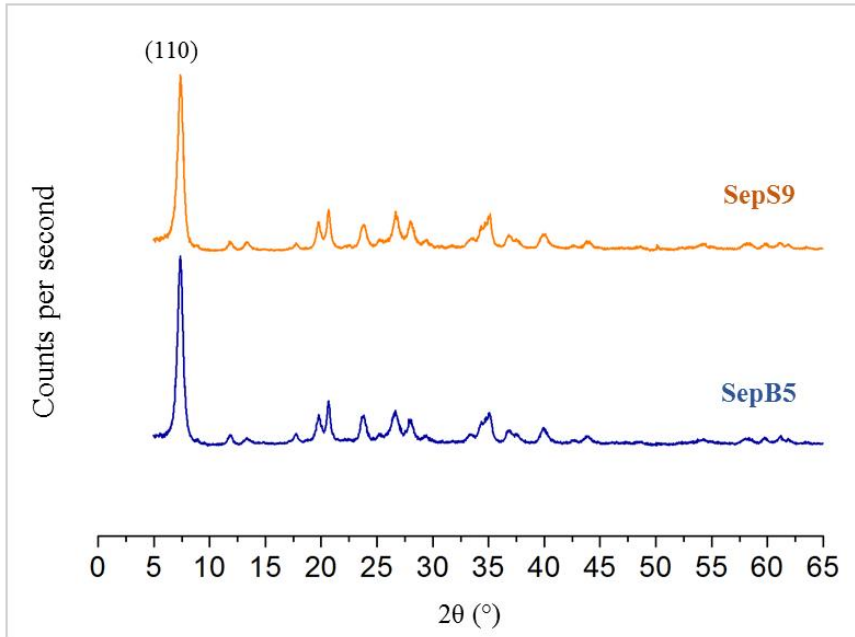


*Figure 2-6. XRD pattern of SepS9 (orange line) and SepB5 (blue line).*

The characteristic reflections at  $2\theta = 7.3^\circ$ ,  $12.3^\circ$ ,  $17.7^\circ$ ,  $19.8^\circ$ ,  $35.0^\circ$  correspond to the (110), (130), (150), (060) and (371) crystal planes of Sep, respectively.<sup>12</sup>

SepS9 and SepB5 have been characterized by FTIR (*Figure 2-7*). The relative band assignment is given in *Table 2-6*.<sup>13</sup>

In this thesis, Sep Pangel S9 (SepS9) and the organically modified Sep Pangel B5 (SepB5, organically-modified with N,N-didodecyl-N-methyl-benzylammonium) were supplied by Tolsa and extracted from the landfill of Vallecas (Spain).

The hydrophilic nature of silica-based fillers requires their compatibilization to rubber. A good compatibilization is reflected on the filler dispersion, which is crucial to obtain good mechanical properties.

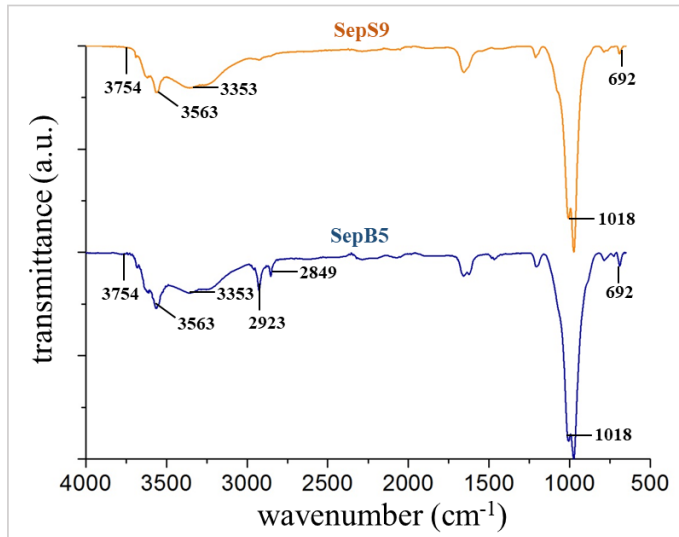


Figure 2-7. FTIR of SepS9 (orange line) and SepB5 (blue line).

Table 2-6. FTIR peak assignments for Sep.

Wavenumber (cm <sup>-1</sup> )	assignment
<b>pristine</b>	
<b>3700-3650</b>	$\nu$ MgO-H
<b>3600-3200</b>	$\nu$ OH
<b>1661</b>	$\delta$ H-O-H
<b>1209, 1005</b>	$\nu$ Si-O asymmetric
<b>975</b>	$\nu$ Si-OH
<b>692</b>	$\delta$ Mg-OH
<b>organically modified</b>	
<b>2923</b>	$\nu$ CH <sub>3</sub> asymmetric
<b>2849</b>	$\nu$ CH <sub>2</sub> asymmetric

### 2.1.3 Coupling agents

Coupling agents are molecules which provide the formation of chemical interactions between two dissimilar materials, usually of inorganic and organic nature, respectively. Thanks to a double functionality, they are able to bind to silica-based fillers with a silicon-functional moiety and to rubber with an organo-functionality creating a filler-polymer network which imparts high reinforcement



to the material. The silicon functional moieties are halides, alkoxides or acyloxy, while the organo-functional ones consist of an amino, methacrylate, epoxy, mercapto-group.<sup>14</sup>

One of the most common coupling agents applied in tyre compounding is bis(3-triethoxysilylpropyl)tetrasulfide (TESPT) (*Figure 2-8*). It has been used in this thesis and purchased from Aldrich.

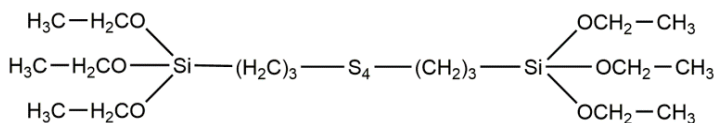


*Figure 2-8. Chemical structure of TESPT.*

The functionalization of the silica-based fillers usually takes place during mixing where the triethoxysilyl groups of the TESPT are hydrolyzed and then undergo condensation with the silanol groups of silica with ethanol loss at 120°C (*Figure 2-9 a*). The surface chemistry of the filler changes and the surface free energy is reduced. This enhance its dispersability within the polymer matrix.<sup>15</sup>

During the vulcanization at 170°C, TESPT disproportionate into bis(3-triethoxysilylpropyl)-disulfide and bis(3-triethoxysilyl propyl)-polysulfides and then reacts as a sulfur donor, ending in the saturation of polymer double bonds and creating a sulfur bridges (*Figure 2-9 b*). Thanks to these reactions, TESPT acts as linker between filler and rubber, producing the so-called filler-rubber network.<sup>16</sup>

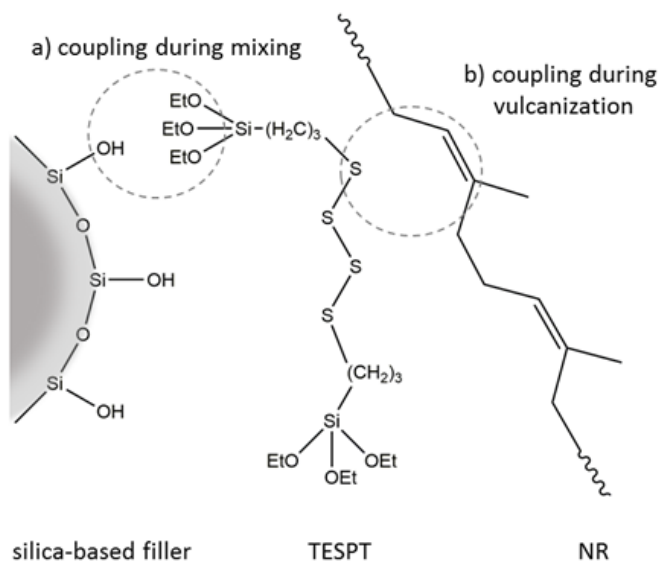


*Figure 2-9. Functionalities of TESPT involved in the formation of filler-rubber network.*

Sarkawi, through a quantification of the bound rubber which is only loosely or physically bound to silica filler particles, showed that, even without silanization, some silica-NR interactions are present.<sup>17</sup> As concern NR nanocomposites, the comparison among NRs having different amount of proteins demonstrated that non-rubber compounds increase the filler-rubber interactions because of the lowering of the hydrophilicity of the silica surface, which enable to disrupt the silica-silica networking. In the presence of both coupling agent and proteins it was revealed a complicated antagonistic effect in silica reinforcement in NR.<sup>17</sup> Since this PhD work makes use of NR, aspects related to the presence of proteins has been taken into account.

#### 2.1.4 Curing agents and additives

The vulcanization process makes use of activants and accelerants. Briefly, the formation of sulfurating complexes involves the use of stearic acid which interacts with ZnO, making  $Zn^{2+}$  available for the formation of intermediates with N-cyclohexyl-2-benzothiazole sulfenamide (CBS) and sulfur. These sulfurating complexes act creating mono- and multi-sulfur bonds between rubber chains.<sup>18</sup> In this thesis work, stearic acid (Stearina TP8) was purchased from Undesa, sulfur from Zolfoindustria, zinc oxide from Zincol Ossidi and CBS (Vulkacit CZ/C) from Lanxess.

To avoid degradation of rubber usually the antioxidants N-(1,3-dimethylbutyl)-N'-phenyl-p-phenylenediamine (6PPD) was used.

## 2.2 Procedures

This thesis proposes the preparation of silica-based/PI nanocomposites through colloidal approaches which enable good dispersion of fillers. In particular, the work is outlined in two different approaches: latex compounding and *in situ* polymerization. Moreover, the materials obtained by colloidal approach have been further compounded to make nanocomposite final materials for tyre application by melt mixing.

LCT is a compounding method which makes use of latexes of polymers, like NRL, and water filler dispersions with the production of masterbatches (MB, i.e. coagulated filled rubber material). MB is a term used to identify materials which have been processed but are not final materials, since their aim is to impart properties to polymeric composites. It may refer to any process stage intermediate between raw materials and final formulate products. MBs are usually concentrated mixture of ingredients/additives in a polymeric matrix. They can transfer properties by mixing with other polymeric composites. MBs are useful when the direct compounding of ingredients in the final material retains some problems, i.e. dispersion, aggregation and so on. The term is usually referred to "colored masterbatch", materials applied to transfer pigments in plastics. In our

case, MBs are concentrated filler-polymer materials, where the filler is pre-dispersed with the aim of increasing dispersion in the final composites. The application of MB seems particularly suitable in the case of dusty fillers like clays. The MBs have been produced by LCT and then compounded to the other ingredients for tyre application by melt mixing.

For the *in situ* polymerization, polyisoprene has been synthesized by a Pickering emulsion polymerization of silica-based nanoparticles. This approach provides an intimate filler-polymer interaction which determines the formation of highly dispersed silica-based filler/polyisoprene nanocomposites.

### 2.2.1 Latex compounding technique

A dispersion of 20 g of silica-based filler ( $\text{SiO}_2$ , SepS9 and SepB5) in 400 ml of water is prepared and stirred with a mechanical stirrer (Velp Scientifica Stirrer DLS) at 200 rpm (rounds per minute) for 10 minutes. The type of silica used is a commercial product appropriate for colloidal chemistry where the silica particles are very stable thanks to the ions in solution ( $\text{NH}_4^+$  in the case of LUDOX® AS40). The dilution of  $\text{SiO}_2$  appears immediately homogeneous thanks to the high dispersability of the  $\text{SiO}_2$  particles, unlike the Sep dispersion which requires some efforts to produce an homogeneous dispersion. SepX, instead, is mixed with a mechanical stirrer (Velp Scientifica Stirrer DLS) at 200 rpm. The mixing time is 60 min for SepS9 and 20 min for SepB5, corresponding to the optimal colloid relative dispersion needed to the following flocculation process (the optimal viscosity was identified by testing different mixing time). Subsequently, Sep dispersion is sonicated for 10 min and mixed again for 10 min.

In another vessel, 33 g of NRL are diluted with 100 ml of distilled water and stirred for 10 min at 100 rpm with a mechanical stirrer. Successively, 0.2 g of finely ground 6 PPD antioxidant is added to the solution.

In the case of  $\text{SiO}_2$ , the filler dispersion is poured into the diluted NRL solution, under stirring at 500 rpm. The system is kept under stirring for 10 minutes. In this time no flocculation is detected. To coagulate the system a solution of  $\text{Mg}(\text{NO}_3)_2 \cdot 6\text{H}_2\text{O}$  in water in the proportion of 2% wt is added to the  $\text{SiO}_2$ /NRL dispersion. Flocculation suddenly happens at the addition of the inorganic salt.

In the case of SepX, the dispersion is poured into the diluted NRL solution, under stirring at 500 rpm. The flocculation of the SepX/NR takes place spontaneously without the addition of any coagulant and is completed in 30 s.

The silica-based filler/NR masterbatch is separated from the liquid phase through filtration, and washed with water to remove ammonium residuals, portioned in small pieces and dried in a vacuum oven (pressure: 10 mbar) at 80 °C for 18 h.

The obtained MB containing 50% wt of filler is further homogenized in a two roll mill at room temperature for 5 min. The obtained composite materials are called MB- $\text{SiO}_2$ /NR and MB-SepX/NR.<sup>19</sup>

Each step of this procedure is shown in pictures and represented in schemes in *Figure 2-10*.

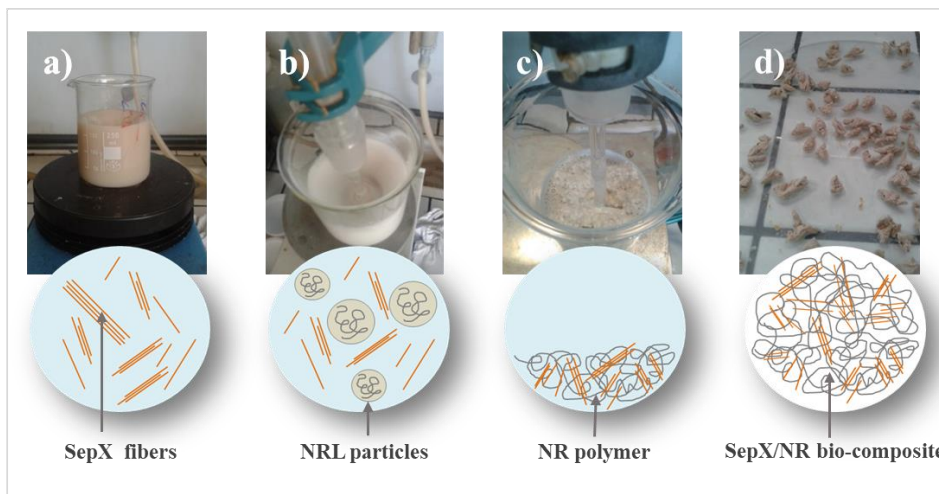


*Figure 2-10. Scheme of the MB-SepX/NR masterbatch preparation: a) SepX dispersion in water; b) mixing of the SepX aqueous dispersion with NRL; c) flocculated MB-SepX/NR; and d) dried MB-SepX/NR.*

### 2.2.2 *In situ* Pickering emulsion polymerization

The synthesis of polyisoprene via Pickering emulsion has been carried out in the presence of silica-based fillers ( $\text{SiO}_2$ , SepS9 and SepB5).

First, 3 ml of isoprene are treated with an alumina phase to remove the inhibitor. Then, the monomer is degassed under nitrogen flux for 20 minutes. In the meantime, a dispersion of 1 % wt of inorganic particles is made over a volume of 30 ml of distilled water. In the case of SepX, the dispersion is left under stirring overnight, while the  $\text{SiO}_2$  dispersion is immediately stable without any dispersion procedure. 120 mg of sodium bicarbonate are added to the silica dispersion to provide a basic pH of 9. Then, potassium persulfate is also added to the dispersion at 1 wt % (41 mg) with respect to the monomer weight. The aqueous dispersion is also degassed for 20 minutes.

After, we unify 118  $\mu\text{L}$  of tert-dodecylmercaptan to the degassed monomer. The presence of thiols is known to be important for the transport of radical species from the aqueous to the oil phase. This mixture is added under stirring and nitrogen flux to the aqueous dispersion with the help of a syringe. The reaction is stirred at room temperature for one hour to create the emulsion. The polymerization is carried out for 2 or 4 days at 75 or 90  $^\circ\text{C}$ . We make use of a vial closed with a teflon tape to avoid evaporation of the monomer which as a low boiling point (34 $^\circ\text{C}$ ). Anyway, small evaporation of the monomer are not to be excluded. In *Figure 2-11* it is shown a picture of the polyisoprene latex polymerized via Pickering emulsion with silica particles.



Figure 2-11. Polyisoprene latex with silica particles via Pickering emulsion.

### 2.2.3 Preparation of composite materials for tyre application

The relative quantity of ingredients used to prepare the composite materials is listed in *Table 2-7*. Composite materials are compounded through melt mixing, using a Brabender Plasti-Corder Lab station internal mixer (65 mL mixing chamber, 0.6 filling factor). The mechanical properties of composite materials compounded with MBs (named: NC(MB-SepX/NR) and NC(MB-SiO<sub>2</sub>/NR)) are then compared to the ones of reference materials, whose compounding is completely made by melt mixing (named: REF-SepX and REF-SiO<sub>2</sub>). All the compounds have a total amount of filler of 32 phr. The compounds containing Sep are always compounded with the same phr of silica. In the case of NC(MB-SiO<sub>2</sub>/NR) the filler was added through MBs, while in the case of NC(MB-SepX/NR) silica was introduced without MBs to emphasize the effect of LCT on the compounding of Sep.

The preparation of the composite materials consists of three mixing steps:

- 1<sup>st</sup> step: 120 °C for 7 minutes;
- 2<sup>nd</sup> step: 90 °C for 3 minutes;
- 3<sup>rd</sup> step: 50°C for 3 minutes in an open mixer.

Times and temperatures are determined according to the thermal stability of the reactants and to the workability of rubber. Rubber is first masticated at 120 °C and 60 rpm rotor speed. Then, the relative quantity of MB is added within 1 minutes. Right after, the dry filler is added in subsequent aliquots within 2 minutes, together with the silane. The temperature provides the right energy for the

silanization to take place.<sup>20</sup> The mixing process determines the deformation of the rubber matrix helping the distribution of the components within the matrix and contemporary breakdown of filler agglomerates into fine aggregates. Reference materials are compounded in the same way, but no MB is added. One minute after the last filler addition, 6PPD, zinc oxide and stearic acid are added.

The second step takes place the day after, when the polymer chains are relaxed. The intermediate materials are reloaded in the internal mixer operating at 90 °C at 60 rpm. CBS and sulfur are added in one minute.

In the last step, the day after, the composites are processed in a two-rolling mill at 50 °C for 3 minutes to improve their homogeneity. The material composites containing 32 phr of Sep or silica are vulcanized in a hydraulic press at 170°C and 100 bar for 10 min.

*Table 2-7. Relative quantities of the compounding ingredients in composite materials.*

	NR	SiO <sub>2</sub>	SepX	MB (phr filler)	TESPT	St. acid	6PPD	ZnO	C B S	S
REF-SepX/NR	100	16	16	-	2,56	2	2	3,5	3	1
NC(MB-SepX/NR)	100	16	-	16	2,56	2	2	3,5	3	1
REF-SiO <sub>2</sub> /NR	100	32	-	-	2,56	2	2	3,5	3	1
NC(MB-SiO <sub>2</sub> /NR)	100	-	-	32	2,56	2	2	3,5	3	1

## 2.3 Bibliography

- 1 S. Thomas and R. Stephen, *Rubber nanocomposites: preparation, properties, and applications*, John Wiley & Sons, 2010.
- 2 S. Thomas, R. K. R., H. J. Maria, C. H. Chan and L. a. Pothen, 2014, **2**, 634.
- 3 S. Thomas, H. C. Chin, L. A. Pothen, K. R. Rajisha and H. J. Maria, *Nat. Rubber Mater.*, 2014, **1: Blends**, 107–131.
- 4 D. Liu, D. Cui and W. Gao, *Sci. China Chem.*, 2010, **53**, 1641–1645.
- 5 L. Tarachiwin, Y. Tanaka and J. Sakdapipanich, *Kautschuk Gummi Kunststoffe*, 2005, **58**, 115–122.
- 6 B. Huneau, *Rubber Chem. Technol.*, 2011, **84**, 425–452.
- 7 E. C. Gregg Jr and J. H. Macey, *Rubber Chem. Technol.*, 1973, **46**, 47–66.
- 8 A. B. Othman and H. Hasma, in *Proceedings International Rubber Technology Conference*, 1988, pp. 166–177.
- 9 L. Tarachiwin, J. Sakdapipanich, K. Ute, T. Kitayama and Y. Tanaka, *Biomacromolecules*, 2005, **6**, 1858–1863.
- 10 F. J. Lu and S. L. Hsu, *Rubber Chem. Technol.*, 1987, **60**, 647–658.
- 11 J. Santaren, *Clays Clay Miner.*, 1990, **38**, 63–68.
- 12 J. E. Post, D. L. Bish and P. J. Heaney, *Am. Mineral.*, 2007, **92**, 91–97.
- 13 J. L. Acosta, M. C. Ojeda, E. Morales and A. Linares, *J. Appl. Polym. Sci.*, 1986, **31**, 1869–1878.
- 14 G. Burrowes and B. Rodgers, 2004.
- 15 S. S. Sarkawi, W. K. Dierkes and J. W. M. Noordermeer, *Rubber Chem. Technol.*, 2015, **88**, 359–372.
- 16 S. Wolff, *Kautsch. Gummi, Kunstst.*, 1981, **34**, 280.
- 17 S. salina Sarkawi, *Nano-Reinforcement of Tire Rubbers: Silica-technology For Natural Rubber*, 2013.
- 18 A. Susanna, M. D'Arienzo, B. Di Credico, L. Giannini, T. Hanel, R. Grandori, F. Morazzoni, S. Mostoni, C. Santambrogio and R. Scotti, *Eur. Polym. J.*, 2017, **93**, 63–74.
- 19 B. Di Credico, I. Tagliaro, E. Cobani, L. Conzatti, M. D'Arienzo, L. Giannini, S. Mascotto, R. Scotti, P. Stagnaro and L. Tadiello, *Nanomaterials*, 2019, **9**, 46.
- 20 S. Wolff, *Rubber Chem. Technol.*, 1996, **69**, 325–346.





## Chapter 3.

### Latex compounding technique for preparing silica-based natural rubber masterbatches

Chapter 3 describes the preparation of highly-loaded homogeneous SiO<sub>2</sub> and Sep masterbatch (*i.e.* coagulated filled rubber material) by applying LCT approach with NRL.

The main physicochemical parameters which control aggregation processes in the aqueous medium, *i.e.* pH, ζ-potential, concentration of colloidal systems, as well as the morphological features of the final filler/NR composites, were comprehensively investigated to highlight the filler-NR interactions and to propose a flocculation mechanism.

Filler/NR MBs were fully characterized and used to prepare composites by conventional melt mixing.



### 3.1 Characterization of colloidal dispersions

#### 3.1.1 NRL

Dynamic Light Scattering (DLS) analysis of NRL evidences a bimodal distribution of the hydrodynamic radius, indicating the presence of a fraction of particles with an average size of  $\sim 300 \pm 130$  nm (65%), and a second population (35%) with an average size of  $\sim 1200 \pm 500$  nm (*Figure 3-1*).<sup>1</sup> The analysis of NRL particle size may be affected by the presence of other spherical structures which are naturally present from the extraction from the tree of NRL, such as lutoids or Frey-Wyssling complexes.<sup>2</sup> The amount of these structures may vary depending on several factors like the season of extraction, climate changes etc, as reported in Chapter 1 Paragraph 4.1.2.

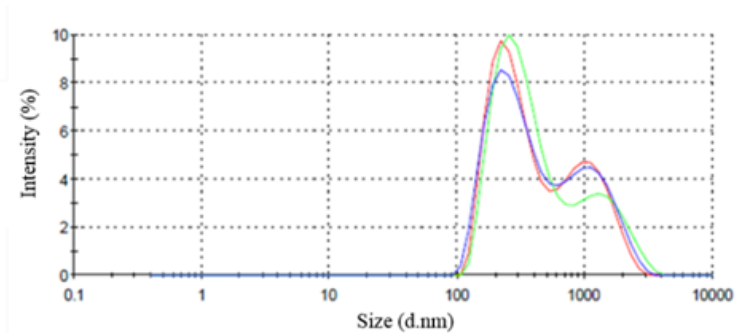


*Figure 3-1. DLS analysis of NRL particles (red, green and blue lines are respectively the first, second and third measurement).*

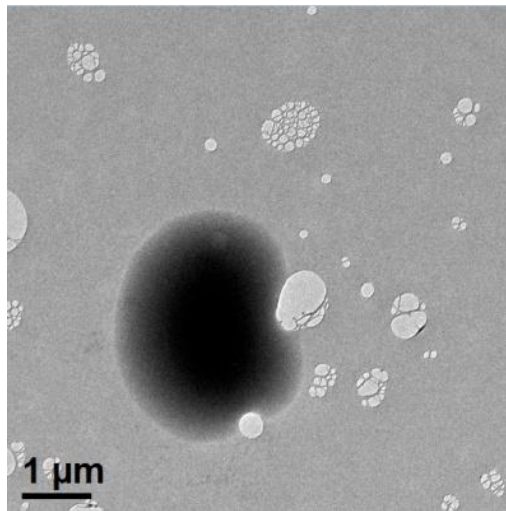


*Figure 3-2. TEM image of NRL.*

Transmission Electron Microscopy (TEM) images of NRL (*Figure 3-2*) reveal that NRL particles are spherical with a diameter of about 2  $\mu\text{m}$ , in line with DLS analysis. In *Figure 3-2*, the NRL particles are visible like black shadows with a darker center and lighter borders. Elsewhere the lighter region has been identified as the proteic-phospholipidic layer which surrounds the NRL particles.<sup>1</sup> The clear spots in TEM image are more likely parts of Frey-Wyssling complexes, i.e. lipids or vesicles.<sup>2</sup>

The  $\zeta$ -potential of the NRL particles has been determined in order to define the charge of the electric double layer of this colloidal system and to investigate the colloid stability. The  $\zeta$ -potential of NRL-MA at pH 7 is  $-28 (\pm 2)$  mV. Since relatively high absolute values of  $\zeta$  ( $\pm 30$  mV) indicate significantly stable systems, the measurement supports the good stability of NRL dispersion. The negative surface charge is most likely provided by proteins and phospholipids amino and carboxyl functional groups, which can be easily ionized and whose charge balance give rise to a negative electric double layer.<sup>3</sup> The evolution of the  $\zeta$ -potential changing the pH demonstrates how the electric double layer of NRL is affected by ions in the medium. Decreasing the pH,  $\zeta$  of NRL increases (*Figure 3-3*), reaching the IEP at pH 3, in agreement with the literature.<sup>4</sup>

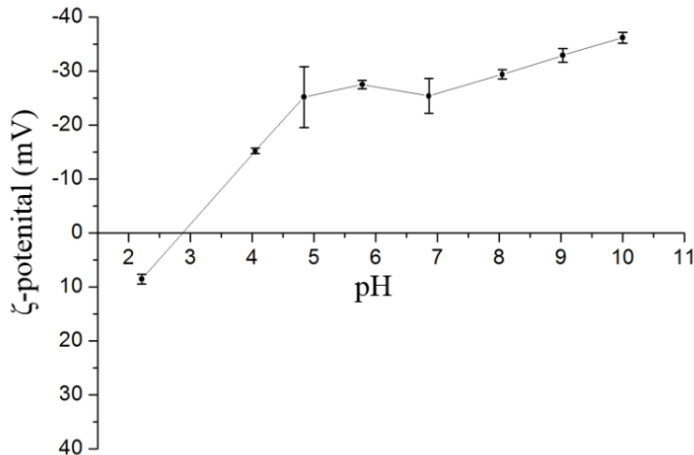


*Figure 3-3. Trend of  $\zeta$ -potential vs. pH for NRL.*

### 3.1.2 $\text{SiO}_2$ dispersion

The hydrodynamic radius value of commercial  $\text{SiO}_2$  particles has been measured by DLS and reported in the *Table 3-1*. The nominal value of the particle radius is 22 ( $\pm 6$ ) nm, which is confirmed by SEM analysis, while the hydrodynamic radius of around 20 ( $\pm 2$ ) nm.

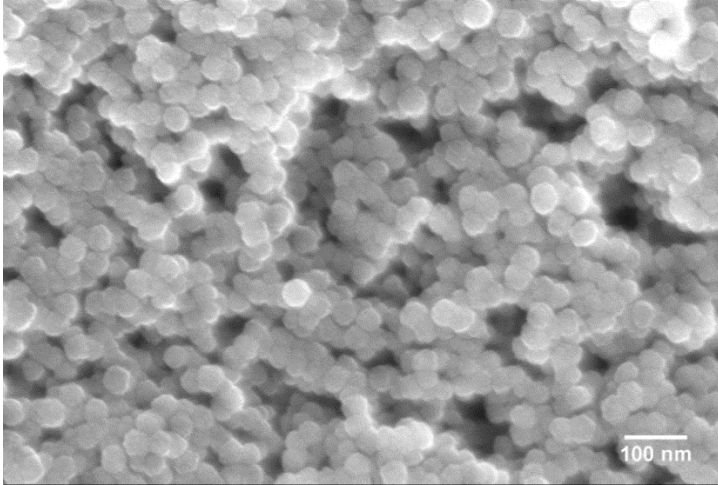


Figure 3-4. SEM image of SiO<sub>2</sub> particles.

The  $\zeta$ -potential of SiO<sub>2</sub> at pH 7 is  $-42 (\pm 1)$  mV, which indicate high colloidal stability.

The negative charge of the particles is the result of dehydroxylation or deprotonation of the SiO<sub>2</sub> surface at this pH value. Changing the pH of the medium the module of the  $\zeta$ -potential increases accordingly to literature.<sup>5</sup>

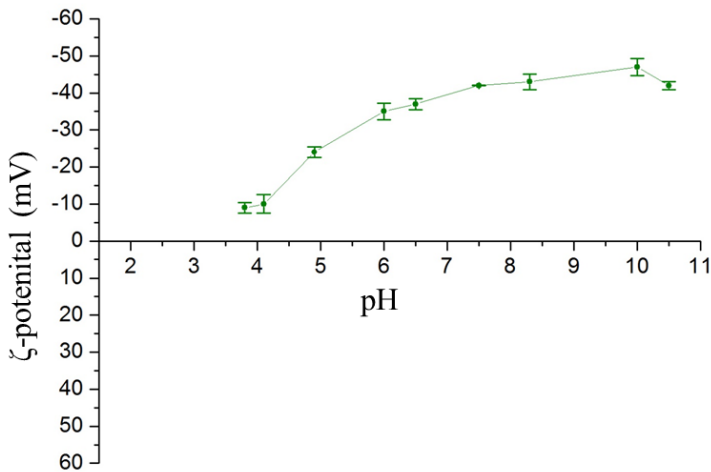
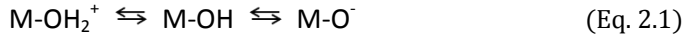


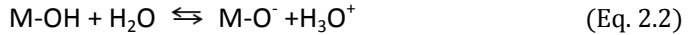
Figure 3-5. Trend of  $\zeta$ -potential vs. pH for SiO<sub>2</sub>.

It is well known that for hydrous oxides, H<sup>+</sup> and OH<sup>-</sup> are most likely the potential-determining ions (pdi). The pdi are specifically bound cations or anions that result in net surface charge. The potential determining role of H<sup>+</sup> and OH<sup>-</sup> is most readily

accounted by realizing that the pH-dependent charge of an oxide results from acid–base reactions at the surface:<sup>6</sup>



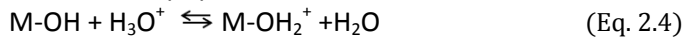
where M stands for a metal or metalloid central ion, i.e. Si or Mg. It is convenient to visualize the surface sites as converted on hydration to surface hydroxyl groups of M–OH groups that can dissociate protons:



or



or accept protons:



or



The increase of pH results in an increase of M–O<sup>−</sup> or M–(OH)<sub>2</sub><sup>−</sup> in terms of reaction (2), i.e. the negative charge of the particles is the result of dehydroxylation or deprotonation of the surface.

In the case of commercial SiO<sub>2</sub>, since the product is ammonia stabilized, the colloidal stability is due to the presence of NH<sub>4</sub><sup>+</sup> ions which are useful to increase the charge of the electric double layer of the silica particles.

*Table 3-1. Significant parameters of SiO<sub>2</sub> dispersion.*

*SEM (nm)   Hydrodynamic radius (nm)   ζ-potential (mV) pH 7*

22	45	-42.6
----	----	-------

### 3.1.3 SepS9 and SepB5 dispersions

Sep bundles, once dispersed in the aqueous medium, form an arrangement of randomly intermeshed elongated fibers, kept together by physical interactions and hydrogen bonding. Water can easily penetrate through these structures, thus increasing the viscosity of the suspension.<sup>7</sup>

To obtain stable dispersions, SepX undergoes cycles of stirring and sonication to break the natural aggregates of the clay. The mixing time has been established at 60 min for SepS9 and 20 min for SepB5, corresponding to the optimal dispersion condition needed to get the proper viscosity. Subsequently, SepX dispersion is sonicated for 10 min and mixed again for 10 min.

SEM micrographs on Sep fibers reveals that both SepS9 and SepB5 appear as rod like particles with similar AR strongly interconnected in bundles-like aggregates (*Figure 3-6*).

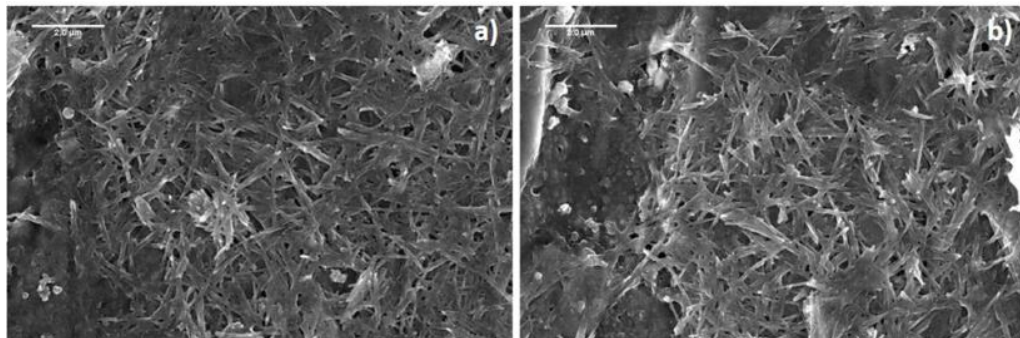


*Figure 3-6. SEM micrographs of a) SepS9 and b) SepB5.*

The characterization of a Sep dispersion through DLS has not been performed, since the high anisotropy of the fibers does not supply a representative result of the particle dimensions and because the presence of the organic modifier in SepB5 may affect the size measurement.

SepS9 particles dispersed in aqueous environment are charged solids surrounded by a diffuse ionic atmosphere. They carry a net negative charge due to the unbalance in its crystal lattice. The crystalline structure is not ideal and the presence of defects determine the formation of vacancies which cause attraction of counter ions. Ions of opposite charge are adsorbed onto the surface, neutralizing the charge developed at the surface. The diffuse ionic layer is composed of opposite charged ions and bound dipoles of water molecules which gather around the particle.

The analysis of  $\zeta$  at pH 7 are  $-34.8 (\pm 0.05)$  mV for SepS9, while for SepB5 modified with an alkylbenzyl ammonium salt, a positive  $\zeta$ -potential was measured  $+26.9 (\pm 0.05)$  mV (*Table 3-2*) due to the presence of a quaternary ammonium salt adsorbed onto the fiber surface.

*Table 3-2.  $\zeta$ -potential of SepS9 and SepB5 at pH7.*

	$\zeta$ -potential (mV)
SepB5	$+26.9 (\pm 0.05)$
SepS9	$-34.8 (\pm 0.05)$

SepS9 suspension (orange line in *Figure 3-7*) has a slightly positive  $\zeta$  values ( $+0.38$  mV at pH 2) at low pH while negative one at high pH.<sup>8</sup> The IEP lies at pH 2.4. As reported by Alkan et al.,<sup>6,8</sup> at acidic pH, SepS9 fibers in water solution display a

positive  $\zeta$ -potential due to the protonation of the surface groups, which undergo dehydroxylation or deprotonation at higher pH, leading to significant decrease of the  $\zeta$  value. SepB5 (blue line in *Figure 3-7*) suspension shows, instead, a positive  $\zeta$ -potential in the whole pH range, again ascribable to the presence of alkylammonium salt as functionalizing group at the filler surface.

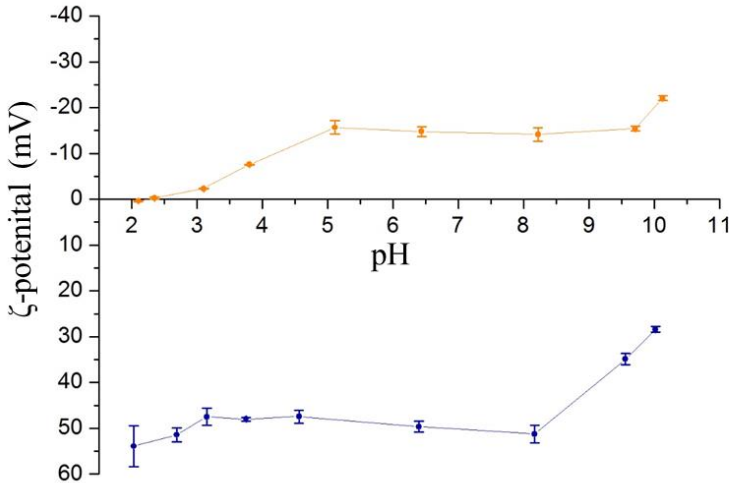


*Figure 3-7. Trend of  $\zeta$ -potential vs. pH for SepS9 (orange line) and SepB5 (blue line).*

### 3.1.3.1 SepS9 dispersion stability evaluation

Further characterizations have been performed in order to evaluate all the electro-kinetic and adsorption properties, in particular for pristine SepS9 colloidal system, which can be more affected by the environmental conditions compared to SepB5 whose surface is covered and protected by a functional organic group. The change of  $\zeta$ -potential over time of mixing is evaluated in *Figure 3-8*.

A shift of the  $\zeta$ -Potential to more positive values of about +5 mV is appreciable increasing the mixing time from 20 min up to 3 h. This effect suggests a possible leaching of  $Mg^{2+}$  ions, which turn the  $\zeta$ -potential of the fibers into more positive values.

As explained in Chapter 1 Paragraph 4.1, the colloidal stability of dispersions depends on the presence of ions in solution.<sup>9</sup> Since it has already been reported that a small amount of  $Mg^{2+}$  ions are released when Sep is dispersed in water,<sup>10</sup> we evaluated the leaching of  $Mg^{2+}$  ions after dispersion of Sep fibers in aqueous medium and its effect on the stability.

For this, the leaching of magnesium is evaluated as a function of mixing by means of Inductively Coupled Plasma Optical Emission Spectrometry (ICP-OES) (*Table 3-3*). Capillary Electrophoresis (CE) analysis has been performed in order to



confirm the presence of magnesium cations, not coordinated in chemical molecules, such as  $\text{Mg}(\text{OH})_2$ .

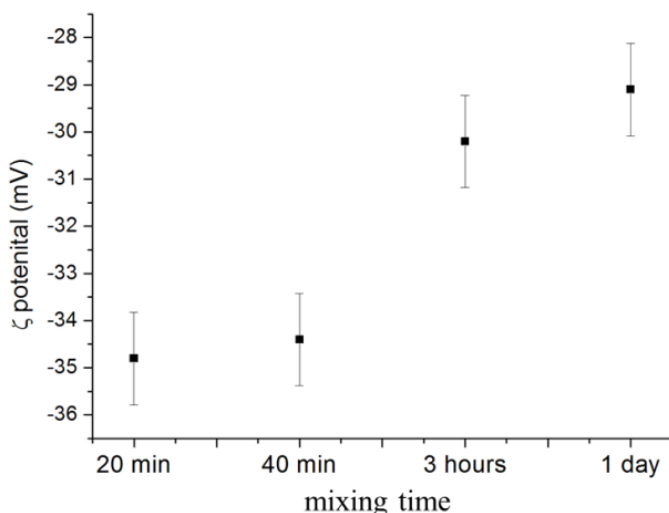


Figure 3-8.  $\zeta$ -Potential of SepS9 after 20 min, 40 min, 3 h and 24 h of mixing.

Table 3-3.  $\text{Mg}^{2+}$  amount released at different mixing time of SepS9 dispersion.

	ICP-OES ( $\text{mgL}^{-1}$ )	CE ( $\text{mgL}^{-1}$ )
20 min	3.07	3.23
1 day	4.69	4.13

As expected, the results show that the concentration of  $\text{Mg}^{2+}$  released in solution is very low but not negligible.

The  $\text{Mg}^{2+}$  ions once released in the water environment will adsorb onto particles surface and take part in determining the electric double layer of all the particles present in the dispersion and, thus, may affect the stability of the colloids.

In the NRL, the addition of ammonia has the effect of inhibiting bacteria action arising from neutral pH condition, hydrolyzing fatty acid and proteins which stabilize the emulsified polymer. On the other hand, Sep has a specific affinity for ammonia to the point that Sep and similar clays seems to be efficient material for the removal of  $\text{NH}_4^+$  from drinking water and wastewater.<sup>11</sup> On this basis, ammonium adsorption on SepS9 has been determined using the Nessler method.<sup>12</sup>

The corresponding kinetic data for SepS9 are depicted in Figure 3-9. The adsorption of  $\text{NH}_4^+$  and the contemporary release of  $\text{Mg}^{2+}$  ions has the effect of

increasing the ionic strength of the solution because of the substitution of ions with single positive charge and higher dimension with smaller ions with a double positive charge. Although the amount of ions taken in consideration is low, this mutual effect may alter the stability of the dispersion.

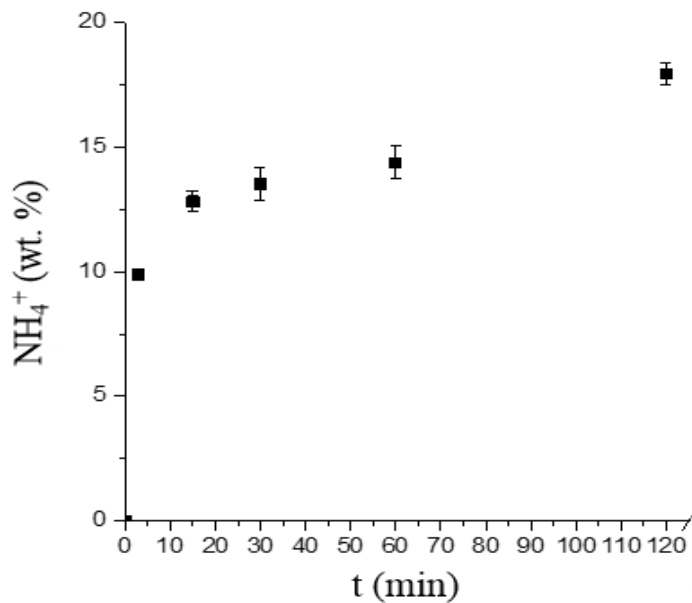
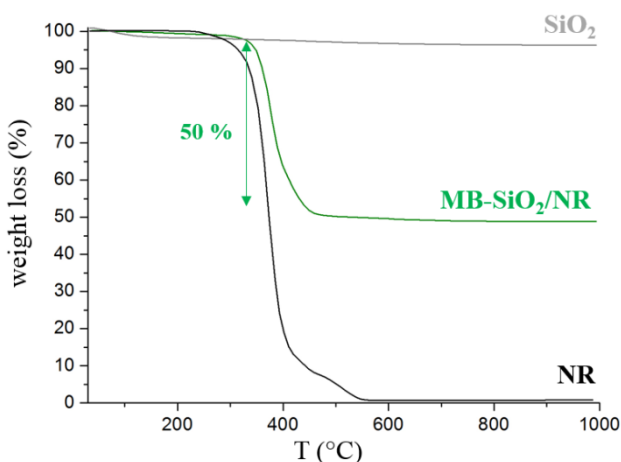


Figure 3-9. The amount of ammonium ions physi/chemisorbed onto SepS9 fibers as function of mixing time.

## 3.2 Thermal, spectroscopic and morphological characterization of filler/NR masterbatches

### 3.2.1 SiO<sub>2</sub>/NR masterbatch

The amount of SiO<sub>2</sub> particles in MB is evaluated by TGA analysis (*Figure 3-10*). In detail, MB-SiO<sub>2</sub>/NR displays a slight weight loss (~1 wt. %) at 100 °C attributed to physisorbed water, while a major weight loss is detectable from 300 to 500 °C, due to thermal degradation of the rubber component. The total amount of SiO<sub>2</sub> in MB thus matches with the remaining weight percentage at the end of the thermal evolution, and corresponds to 50 % wt. The total amount of SiO<sub>2</sub> is evaluated by the net weight loss of MB-SiO<sub>2</sub>/NR (green line in *Figure 3-10*) between 200 °C and 1000 °C. The filler weight loss (gray line) is subtracted from the total weight loss of MB-SiO<sub>2</sub>/NR, considering that rubber will be completely degraded at 1000 °C (black line).



*Figure 3-10.* TGA curves of NR (black line), SiO<sub>2</sub> (grey line) and MB-SiO<sub>2</sub>/NR (green line).

ATR-FTIR spectrum of MB-SiO<sub>2</sub>/NR (*Figure 3-11*) has been collected and compared to those of pristine NR (black line) and SiO<sub>2</sub> particles (gray line), already described in the Chapter 2 Paragraph 1.

The spectrum shows the peaks characteristics of both pristine materials: the asymmetric stretching vibrations of Si–O–Si in the 1090–1070 cm<sup>-1</sup> region, the corresponding symmetric stretching vibration at 800 cm<sup>-1</sup>,<sup>13</sup> the bands in the 3100–2850 cm<sup>-1</sup> region due to the stretching of C–H bonds of NR and those in the 1600–1350 cm<sup>-1</sup> range, attributed to the stretching of C–C bonds and bending of C–H bonds; the C–H out-of-plane bending typical of the poly(1,4-cis-isoprene) chains at 840 cm<sup>-1</sup>; and the bands typical of non-rubber components, such as those of NH

groups of amines ( $3283\text{ cm}^{-1}$ ), carbonyl groups of esters ( $1748\text{-}1738\text{ cm}^{-1}$ ), carboxylic acids ( $1711\text{ cm}^{-1}$ ), and amides ( $1630$  and  $1541\text{ cm}^{-1}$ ).

It is worthy to note that the stretching vibration of Si-OH at  $950\text{ cm}^{-1}$  in MB-SiO<sub>2</sub>/NR resulted slightly shifted to higher wavenumbers (selected green region in *Figure 3-11*), suggesting an interfacial interaction occurring between silica and NR. This interaction may be caused by physical adsorption of polymer polar or non-polar components present in NR onto SiO<sub>2</sub> surface.<sup>14</sup>

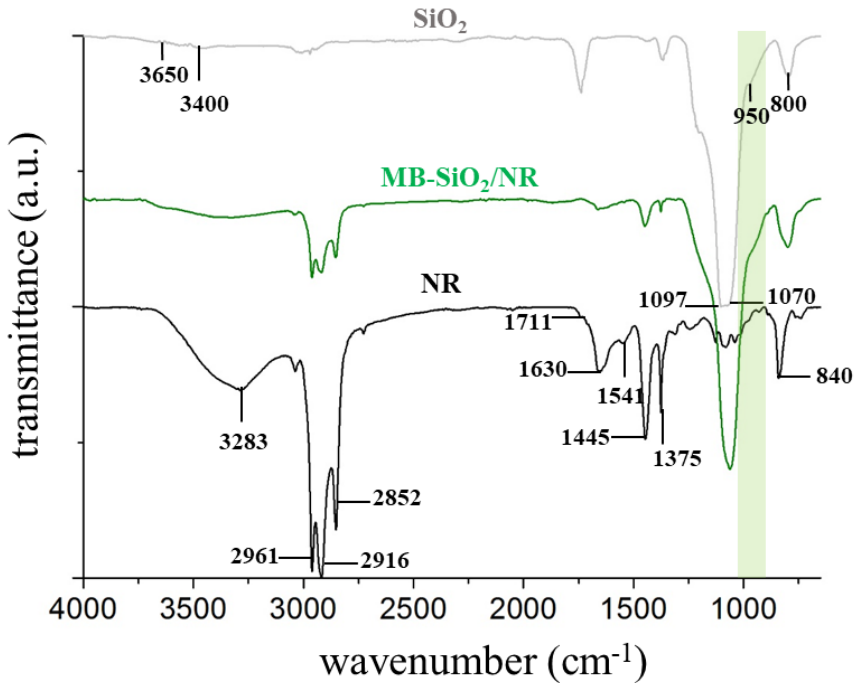


*Figure 3-11. FTIR spectra of NR (black line), SiO<sub>2</sub> (gray line), MB-SiO<sub>2</sub>/NR (green line). The light green shadow area highlights the most significant spectral regions.*

SEM micrographs of MB-SiO<sub>2</sub>/NR (*Figure 3-12*) reveals an homogeneous material with a good distribution of SiO<sub>2</sub> through the polymer matrix, as assessed by Si elemental mapping Energy Dispersive X-ray Analysis (EDX). Phase separation or large filler agglomerates are not detectable.

The X-Ray Diffraction (XRD) pattern of MB-SiO<sub>2</sub>/NR has not been analyzed because of the amorphous nature of SiO<sub>2</sub>.

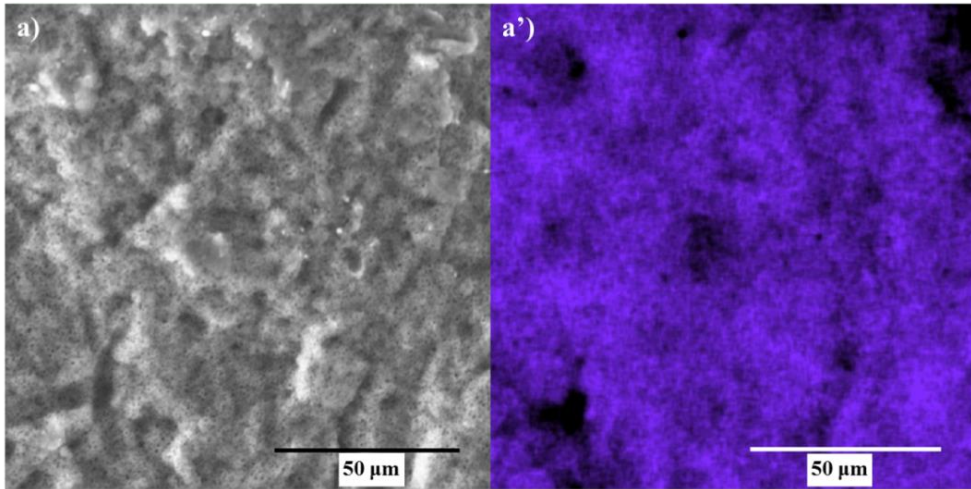


Figure 3-12. SEM micrographs of (a) MB- SiO<sub>2</sub>/NR and (a') the silicon-mapping performed by EDX on MB- SiO<sub>2</sub>/NR.

The silica MB morphology has been characterized by Small-angle X-ray Scattering (SAXS) analysis. Scattering curve of silica particles and the corresponding fitting curve are shown in *Figure 3-13 a*.

In detail, to estimate the silica particles size and their packing, the Percus-Yevick model<sup>15</sup> is applied (*Figure 3-13 b*). This model is made for hard-spheres with surface adhesion and is usually applied in low ordered porous polydispersed systems. The MB-SiO<sub>2</sub>/NR at different loading of silica (9, 23, and 50%) are analysed and fitted (*Figure 3-14 a*) through a model without a lattice, thus avoiding to take into account any structure factor. In *Table 3-4* we report the particle size obtained by the fitting of the curves.

In the case of the bare silica particles, the radius of the sphere in the aqueous dispersion ( $R_{\text{sphere}}$  in *Table 3-4*) is in good agreement with the specification of the commercial product (radius= 11 nm). The radius of the particles in a low ordered packing ( $R_{\text{effective}}$  *Table 3-4*), calculated on the basis of Percus-Yevick model, is higher than the  $R_{\text{sphere}}$  value.

Comparing these data with the higher value of  $R_{\text{sphere}}$  calculated for the MB (15 nm), we may hypothesize the formation of a polymer shell (4 nm) tightly bound to the silica particle.<sup>16</sup> This effect is visible for all MB-SiO<sub>2</sub>/NR at different silica loading, but we show the fitting of just one curve to be concise (*Figure 3-14 b*). *Figure 3-14 a* shows an increase of the intensity the higher the filler loading. This is due to the fact that the scattering intensity is proportional to the relative amount of interface. At small  $q$  it is possible to see different slopes of the curves. At these angles we may appreciate effects given by the structure factor and related to the different arrangements of particles.

Table 3-4. SAXS fitting parameters.

SiO <sub>2</sub>	MB-SiO <sub>2</sub> /NR
R <sub>shpere</sub> = 9.16 nm	R <sub>shpere</sub> = 15.0 nm
R <sub>effective</sub> = 13.9 nm	No lattice

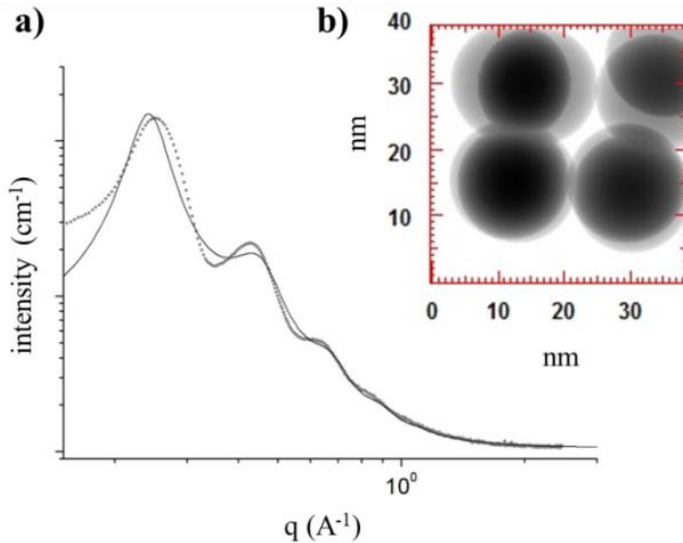


Figure 3-13. a) Scattering curves of silica particles (dotted line) and relative fitting (black line) b) model packing of silica particles through Percus-Yevick model.

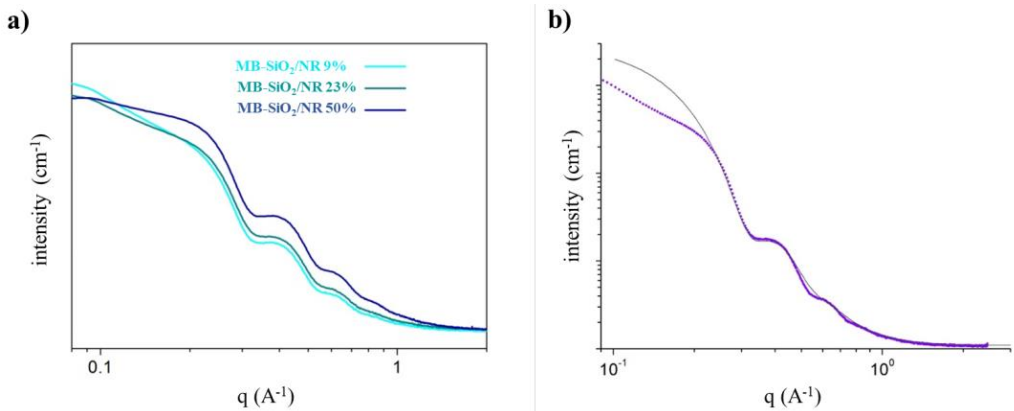
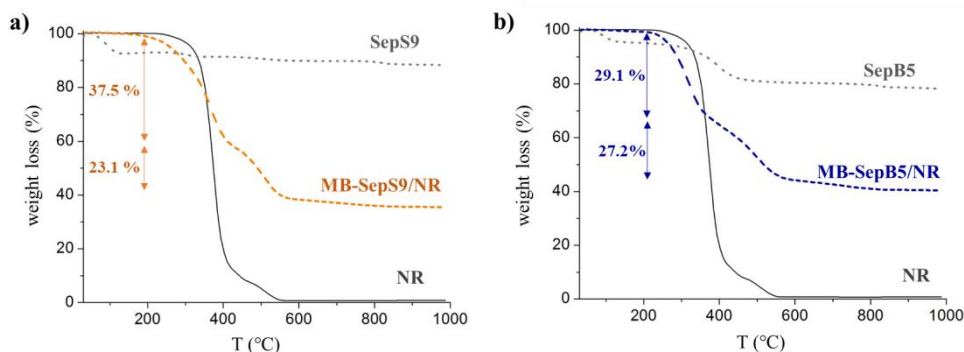


Figure 3-14. Scattering curves of a) MB-SiO<sub>2</sub>/NR with 10 phr of silica (light blue line), 30 phr (green line), 100 phr (blue line) b) MB-SiO<sub>2</sub>/NR with 30 phr of silica (dashed purple line) and its fitting.

## 3.2.2 SepX/NR masterbatch

The loading of Sep fibers in MB has been evaluated by TGA analysis (*Figure 3-15*). In detail, MB-SepX/NR display a slight weight loss ( $\sim 1$  wt. %) at 100 °C attributed to physisorbed water, while a major weight loss is detectable from 300 to 500 °C, due to thermal degradation of the rubber components and to the Sep organo-modifiers, when present (*Figure 3-15 b*).<sup>17</sup> The total amount of SepX fibers of in MB thus matches with the remaining weight percentages at the end of the thermal evolution, and corresponds to 45 and 50 wt. % for SepS9 and SepB5, respectively.



*Figure 3-15 TGA curves of: (a) NR (continuous black line), SepS9 (grey dotted line), MB-SepS9/NR (orange dashed line); and (b) NR (continuous black line), SepB5 (grey dotted line), MB-SepB5/NR (blue dashed line).*

The total amount of Sep has been evaluated by the net weight loss of MB-Sep/NR (dashed colored lines) between 200 °C and 1000 °C. In detail, the filler weight loss (dot grey lines) is subtracted from the total weight loss of MB, considering that rubber will be completely degraded at 1000 °C.

The crystalline structure of Sep fibers inside the MB-SepX/NR is confirmed by XRD.

The XRD pattern of MB-Sep/NR are shown in comparison to that of the fillers in *Figure 3-16*. Both MB-SepS9/NR (orange line) and MB-SepB5/NR (blue line) show distinct diffraction peaks, corresponding to the Sep fibers, confirming that the coagulation process do not alter the Sep crystalline structure. In fact, the diffractograms of the MBs are strictly comparable to those of the pristine Sep (black lines).<sup>18</sup> Only small changes in relative intensity and width of the reflections of Sep samples are observed. It is possible to notice a small shift of the (110) peak to smaller angles in Sep/NR masterbatches. Unlike smectite clays, sepiolite exhibits a structure where tetrahedral and octahedral layers are covalently bound. Therefore, even at highly exfoliated fibrous crystals of sepiolite, the diffraction peak (110) is hardly displaced. Small variations in the XRD pattern could suggest a certain degree of interaction of Sep with the rubber chains indicating the intimate Sep/NR contact.<sup>19</sup>

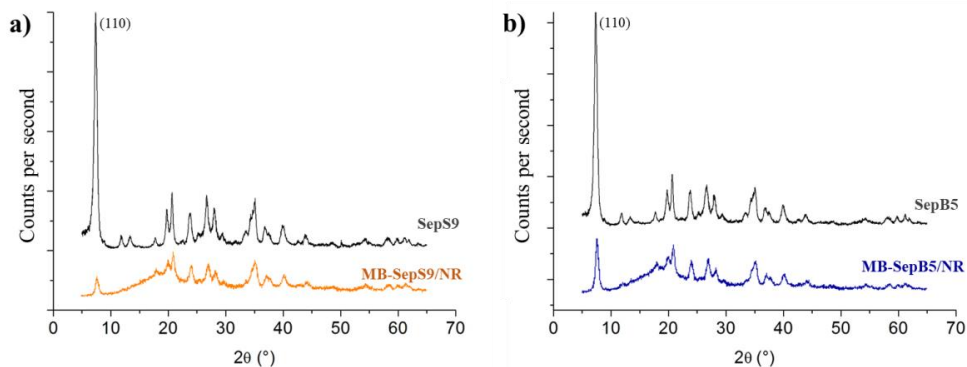


Figure 3-16 XRD patterns of (a) SepS9 (black line) and the corresponding MB-SepS9/NR (orange line), and of (b) SepB5 (black line) and the corresponding MB-SepB5/NR (blue line).

The ATR-FTIR spectra of MB-SepX/NR have been collected and compared to those of pristine NR and Sep fibers (Figure 3-17), in order to highlight the occurrence of potential interactions between Sep surfaces and NR matrix. The characteristic peaks of pristine NR (black line) and SepX fibers (grey line Figure 3-17 a,b), already described in the Chapter 2 Paragraph 1 are present in both MB-SepX/NR spectra. The SepX spectra evidences the adsorption bands at  $3700\text{--}3555\text{ cm}^{-1}$ , attributable to O-H bounded to octahedral magnesium centers stretching vibrations of groups and water molecules, and at  $692\text{ cm}^{-1}$ , attributable to the Mg-O-H bending vibrations. The bands at  $1209$  and  $1005\text{ cm}^{-1}$  are due to the Si-O stretching of tetrahedral sheets and the peak at  $795\text{ cm}^{-1}$  to Si-OH stretching vibrations. As previously mentioned for MB-SiO<sub>2</sub>/NR, the stretching vibration of Si-OH in both MB-SepX/NR, compared to pristine SepX, resulted slightly shifted to higher wavenumbers (selected green region in Figure 3-17 a and b), suggesting an interfacial interaction occurring between Sep and NR. Polar or non-polar components which are present in NR may be physically adsorbed onto Sep surface by polar interactions and cause the shift of peaks relative to silanols.<sup>14</sup> The decrease of intensity of amide stretching bands at  $1541\text{ cm}^{-1}$  (selected violet region in Figure 3-17 a and b) may be due to the occurrence of intermolecular hydrogen bonds between protein molecules in NR and silanol groups of Sep.<sup>20</sup> The interaction between non-rubber components in NR, such as lipids and proteins, and silanol functional groups on Sep surface is known to be relevant in the enhancement of the filler-rubber compatibilization. Protein and phospholipids were found to help in the hydrophobation of the silica surface as reported by Sarkawi.<sup>20</sup> The higher affinity between filler and rubber increases the homogeneous dispersion of silica-based fillers in NR. In Figure 3-18 is reported a schematic representation of possible H-bonding between silanol groups of hydrophilic fillers and functional groups of proteins.



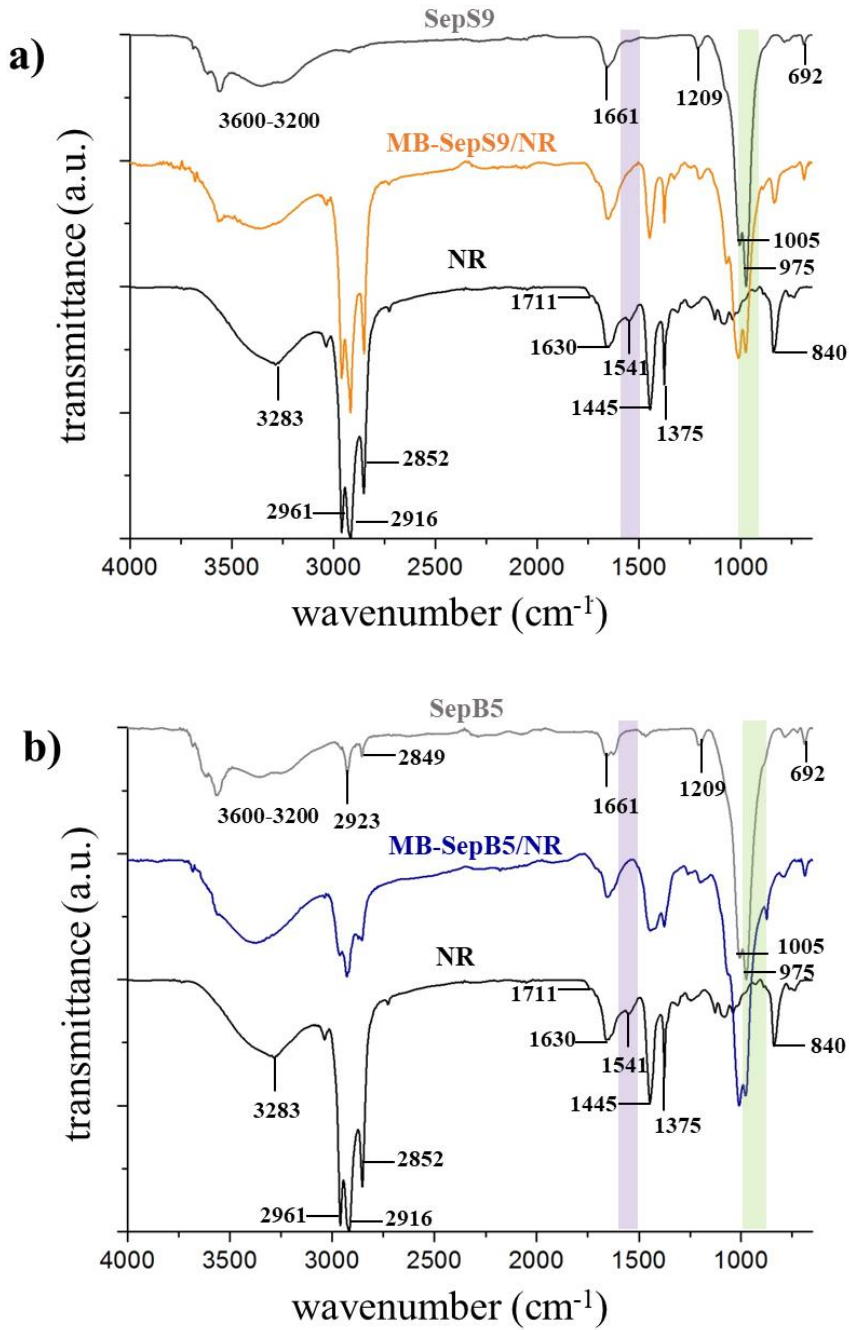


Figure 3-17. FTIR spectra of a) NR (black line), SepS9 (gray line), MB-SepS9/NR (orange line), b) NR (black line), SepB5 (gray line), MB-SepB5/NR (blue line). The light green and violet shadow areas highlight the most significant spectral regions.

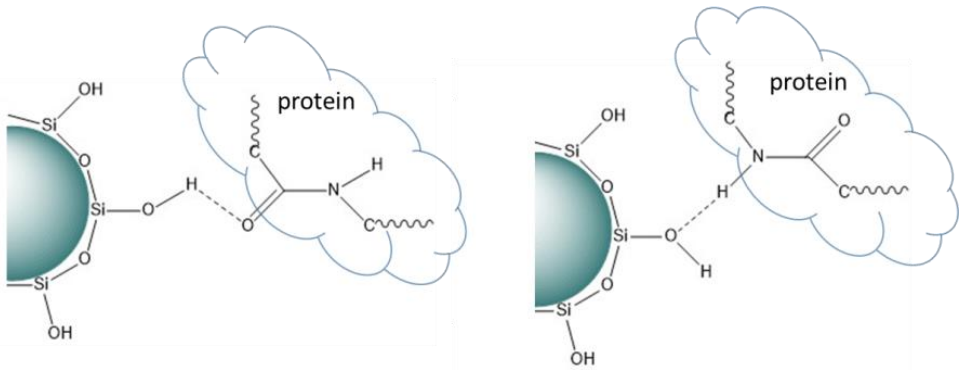


Figure 3-18. Illustration of possible interactions between silanol groups of silica and proteins in natural rubber via hydrogen bonding with functional group: right) amino group, left) carboxyl group.

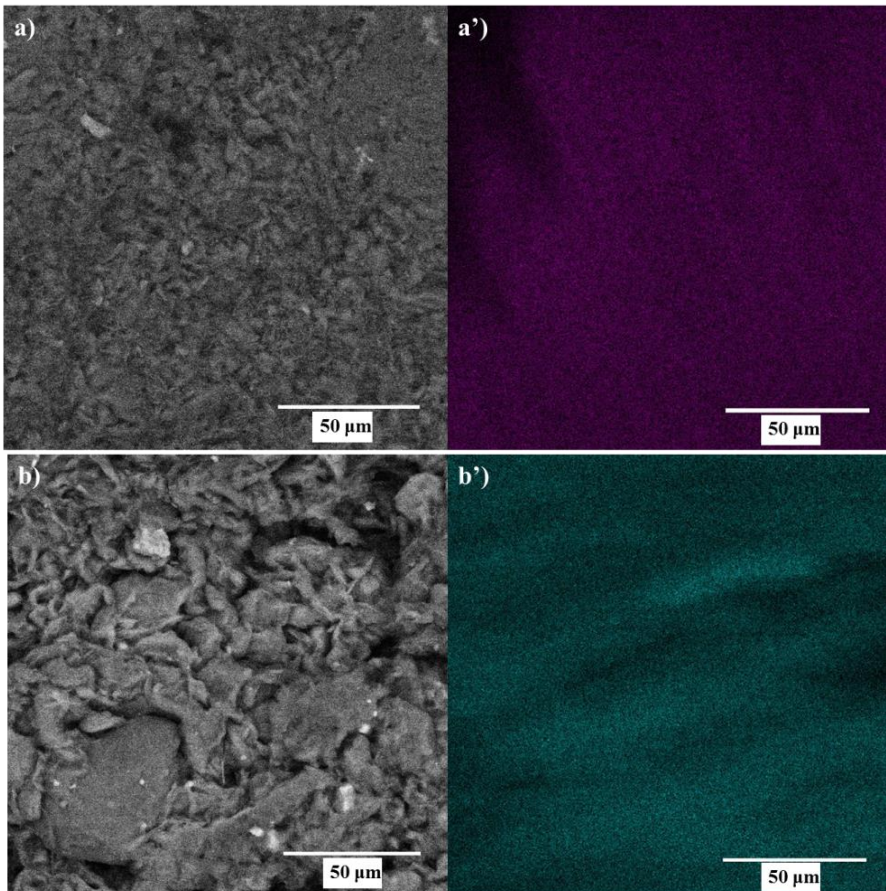
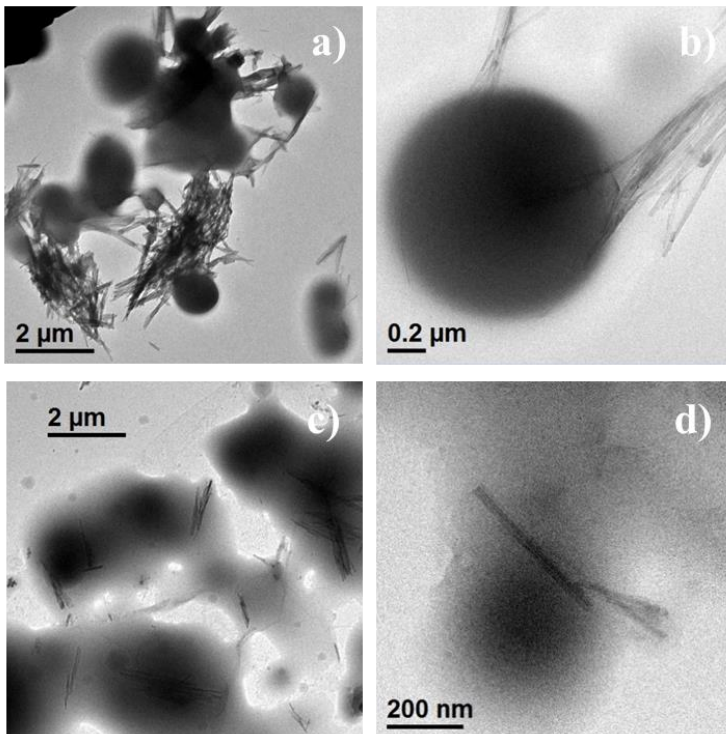


Figure 3-19. SEM micrographs of (a) MB-SepS9/NR and (b) MB-SepB5/NR and the corresponding silicon-mapping performed by EDX on (a') MB-SepS9/NR and (b') MB-SepB5/NR.

SEM micrographs (*Figure 3-19*) reveal a very good distribution of SepX through the NR matrix without any phase separation, thus supporting the formation of homogeneous MB-SepX/NR composites. The absence of fibers agglomerates have been assessed by Si elemental mapping.

Performing TEM analysis during the flocculation process, we managed to gain additional informations on the possible interaction between Sep surfaces and NRL. During the initial steps of mixing, i.e. before flocculation starting, TEM images revealed the presence of small filler aggregates which lie among or in the periphery of the rubber micelles, indicating poor surface-mediated interactions between SepS9 and (Figure 3-20 a, b). Homo-aggregated spherical NRL micelles<sup>21</sup> embedding some SepB5 fibers, some of which organized in bundles (Figure 3-20 c, d), are visible instead in SepB5/NR system. These images support the existence of weak attractive interactions between SepB5 and NRL, which may favour the adsorption of polymer chains onto Sep surfaces. These results seem to support the FTIR findings, suggesting the occurrence of interactions among filler and rubber components.



*Figure 3-20. TEM images at different magnifications of dilute dispersions of SepX in NRL allowed to dry on a carbon-coated TEM grid: (a, b) SepS9/NR and (c, d) SepB5/NR colloidal systems.*

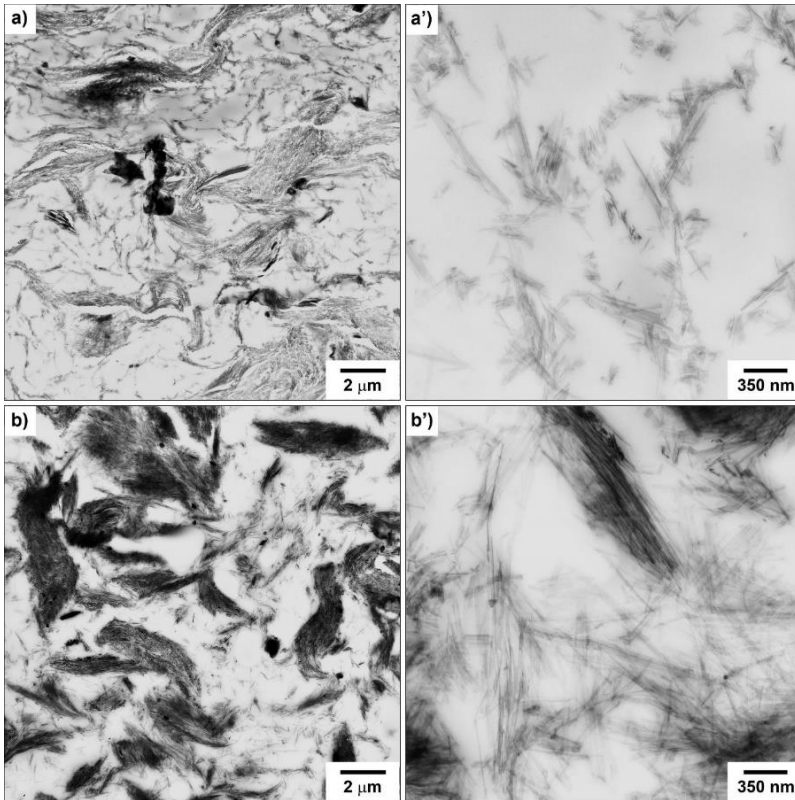


Figure 3-21. TEM micrographs at different magnifications of (a, a') MB-SepS9/NR and (b, b') MB-SepB5/NR.

TEM images collected on MB-SepX/NR, i.e. after the flocculation process, are shown in *Figure 3-21*. A percolative network, made of interconnected and partially oriented Sep fibers domains which extends through the whole polymer matrix, is detectable *Figure 3-21 a, b*). The alignment may be connected to the significant interface interaction of the anisotropic Sep fibers which leads to their preferential orientation along the main axis. In detail, MB-SepS9/NR show aggregates with cross-section of  $\sim 100$  nm, which are poorly compact and separated by small NR regions (*Figure 3-21 a'*). MB-SepB5/NR presents instead larger SepB5 domains with cross-section  $\sim 400$  nm and constituted by highly interconnected Sep particles bridged by much thinner rubber layers (*Figure 3-21 b'*).

The occurrence of weak attractive interactions between SepB5 and NRL, instead less pronounced in the SepS9/NR system, are confirmed by these results. Because of the good dispersion and of the filler-polymer interactions, improved mechanical properties are expected.

The MB-SepX/NR have been analyzed by SAXS with the aim to characterize in depth the nanostructure of NR, Sep, and their assembly in the final composites. The obtained scattering curves are shown in *Figure 3-22*. The typical reflections of

the orthorhombic unit cell of NR are observed in the SAXS pattern of NR (*Figure 3-22 a*) at high scattering vectors ( $q > 10^{-1} \text{ \AA}^{-1}$ ).<sup>22</sup> The remaining part of the curve can be described combining the scattering from aggregates<sup>23</sup> with the Debye approximation,<sup>24</sup> as already proposed by Karino and coworkers.<sup>25</sup> The signal centered at  $q$  values around  $10^{-2} \text{ \AA}^{-1}$  indicates the presence of 19 nm scattering bodies, probably ascribable to the crystalline domains in the rubber. At lower  $q$  the power law decay of -3.8 refers to interparticle scattering originated by micrometer sized particles with rough surface. There is a close similarity between the SAXS curves of the different Sep fillers (dark grey lines in *Figure 3-22 a* and *b*). Just one peak can be detected at  $q = 0.5 \text{ \AA}^{-1}$ , which is relatable to the channel structure of the fillers.<sup>26</sup> By means of the Guinier approach (*Figure 3-23* and *Table 3-5*), the scattering of the Sep fibers has been analysed assuming a rod-like form factor.

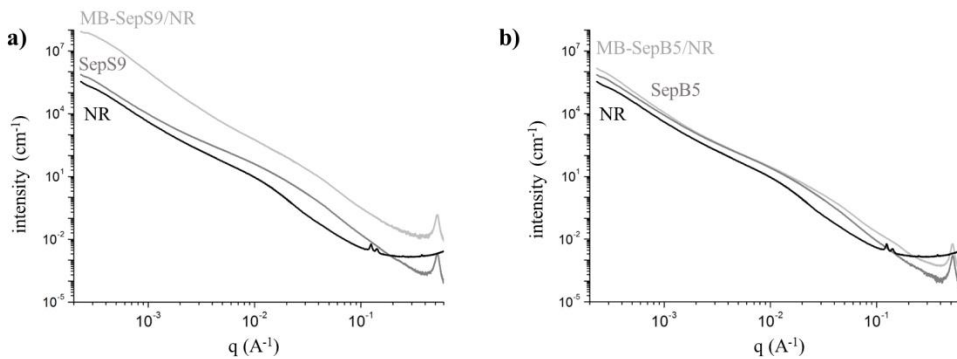


*Figure 3-22* Scattering curves of a) NR (black line), SepS9 (dark gray), MB-SepS9/NR (light gray), b) NR (black line), SepB5 (dark gray), MB-SepB5/NR (light gray).

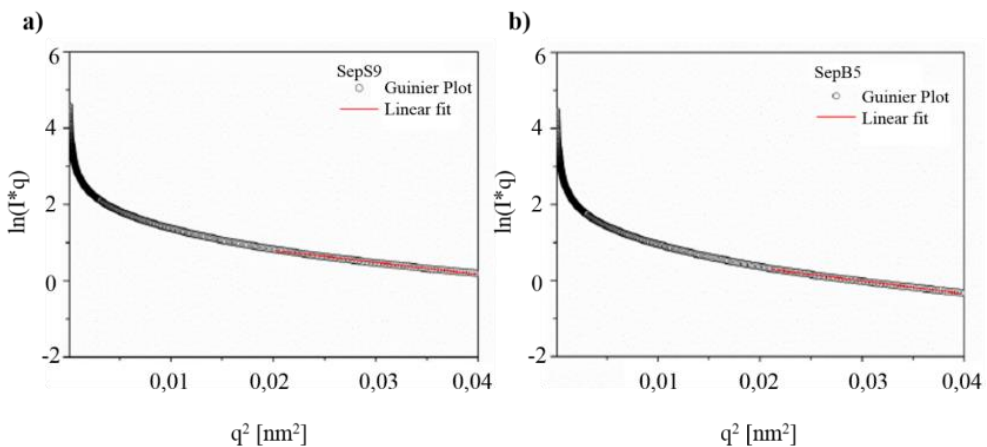


*Figure 3-23.* Guinier plot (circles) and liner fit (red line) of a) SepS9 and b) SepB5.

Table 3-5. Parameters of the Guinier analysis of the SepX SAXS curves.

	Slope (nm)	Rg (nm)	R (nm)
<i>SepS9</i>	31	7.9	11
<i>SepB5</i>	33	8.1	11.5

From the intermediate part of the curve the fibers radii of are estimated as 11.5 nm and 11 nm for B5 and S9 samples, respectively, in good agreement with the SEM and TEM analyses. In principle, this approach allows also the determination of the length of the scattering bodies, but this parameter can only be assessed if the forward scattering at very low  $q$  vectors is visible. Therefore, since the Sep fibers form bundle-like aggregates (steep power law at  $q < 0.002 \text{ \AA}^{-1}$ ), only the radii of the fibers, from the intermediate part of the curve, can be determined.

Regarding the MB-SepX/NR samples (light grey lines), the peak at  $q = 0.5 \text{ \AA}^{-1}$  indicates that the filler is incorporated in the Sep/NR material. The patterns show a different course with respect to the curves of the single systems, particularly in the MB-SepS9/NR small scattering vectors. The higher scattering intensity is directly related with an enhancement of the interface area between the SepS9 fibers, thus suggesting that these inorganic fillers are much more homogeneously distributed in the polymer than SepB5. This is supported by the TEM results. The disappearance in the MB-SepS9/NR of the signals at approx.  $q = 10^{-1} \text{ \AA}^{-1}$  in the NR curve, proper of the crystalline domain of the rubber is not so evident in the MB-SepB5/NR. This result supports also the difference in the filler distribution between the two systems. The analysis may suggest that polymer chains unfold much better in the presence of SepS9 that with SepB5, further showing that weak interactions are established between organic and inorganic components.

In summary, the combined SAXS-TEM approach seems to support the formation of different structural arrangement depending on the filler type used.

In particular, the presence of a polymer shell tightly bounded to the surface in the case of MB-SiO<sub>2</sub>/NR and the increase of intensity of MB-SepS9/NR with respect to MB-SepB5/NR, support the idea that LCT is a suitable and green approach able to highly disperse hydrophilic particles in hydrophobic matrices, thanks to the use of water dispersions.

### 3.3 Dynamic-mechanical properties of MB-SepX/NR

MB-SepX/NR have been characterized in the dynamic-mechanical behaviour and compared to reference composite (REF-SepX/NR), with the same filler content and obtained by conventional blending technique. The percolated solid phase of filler particles embedded in a polymer matrix which make the filler network is evaluated by strain sweep. The measurement is carried out at 100°C until large

deformations. The results are shown in terms of storage ( $G'$ ) and loss moduli ( $G''$ ), for both SepS9 (Figure 3-24 a) and SepB5 (Figure 3-24 b) fillers.

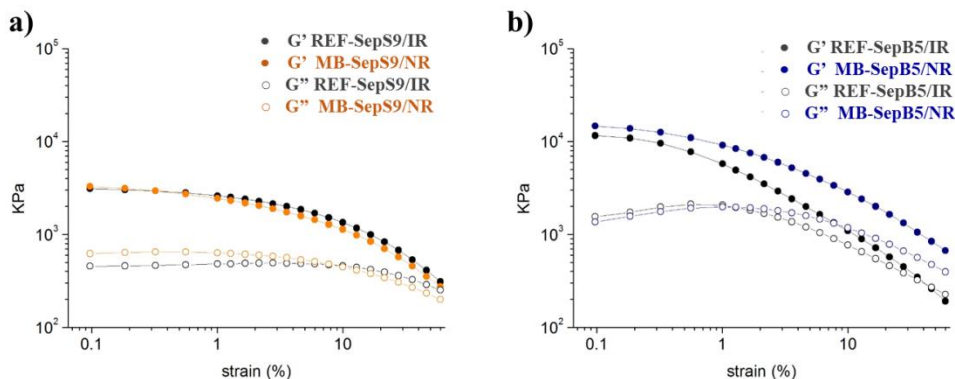


Figure 3-24. Storage modulus  $G'$  (plain circle lines) and loss modulus  $G''$  (empty circle lines) vs strain for a) MB-SepS9/NR (orange lines), REF-SepS9/NR nanocomposite (black lines) and for b) MB-SepB5/NR (blue lines), REF-SepB5/NR (black lines).

The storage modulus  $G'$  decreases with increasing amplitude from 0.01 to 60% in all uncured samples. From low strain to high strain values, the short-distance forces between filler particles decrease strongly and affect  $G'$ . This effect is commonly related to the filler-filler network breakdown (Payne Effect)<sup>27</sup>. The Payne Effect is known to be dependent only from the filler-filler network and independent from the other factors affecting the whole composite reinforcement. Thus, it is sensitive to the dispersion of the filler in the polymer matrix.

The strain sweep of MB-SepS9/NR and REF-Sep9/NR show very similar results at both low and high strain (Figure 3-24 a). This suggests that the incorporation method poorly affects the filler-filler interactions.

A decrease in the Payne Effect is visible comparing MB-SepB5/NR to REF-SepB5/NR (Figure 3-24 b). This may be associated with the obtention of lower filler-filler network through LCT, with benefits of the filler-rubber interactions. So, in this case, the LCT seems to impact positively on the mechanical properties.<sup>28</sup>

A low Payne Effect is usually related to fast recovery of the filler network after a single large-amplitude deformation, as seen in both the cases of SepX. The high reinforcement with low Payne Effect must have a correlation with the peculiar self-assembly and alignment of Sep fibers, which improve their interfacial interaction with rubber.

The energy dissipation during deformation is commonly related to the loss modulus ( $G''$ ).  $G''$  is also associated with the breakage and rebuilding of filler-filler network and slippage of the polymer chains. Thus  $G''$  gives an effective quantification of the viscous behaviour of a nanocomposite. In the MB-SepX/NR

and REF-SepX/NR, the energy dissipation processes seem to be quite similar from the  $G''$  behaviour.

Like the storage modulus,  $G''$  decreases at high strain amplitudes, but MBs enclosing Sep fibers show only a moderate decay of  $G''$ . The aforementioned Sep rubber interactions, which hinder the slippage of the macromolecular chains, may be relevant in the lowering of the  $G''$  decay.

Moreover, the maximum peak in  $G''$  curves is slightly broaden and shifted to the higher strain amplitude for MB-SepX/NR in comparison with reference materials, suggesting that the filler network stability during the strain sweep is improved by LTC.<sup>29</sup>

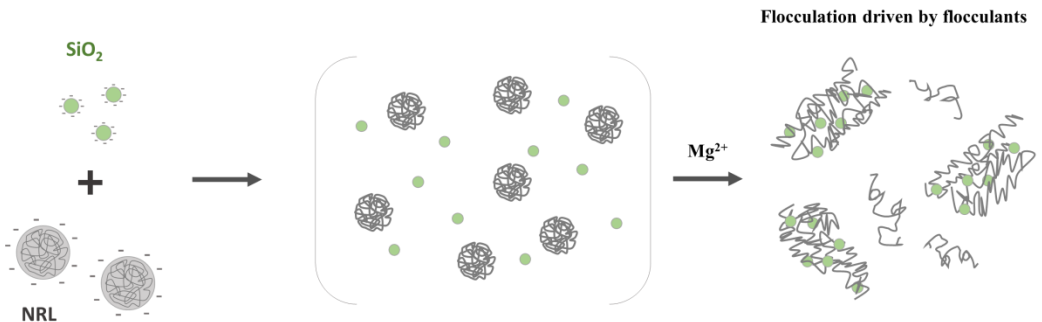
### 3.4 Discussions on flocculation mechanisms

Based on the above characterizations, a flocculation mechanism is proposed for each analysed system.

In a general case, to induce flocculation in aqueous dispersions of polymer lattices and inorganic particles which do not have particular affinity or destabilizing charge interactions, the use of electrolytes as suitable coagulating agents it is required in order to produce filler-rubber MBs. Usually in LCT these species are inorganic salts or acids.

In the case of  $\text{SiO}_2$ /NRL system, when magnesium nitrate is added to the  $\text{SiO}_2$ /NRL dispersion, coagulation suddenly occurs.  $\text{Mg}^{2+}$  ions, having a relatively high charge/radius ratio, screen the electric double layer on the NRL and  $\text{SiO}_2$  particles, thus determining the flocculation of the system (*Scheme 3-1*).

The peculiarity of the SepX/NRL system is that the flocculation occurs in the absence of any organic solvent, surfactant or flocculating agent. Considering this particular behaviour and the main physicochemical parameters, a flocculation mechanism characteristic of each Sep/NR system has been proposed (*Scheme 3-2*).



*Scheme 3-1. Flocculation mechanism of  $\text{SiO}_2$ /NRL system driven by magnesium nitrate.*



In the case of SepB5/NRL (*Scheme 3-2 a*), a mechanism simply based on charges neutralization can be inferred. In fact, at the working pH range (9-10),  $\zeta$ -potential of SepB5 and NRL displays an opposite sign, suggesting that repulsive forces between particles are overcome by attractive forces, thanks to the collision of particles by Brownian motions.<sup>30,31</sup> The progressive adsorption of polymer on SepB5 surface, lowers the free energy of interaction among the fibers, decreasing their distance and leading to flocculation. It must be observed that the proposed mechanism is active only at high SepB5 loading.<sup>32</sup>

These considerations are in agreement with the presence at the early stages of mixing of homo-aggregated NRL micelles embedding some SepB5 fibers (*Figure 3-20 c, d*) and also, in MB-SepB5/NR sample, of large domains constituted by aligned Sep fibers bridged by thin rubber layers (*Scheme 3-2, Figure 3-21 b'*).

In the case of the SepS9/NRL system, both the colloidal systems carry a negative surface charge at the working pH. Thus, flocculation cannot be explained simply referring to the  $\zeta$ -potential measurements. In fact, when a significant repulsive contribution to the inter-particle potential is present, experimental conditions other than surface charge should affect the flocculation process. Moreover, the quantification of ions exchange ( $Mg^{2+}$  and  $NH_4^+$ ) in a SepS9 dispersion does not suggest the occurrence of electrostatic screening of the electric double layer of NRL particles able to induce destabilization.

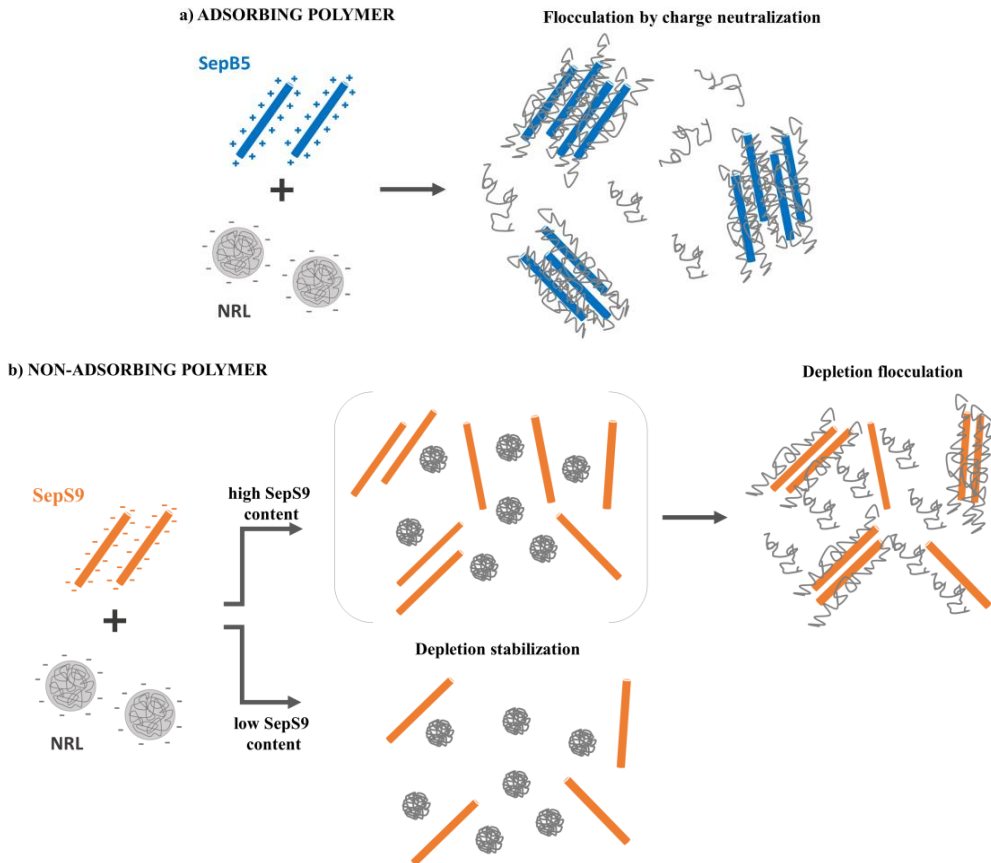
The flocculation of SepS9/NRL is observed only in the presence of the high loading of Sep fibers, while did not occur for more diluted colloid systems. This suggests that high filler content and a relatively low fraction of NR play a key role in promoting flocculation.

Attractions between colloidal particles can be conveniently induced by the addition of non-adsorbing polymers, due to the so-called depletion attraction.<sup>33,34</sup> The driving force of this phenomena lies in the existence of a "depletion zone", generated by the conformational entropic restrictions of the polymer coils. According to depletion flocculation, we can infer that in SepS9/NR system, because of the high filler loading, NR is pushed out from the region among the fibers, leading to a higher concentration of the polymer in the colloidal solution (*Scheme 3-2 b, top*). The difference in the osmotic pressure between these two regions results in the solvent flow out from the gap between Sep particles, inducing attractive forces which drive the flocculation. The hypothesis is supported by the fact that, at low SepS9 content flocculation does not take place, since the binary colloidal systems results sterically stabilized (*Scheme 3-2 b*).

These observations are in accordance with TEM investigation on Sep9/NR which, at the early stages of mixing, shows (*Figure 3-20 a, b*) that Sep bundles lies among or in the periphery of the rubber micelles indicating their poor interactions with NRL, while, after flocculation reveals (*Figure 3-21 a, a'*) the presence of poorly compact filler aggregates in the MB. Moreover, SAXS analysis also supports the

occurrence of weak interactions between the organic and inorganic components in Sep9/NR colloidal system, suggesting that, once in contact with the SepS9 fibers, the polymer chains unfold generating a continuous matrix.

Finally, it has to be mentioned that the efficacy of depletion forces is generally enhanced in the presence of colloidal particles with high AR, because they provide extensive and effective confinement regions.<sup>35–37</sup> This suggests a remarkable influence of Sep anisotropy on the flocculation process of Sep9/NR system, especially considering the comparison with SiO<sub>2</sub>.



*Scheme 3-2. Proposed mechanisms for the flocculation process in a) SepB5/NRL and b) SepS9/NRL systems.*

In summary, the flocculation process in Sep/NRL system can be ascribed to electrostatic or depletion attraction forces for SepB5 and SepS9, respectively. This is strongly connected both to the high filler content and to the peculiar anisotropic features of Sep fibers. While, in the case of SiO<sub>2</sub>/NRL, the absence of particular electrostatic or surface attractions requires the use of flocculants, inducing flocculation by double layer screening of particles by high charge to radius ratio ions.

### 3.5 Conclusions

The proposed LCT method promotes a homogeneous dispersion of hydrophilic Sep fibers in the rubber matrix, allowing the production of high-loaded Sep rubber composites.

The investigation of the flocculation process by TEM performed at the early stages of NRL/Sep dispersion destabilization reveals the production of SepB5-NRL contact between particles, probably induced by the presence of alkylammonium salt functionalities which promotes charge interactions in water, while SepS9 shows poorer interactions with NRL.

TEM analysis performed on MBs reveals the presence of large and compact filler domains constituted by aligned Sep fibers interconnected by rubber for SepB5/NR. SepS9 forms poorly tight filler aggregates in NR MBs indicating the occurrence of weaker interactions between the organic and inorganic components.

SAXS analysis supports these outcomes and points out that NRL, once in contact with the Sep fibers, unfold leading to the formation of a homogeneous materials.

These results allow us to propose a flocculation mechanism characteristic for both SepB5/NR and SepS9/NR systems, based on electrostatic and depletion attraction forces, respectively, and remarkably connected both to the high content (50 wt.%) and to the peculiar anisotropy of Sep fibers. Our results strengthen the idea that high AR rods are affected by depletion forces, respect to the isotropic silica spheres, and are suitable materials for the generation of soft matters.

The uniform Sep distribution in the rubber matrix, characteristic of the proposed LCT approach, and the percolative filler network formed give rise to comparable mechanical properties for SepX/NR MB, in comparison to those of analogous materials prepared by conventional melt blending technique.

## 3.6 Bibliography

- 1 J. Sansatsadeekul, J. Sakdapipanich and P. Rojruthai, *J. Biosci. Bioeng.*, 2011, **111**, 628–634.
- 2 J. B. Gomez and H. Samsidar, *J. Nat. Rubber Res.*, 1989, **4**, 75–85.
- 3 K. Nawamawat, J. T. Sakdapipanich, C. C. Ho, Y. Ma, J. Song and J. G. Vancso, *Colloids Surfaces A Physicochem. Eng. Asp.*, 2011, **390**, 157–166.
- 4 G. De Oliveira, P. Menut, F. Bonfils, L. Vaysse, Y. Hemar and C. Sanchez, *Colloids Surfaces A Physicochem. Eng. Asp.*, 2015, **482**, 9–17.
- 5 C. A. Hall, University of Manchester, 2010.
- 6 M. Alkan, G. Tekin and H. Namli, *Microporous Mesoporous Mater.*, 2005, **84**, 75–83.
- 7 E. A. Hauser, *Clays Clay Miner.*, 1954, **3**, 442–472.
- 8 M. Doğan, A. Türkyilmaz, M. Alkan and Ö. Demirbaş, *Desalination*, 2009, **238**, 257–270.
- 9 M. Kosmulski, *Colloids Surfaces A Physicochem. Eng. Asp.*, 2003, **222**, 113–118.
- 10 F. Wypych, in *Clay surfaces: fundamentals and applications*, Elsevier, 2004, p. 1.
- 11 M. Molina-Sabio, J. C. González and F. Rodríguez-Reinoso, *Carbon N. Y.*, 2004, **42**, 448–450.
- 12 M. S. Çelik, B. Özdemir, M. Turan, I. Koyuncu, G. Atesok and H. Z. Sarikaya, *Water Sci. Technol. Water Supply*, 1998, **1**, 81–88.
- 13 H.-T. Lu, *Colloid J.*, 2013, **75**, 311–318.
- 14 Z. Peng, L. X. Kong, S. D. Li, Y. Chen and M. F. Huang, *Compos. Sci. Technol.*, 2007, **67**, 3130–3139.
- 15 R. O. Watts, D. Henderson and R. J. Baxter, *Adv. Chem. Phys.*, 1971, **21**, 421.
- 16 G. P. Baeza, A. C. Genix, C. Degrandcourt, L. Petitjean, J. Gummel, M. Couty and J. Oberdisse, *Macromolecules*, 2013, **46**, 317–329.
- 17 C. Del Hoyo, C. Dorado, M. S. Rodríguez-Cruz and M. J. Sánchez-Martín, *J. Therm. Anal. Calorim.*, 2008, **94**, 227–234.
- 18 A. Yebra-Rodríguez, J. D. Martín-Ramos, F. Del Rey, C. Viseras and A. Lopez-Galindo, *Clay Miner.*, 2003, **38**, 353–360.
- 19 M. Soheilmoghaddam, M. U. Wahit, A. A. Yussuf, M. A. Al-Saleh and W. T. Whye, *Polym. Test.*, 2014, **33**, 121–130.
- 20 S. S. Sarkawi, W. K. Dierkes and J. W. M. Noordermeer, *Eur. Polym. J.*, 2013, **49**, 3199–3209.
- 21 L. F. Valadares, C. A. P. Leite and F. Galembeck, *Polymer (Guildf.)*, 2006, **47**, 672–678.
- 22 J. Che, C. Burger, S. Toki, L. Rong, B. S. Hsiao, S. Amnuaypornsrri and J. Sakdapipanich, *Macromolecules*, 2013, **46**, 9712–9721.
- 23 C. M. Sorensen, J. Cai and N. Lu, *Langmuir*, 1992, **8**, 2064–2069.
- 24 P. Debye, H. R. Anderson and H. Brumberger, *J. Appl. Phys.*, 1957, **28**, 679–

- 683.
- 25 T. Karino, Y. Ikeda, Y. Yasuda, S. Kohjiya and M. Shibayama, *Biomacromolecules*, 2007, **8**, 693–9.
- 26 R. E. Winans, S. Seifert and K. A. Carrado, *Chem. Mater.*, 2002, **14**, 739–742.
- 27 A. R. Payne, *J. Appl. Polym. Sci.*, 1962, **6**, 368–372.
- 28 M. J. Wang, *Rubber Chem. Technol.*, 1999, **72**, 430–448.
- 29 T. Xu, Z. Jia, J. Li, Y. Luo, D. Jia and Z. Peng, *Polym. Compos.*, 2018, **39**, 377–385.
- 30 W. B. Russel, D. A. Saville and W. R. Schowalter, *Colloidal dispersions*, Cambridge University Press, Cambridge, 1989.
- 31 R. J. Hunter, *Foundations of colloid science*, Oxford University Press, Oxford, 2001.
- 32 C. S. Lee, J. Robinson and M. F. Chong, *Process Saf. Environ. Prot.*, 2014, **92**, 489–508.
- 33 A. Vrij, *Pure Appl. Chem.*, 1976, **48**, 471–483.
- 34 S. Asakura and F. Oosawa, *J. Polym. Sci. Part A Polym. Chem.*, 1958, **48**, 471.
- 35 N. Yasarawan and J. S. Van Duijneveldt, *Soft Matter*, 2010, **6**, 353–362.
- 36 G. A. Vliegenthart, A. Van Blaaderen and H. N. W. Lekkerkerker, *Faraday Discuss.*, 1999, **112**, 173–182.
- 37 G. H. Koenderink, G. A. Vliegenthart, S. G. J. M. Kluijtmans, A. Van Blaaderen, A. P. Philipse and H. N. W. Lekkerkerker, *Langmuir*, 1999, **15**, 4693–4696.



## Chapter 4.

### Nanocomposite materials for tyre applications

Chapter 4 is focused on rubber nanocomposite materials, compounded with MBs prepared by LTC approach. Dynamic-mechanical analysis of composite materials has been performed in order to investigate filler-filler and filler-rubber interactions, in comparison with the reference composite materials obtained by conventional melt mixing procedure.





## 4.1 Mechanical properties of nanocomposite materials

Rubber nanocomposites containing silica and Sep fillers are prepared by combining latex compounding and melt mixing.

A highly filled NR MB, firstly prepared by co-coagulating of NR latex and silica-based filler aqueous suspension, is mixed with the NR rubber matrix together with silane, coupling agent, vulcanizing agents and antioxidants, as explained in Chapter 2 Paragraph 2.3.

LCT associated with melt mixing is a useful approach because: i) improves the hydrophilic filler dispersion, ii) prevents dust from floating in the air during processing in case of compounding filler with a high volatile component, iii) does not imply abrasion and scratching on mixing machines because the fillers are previously dispersed in NR MBs, iv) does not result in high processing temperatures because of the avoidance of severe friction between filler particles. Rheological and dynamic-mechanical analyses of cured and uncured rubber composites have been performed to evaluate the effect of combined techniques with respect to the traditional melt mixing.

Strain sweep tests of rubber samples, before and after the vulcanization, allow to evaluate the materials reinforcement and hysteretic properties.

### 4.1.1 Dynamic-mechanical analysis of cured and uncured nanocomposites prepared by MB-SiO<sub>2</sub>/NR

Curing profiles of uncured nanocomposites are measured by using an oscillating rotor in contact with the compound, which is kept at a given temperature. As vulcanization proceeds, the viscosity of the material increases. This effect is measured by the rise in the torque ( $S'$ ) needed to keep the amplitude of the oscillation constant. Since the measurement is carried out at high temperature, it is assumed that the viscous effect of the material is negligible and that the increase of the torque is proportional to the number of links per unit volume of rubber.

The vulcanization kinetic is usually evaluated by observing the increase of the  $S'$  as a function of time. *Figure 4-1* shows the vulcanization curve of nanocomposite materials compounded by the coupled approach LCT and melt mixing (namely NC(MB-SiO<sub>2</sub>/NR)) (green line) in comparison with the corresponding reference material compounded by melt mixing (namely REF-SiO<sub>2</sub>/NR) (black line).

The vulcanization has been performed at 170 °C for 10 min, corresponding to the stabilization of  $S'$  value and in line with the curing conditions reported for NR composites.<sup>1</sup> The results are of five replicated experiments. The rheometric characteristics of the nanocomposites, expressed in terms of the minimum torque ( $M_L$ ) and the maximum torque ( $M_H$ ) are reported in *Table 4-1*.

The minimum torque ( $M_L$ ) is defined as  $S'$  at the initial stage of vulcanization. It is related to viscosity and, therefore, to the dispersion of the uncured materials.  $M_L$

values of NC(MB-SiO<sub>2</sub>/NR) looks very similar to that of REF-SiO<sub>2</sub>/NR, suggesting similar viscosity. In addition, the incorporation of MB-SiO<sub>2</sub> in NR matrix gives satisfactory value of the maximum torque (M<sub>H</sub>), which is a measure of crosslink density and stiffness of the rubber. In particular, the enhanced M<sub>H</sub> of NC(MB-SiO<sub>2</sub>/NR) suggests excellent interaction between rubber and SiO<sub>2</sub>, introduced by using MB.

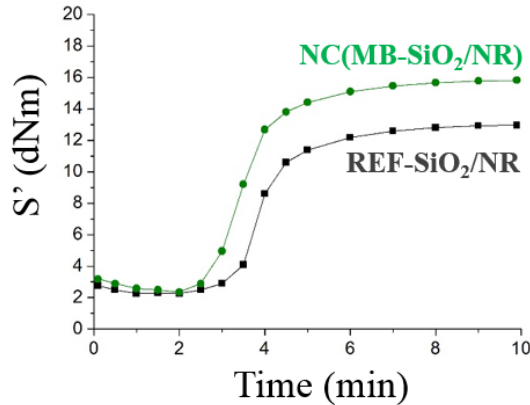


Figure 4-1. Vulcanization curve of NC(MB-SiO<sub>2</sub>/NR) (green line) and REF-SiO<sub>2</sub>/NR (black line).

Table 4-1. Curing characteristics of NC(MB-SiO<sub>2</sub>/NR) and REF-SiO<sub>2</sub>/NR.

	M <sub>L</sub> (dNm)	M <sub>H</sub> (dNm)	M <sub>H</sub> -M <sub>L</sub> (dNm)	scorch time (min)
NC(MB-SiO <sub>2</sub> /NR)	2.35	15.87	13.54	2.51
REF-SiO <sub>2</sub> /NR	2.27	12.95	10.68	2.97

NC(MB-SiO<sub>2</sub>/NR) shows the best interaction with the sulfur-based vulcanization compounds, leading to enhanced mechanical properties in the rubber composite. The presence of ammonium salts, eventually retained in the NR after coagulation, could favor a quicker and more efficient curing of sulfur-based rubber compositions.<sup>2</sup>

After evaluating the effectiveness of curing process, a detailed investigation of the dynamic-mechanical behavior of the composites is performed by RPA analysis, which allows to evaluate the reinforcement and energy dissipation.

The storage modulus (G') of the uncured and cured NC(MB-SiO<sub>2</sub>/NR) has been measured and compared with that obtained via traditional melt mixing (Figure 4-2). A pronounced nonlinear dependence of modulus (Payne effect<sup>3</sup>) is observed in both cases. In fact, the G' value at low strain (G'<sub>0</sub>) decreases rapidly by increasing the strain amplitude and G' value at high strain (G'<sub>∞</sub>) approaches the

lowest values.<sup>4</sup> RPA curves of uncured samples are almost coincident, indicating nearly equivalent filler network structures in the rubber matrix.

After curing (*Figure 4-2 b*), a remarkable increase of the modulus either at low or at high strain is observed for all the composites. In particular the highest  $G'_0$  and value was obtained for NC(MB-SiO<sub>2</sub>/NR), compared with REF-SiO<sub>2</sub>/NR composites. In any case, the composites containing MB-SiO<sub>2</sub>/NR display low decrease of modulus versus strain, that is low Payne effect. This suggests a strong immobilization of the polymer chains close to the silica surfaces or within their network, which increases the mechanical reinforcement of the composites. Evidently by applying LTC, the interaction of silica fillers with the polymer chains is efficient as well as the cross-linking coupling because of the high number of bonding sites (*Figure 4-2*).

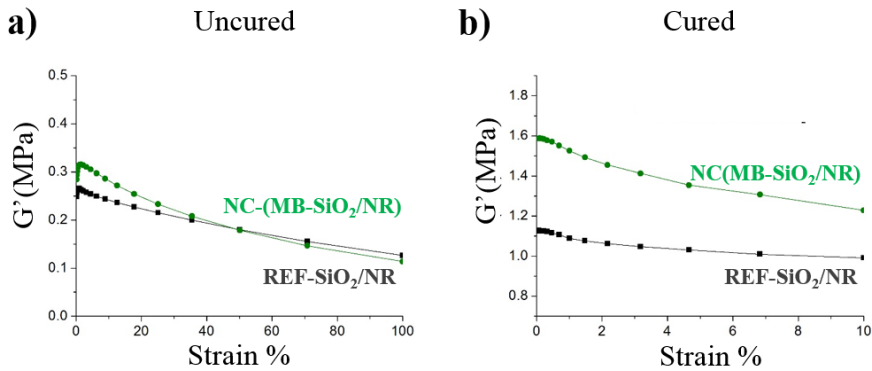


Figure 4-2. RPA analysis of a) uncured NC(MB-SiO<sub>2</sub>/NR) (green line) and REF-SiO<sub>2</sub>/NR (black line) and of b) cured samples NC(MB-SiO<sub>2</sub>/NR) (green line) and REF-SiO<sub>2</sub>/NR (black line).

Table 4-2. Storage modulus of cured and uncured samples of NC(MB-SiO<sub>2</sub>/NR) and REF-SiO<sub>2</sub>/NR.

	Uncured			Cured		
	$G'_{(1\%)}$ MPa	$G'_{(100\%)}$ MPa	$\Delta G'_{(1\%-100\%)}$ MPa	$G'_{(0.5\%)}$ MPa	$G'_{(9\%)}$ MPa	$\Delta G'_{(0.5\%-9\%)}$ MPa
NC(MB-SiO <sub>2</sub> /NR)	0.31	0.13	0.18	1.55	1.25	0.30
REF-SiO <sub>2</sub> /NR	0.26	0.11	0.15	1.08	0.99	0.09

To better understand the variation in mechanical properties we report the values of  $G'$  at high and low strain and  $\Delta(G'_0 - G'_\infty)$ , which represent respectively the measure of reinforcement and Payne effect in vulcanized rubbers (*Table 4-2*). For uncured samples these values give information on the filler dispersion.

The NC(MB-SiO<sub>2</sub>/NR) shows a higher G' value of about 0.5 MPa respect to the reference material at low strain and about of 0.3 MPa at high strain. The low Payne effect and the high G' value, together with high M<sub>H</sub> indicate a good quality of rubber composite obtained by LCT approach.

#### 4.1.2 Dynamic-mechanical analysis of cured and uncured nanocomposites prepared by MB-SepX/NR

Mechanical analysis of both SepS9 and SepB5 nanocomposite materials prepared by combining LCT and melt mixing (named: NC(MB-SepX/NR)) are performed and compared with those of reference materials compounded only by melt mixing (named: REF-SepX/NR).

The vulcanization curves of NC(MB-SepX/NR) are reported in *Figure 4-3*. The vulcanization curves of both NC(MB-SepX/NR) samples show lower values of M<sub>L</sub> and M<sub>H</sub> compared to REF-SepX/NR (*Table 4-3*).

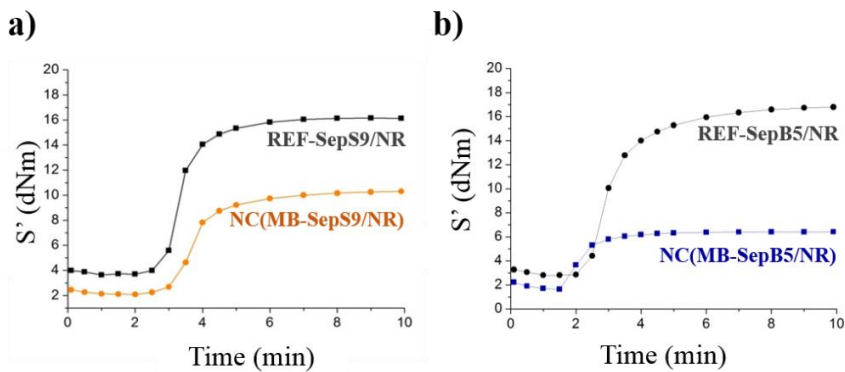


*Figure 4-3. Vulcanization curve of a) NC(MB-SepS9/NR) (orange line) and REF-SepS9/NR (black line) and b) NC(MB-SepB5/NR) (blue line) and REF-SepB5/NR (black line).*

*Table 4-3. Curing characteristics of NC(MB-SepX/NR) and REF-SepX.*

	M <sub>L</sub> (dNm)	M <sub>H</sub> (dNm)	M <sub>H</sub> -M <sub>L</sub> (dNm)	scorch time (min)
NC(MB-SepS9/NR)	2.10	10.26	8.16	2.49
REF-SepS9/NR	3.65	16.19	12.54	2.51
NC(MB-SepB5/NR)	1.85	6.72	4,87	1.32
REF-SepB5/NR	2.79	16.77	13,97	2.00

It is well known that M<sub>L</sub> is an index of the nanocomposite viscosity. Usually a low viscosity has been related to the occurrence of degradative reactions which alter

rubber polymer with the shortening of the long molecular chains. Among degradative reactions, oxidation phenomena frequently affect NRL and NR composite material. It is worth reminding that NR exists as high polymer in latex. The fresh NRL is sensible to oxidation from the time of the tapping to its vulcanization and final use. Reaction with oxygen may affect its properties, even if the changes are small and not usually significant since latex of commerce is preserved with ammonia.

On the other hand, it could not be excluded that oxidation phenomena could occur during the MB preparation. If present, oxidation phenomena could negatively affect the vulcanization process.

Actually, a lowering of  $M_L$  and  $M_H$  values has been observed in the rubber nanocomposite obtained with both MB-SepS9/NR and MB-SepB5/NR (Figure 4-3), but not in the case of MB-SiO<sub>2</sub>/NR (Figure 4-1). This suggests a specific drawback involving MBs with Sep. These samples have been investigated in Paragraph 1.3.

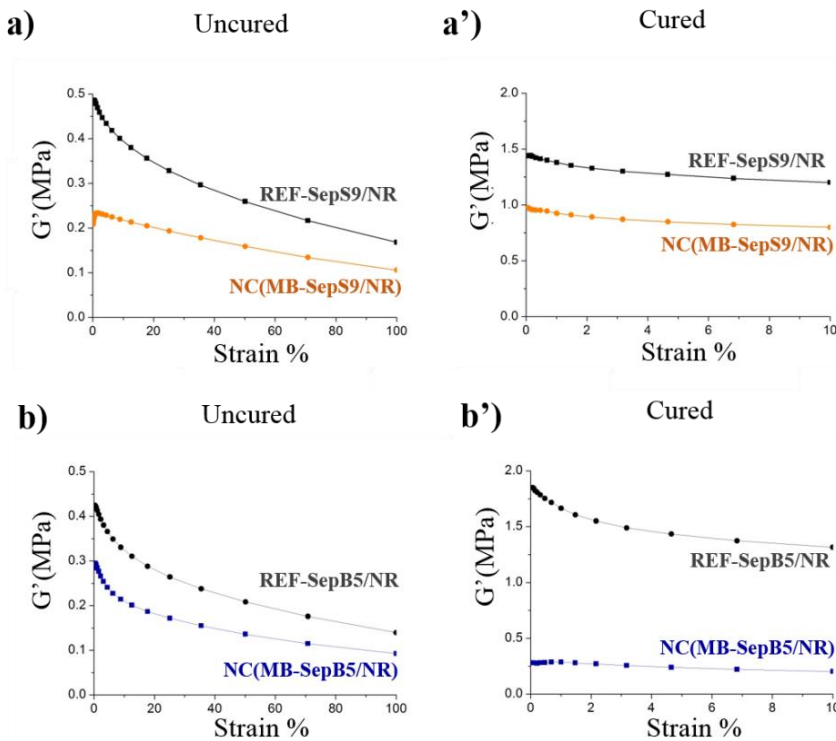


Figure 4-4. RPA analysis of uncured a) NC(MB-SepS9/NR) (orange line) and REF-SepS9/NR (black line), b) NC(MB-SepB5/NR) (blue line) and REF-SepB5/NR (black line); RPA analysis of cured a') NC(MB-SepS9/NR) (orange line) and REF-SepS9/NR (black line), b') NC(MB-SepB5/NR) (blue line) and REF-SepB5/NR (black line).

*Table 4-4. Storage modulus of cured and uncured NC(MB-SepS9/NR), REF-SepS9/NR, NC(MB-SepB5/NR), REF-SepB5/NR.*

	Uncured			Cured		
	$G'_{(1\%)}$ MPa	$G'_{(100\%)}$ MPa	$\Delta G'_{(1\%-100\%)}$ MPa	$G'_{(0.5\%)}$ MPa	$G'_{(9\%)}$ MPa	$\Delta G'_{(0.5\%-9\%)}$ MPa
NC(MB-SepS9/NR)	0.23	0.11	0.12	0.93	0.80	0.13
REF-SepS9/NR	0.49	0.18	0.31	1.39	1.21	0.18
NC(MB-SepB5/NR)	0.28	0.10	0.18	0.27	0.20	0.07
REF-SepB5/NR	0.41	0.15	0.26	1.66	1.34	0.32

The dependence of storage modulus vs strain is evaluated for NC(MB-SepX/NR) and REF-SepX/NR before and after curing (*Figure 4-4*).

NC(MB-SepX/NR) uncured samples show lower values of  $G'$  than reference materials at low and high strain (*Figure 4-4 a and b*). Straining the materials to 100%, a lowering of the  $G'$  is observed in all the materials, i.e. the Payne effect.

After curing (*Figure 4-4 b'*), an increase of the modulus either at low or at high strain is observed for all the composites. On the other hand, it is evident that the composites containing MB-SepX/NR display worse mechanical properties with respect to the reference materials, as also shown the values of  $G'_{(9\%)}$  and  $\Delta(G'_{\infty}-G'_0)$  (*Table 4-4*). These results could be ascribable to eventual oxidation phenomena against NC(MB-SepX/NR) samples.

#### 4.1.3 More-in-depth analysis of composite materials: the oxidation process of NC(MB-SepX/NR)

With the aim of solving the problems related to the NC(MB-SepX/NR), a more-in-depth analysis of composite materials has been performed.

Firstly, occurring oxidation phenomena are verified by DSC analysis, which can highlight the endothermic or exothermic processes happening in the materials, giving information on the occurring reactions at a specific temperature. Oxidative reactions are exothermic peaks.

*Figure 4-5* shows the heat flow at increasing temperature of the fillers SepS9 and SepB5 (a and b in figure) and related MB (c and d in figure), prepared by LTC.

DSC analysis of the pristine fillers does not present any peak from 30 to 170°C. Both DSC curves of MB-SepX/NR samples show an exothermic peak at around 150°C. This suggests the possible oxidation of rubber polymer matrix favored by high temperature. A mechanism of NR oxidation is reported in *Figure 4-6*.



To support this, TGA analysis of both MB-SepS9/NR and MB-SepB5/NR, having low  $M_L$  and  $M_H$ , has been performed. *Figure 4-7* shows a slight increase of weight around 200 °C (in highlighted colored region) for both sample (a and b in figure).

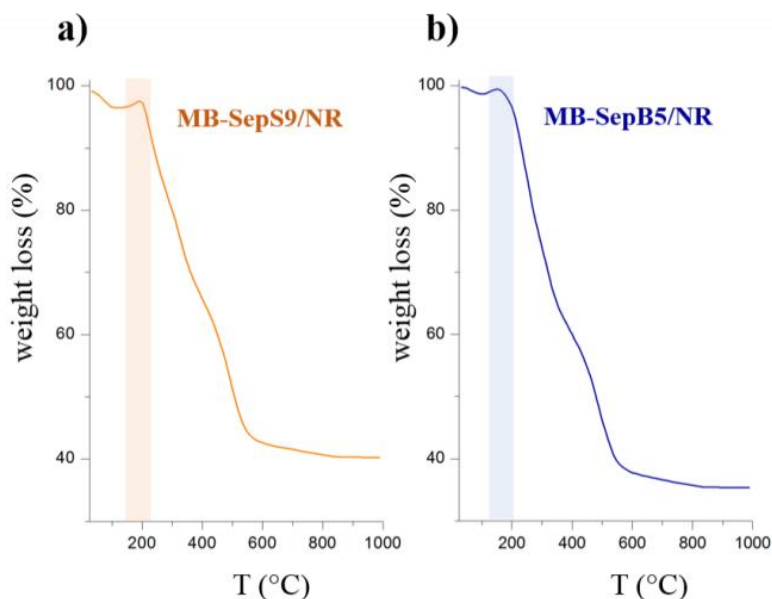


*Figure 4-7. TGA analysis of a) MB-SepS9/NR and b) MB-SepB5/NR.*

According to the literature,<sup>5</sup> this weight increase could be associated to an oxygen uptake.

DSC and TGA analyses support that oxidation processes occur in the NC(MB-SepX/NR) which in turn affect the mechanical properties of final rubber nanocomposites prepared by using MB-SepX/NR.

These findings make us questioning about the possible persistence of water, entrapped into Sep mesopores during the aqueous dispersion process, which may conveyed oxygen. During vulcanization, the high temperature reached in a non-controlled environment rich of oxygen solubilized in water might trigger oxidation phenomena.

In addition some metallic ions, released by Sep fibers, could act as catalysts. To assess the presence of metallic ions on the Sep surface, XRF analysis has been carried out. Beyond magnesium, a structural ion of Sep crystalline structure, Al, Cl, K, Ti, Ca and Mn elements are detected in small amounts as shown in the in *Table 4-5*. Low but not negligible percentage of iron ions have been found in both SepS9 and SepB5 dispersions. The presence of iron ions could activates oxidative processes of an organic compound. Natural surface-adsorbed  $Fe^{3+}$  and octahedral  $Fe^{3+}$  of Sep were proved to catalyze oxidation in other studies.<sup>6</sup>



Table 4-5. XRF of SepS9 and SepB5 dispersions (amount in wt%).

	Mg	Al	Cl	K	Fe	Ti	Ca	Mn	Cu	Zn	Rb
<b>SepS9</b>	13,2	1,3	-	0,63	0,58	0,06	0,27	0,02	T	T	T
<b>SepB5</b>	12,7	0,27	1,3	0,68	0,61	0,07	0,25	0,01	T	T	T

\*T=traces (<0.01 %)

On the basis of above, a controlled drying process of MB-SepX/NR has been applied to avoid oxidation process.

MB composites are dried in a controlled environment under vacuum at 80 °C for 18 h. Figure 4-8 shows the curing curve of NC(MB-SepB5/NR) compounded with MBs dried by the controlled method and compared with reference materials.

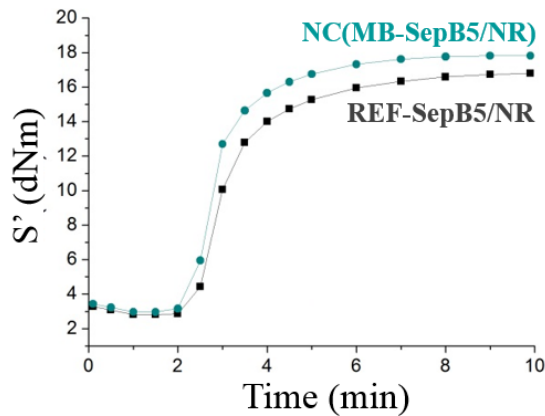


Figure 4-8. Vulcanization curves of NC(MB-SepB5/NR) (light blue line) and REF-SepB5/NR (black line).

Table 4-6. Curing characteristics of NC(MB-SepB5/NR) and REF-SepB5/NR.

	$M_L$ (dNm)	$M_H$ (dNm)	$M_H - M_L$ (dNm)	scorch time (s)
NC(MB-SepB5/NR)	2.95	17.89	14.94	2.00
REF-SepB5/NR	2.79	16.77	13.98	2.01

In this case, the vulcanization curves of NC(MB-SepB5/NR) and REF-SepB5/NR are similar.  $M_L$  and  $M_H$  values of NC(MB-SepB5/NR) are in line with the reference materials. Also the scorch time is restored to very similar values.

Therefore, dynamic-mechanical properties are investigated (Figure 4-9 and Table 4-6).

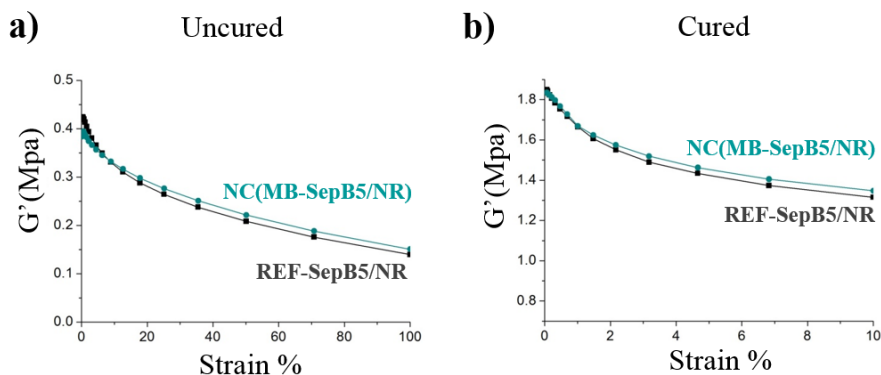


Figure 4-9. RPA of a) uncured NC(MB-SepB5/NR) (light blue line) and REF-SepB5/NR(black line) and of b) cured samples NC(MB-SepB5/NR) (light blue line) and REF-SepB5/NR (black line).

Table 4-7. Storage modulus of cured and uncured samples of NC(MB-SepB5/NR) and REF-SepB5/NR.

	Uncured			Cured		
	$G'_{(1\%)}$ MPa	$G'_{(100\%)}$ MPa	$\Delta G'_{(1\%-100\%)}$ MPa	$G'_{(0.5\%)}$ MPa	$G'_{(9\%)}$ MPa	$\Delta G'_{(0.5\%-9\%)}$ MPa
NC(MB-SepB5/NR)	0.39	0.16	0.23	1.82	1.36	0.46
REF-SepB5/NR	0.41	0.15	0.26	1.66	1.34	0.32

$G'$  of the NC(MB-SepB5/NR) is completely comparable with the  $G'$  at high and low strain of the REF-SepB5/NR (Figure 4-9), both in the uncured and in the cured material composites.

The dynamic-mechanical analysis of NC(MB-SepS9/NR) (here not reported) prepared by MBs dried in controlled environment did not showed the same improvements as in the case of SepB5. This is probably due to the fact that in the case of SepB5 the pores are partially protected by the presence of the alkyl ammonium salt, which prevents the strong water adsorption, while in SepS9 they are more exposed.

To avoid this, freeze drying approach is being studied on the drying process of MB-SepS9/NR with promising results.

## 4.2 Conclusions

Rubber nanocomposites containing silica and Sep fillers are prepared by combining latex compounding and melt mixing.

A highly filled NR MBs, firstly prepared by co-coagulating of NR latex and silica-based filler aqueous suspension, are mixed with the NR rubber matrix together with coupling agents, vulcanizing agents and antioxidants.

LCT seems to be a good approach for incorporating hydrophilic filler thanks to the good dispersion obtained in the MBs, but presents some issues linked to the porous nature of clays.

In detail, compounds containing silica MBs shows the best interactions with the sulfur-based vulcanization compounds, leading to good reinforcement and low energy dissipation.

Unfortunately, during MB preparation, Sep fibers with high porosity adsorb and retain water and oxygen that negatively affect the vulcanized materials. By employing a controlled drying process, it is possible to overcome this drawback, avoiding eventual oxidation processes and obtaining composite materials having good mechanical properties.

### 4.3 Bibliography

- 1 S. S. Sarkawi, W. K. Dierkes and J. W. M. Noordermeer, in *Proceedings of the Polymer Processing Society 28th Annual Meeting*, 2012, pp. 13–16.
- 2 M. Galimberti, M. Martino, M. Guenzi and G. Leonardi, *e-Polymers*, 2009, **56**, 1–14.
- 3 A. R. Payne, *J. Appl. Polym. Sci.*, 1962, **6**, 368–372.
- 4 M.-J. Wang, *Rubber Chem. Technol.*, 1998, **71**, 520–589.
- 5 S. A. Kyriakou, M. Statheropoulos, G. K. Parissakis, C. D. Papaspyrides and C. N. Kartalis, *Polym. Degrad. Stab.*, 1999, **66**, 49–53.
- 6 J. Cornejo, M. C. Hermosin, J. L. White, J. R. Barnes and S. L. Hem, *Clays Clay Miner.*, 1983, **31**, 109–112.





## Chapter 5.

### Pickering emulsion polymerization for preparing silica-based waterborne latexes

Chapter 5 describes the preliminary study on the preparation of silica-based latex nanocomposites by applying Pickering emulsion polymerization. In such approach, the production of composite materials is based on the polymerization of the organic isoprene monomer in aqueous emulsion, in the presence of silica-based inorganic colloidal particles, such as silica and Sep, as emulsion stabilizer.

This study was carried out in the Weitz Lab (Department of Engineering and Applied Science, Harvard University) under the supervision of Prof. David Weitz.





## 5.1 Waterborne silica-based polymer nanocomposites by Pickering emulsion polymerization

Pickering emulsion polymerization is a useful technique for synthesizing polymeric particles covered with inorganic nanoparticles. The resulting latex nanocomposite can have intriguing properties and features not present in conventional polymer latexes, such as superior stability, adjustable permeability and low toxicity, thanks to the absence of surfactants.<sup>1</sup>

The Pickering emulsion polymerization technique owns several positive aspects:

- no sophisticated instrumentation is required;
- nanoparticle solution are used without further treatment;
- it is a one-step synthesis;
- the produced polymer-particle dispersion is surfactant-free.<sup>1</sup>

On the basis of these advantages, the latex nanocomposites by Pickering emulsion polymerization can be considered as an innovative way of incorporation of inorganic nanofillers into polymers, potentially offering different mechanical properties because of the obtainment of particular particles arrangement in the polymeric matrix and reduced permeability compared to pure polymers. This approach makes also possible an increase of inorganic particles dispersion thanks to an intimate contact with the waterborne polymer and an orientation of the colloidal components.

A subsequent processing or application step, such as a MB formation obtained after drying the latex nanocomposite, may be seen as an alternative way respect to LCT to compound silica-based fillers and polymers.

It is worthy to note that so far, Pickering emulsion polymerization as means to homogeneously disperse the silica and clay nanoparticles into IR or PI has not been documented.

Poochai<sup>2</sup> et al. reported the preparation of PI-coated silica by admicellar polymerization in the presence of surfactants. In this study, isoprene has been polymerized with a coating of silica particle surface in order to improve the compatibility between the silica surface and IR. The stability of an oil solution of PI, in the presence of silica nanoparticles and an aqueous solution of hydroxypropyl cellulose, was studied to understand the role of solid particles in emulsions.<sup>3</sup> This study suggested that the addition of nanoparticles increases the elasticity of the emulsions, due to the increased stability. To the best of our knowledge, there are no examples in the literature of Pickering emulsion polymerization of PI with silica or Sep nanoparticles.

Thus, the object of this work is to investigate the surfactant-free emulsion polymerization of PI, carried out in the presence of silica or Sep nanoparticles to obtain 1,4-PI latex nanocomposites, following the procedure reported in the Chapter 2 Paragraph 2.2. The synthesis is performed in the presence of KPS as radical polymer initiator under N<sub>2</sub> atmosphere at 75 °C. The operating pH (9),

provided by the presence of sodium carbonate, is required to keep the thiol in the unprotonated form, thus helping the transfer of radicals from the aqueous to the oil phase.

## 5.2 SiO<sub>2</sub>/polyisoprene latex nanocomposite

Polymerization of isoprene has been performed in the presence of silica Ludox TM-50, having a diameter of 22 nm and  $\zeta$ -potential of  $-38.6 (\pm 2.5)$  mV in order to obtain 1,4-PI latex nanocomposite (named: L-SiO<sub>2</sub>/PI).

DLS analysis of latex, synthesized via Pickering emulsion polymerization, shows particles with a diameter of about 207 ( $\pm 1.7$ ) nm (*Figure 5-1*). This value is in agreement with the average particle size reported for emulsion polymerization approach.<sup>4</sup> The polydispersity of the L-SiO<sub>2</sub>/PI is relatively narrow with the polydispersity index of 0.02, typical of very monodisperse systems. The particle size can be related to the presence of SiO<sub>2</sub>/PI latex particles.

Particles size values in the range of 20-45 nm, associable to the presence of free silica particles dispersed in the latex, are not present.

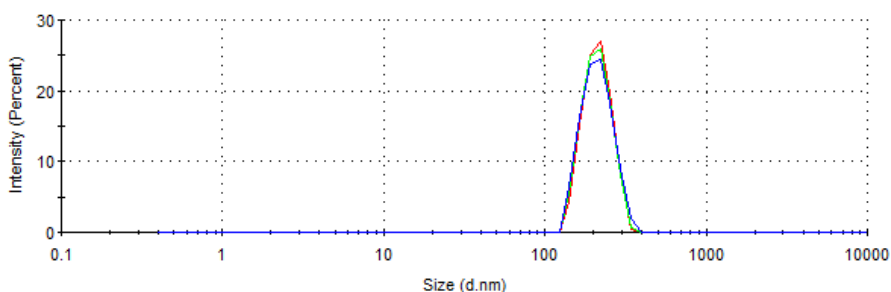


*Figure 5-1. DLS analysis of L-SiO<sub>2</sub>/PI (red line first record, green line second record, blue line third record).*

To assess the best reaction conditions for the synthesis of SiO<sub>2</sub>/PI latex nanocomposite, the Pickering polymerization has been carried out at different temperatures and times. The DLS analysis is reported in the *Table 5-1* for each reaction.

*Table 5-1. Size of L-SiO<sub>2</sub>/PI obtained at different times and temperatures.*

Time (h)	Temperature (°C)	Size (nm, DLS)
24	75	150 ( $\pm 1.3$ )
48	75	190 ( $\pm 2.0$ )
48	90	220 ( $\pm 2.9$ )
96	90	240 ( $\pm 2.0$ )

By increasing the time of reaction, it is observed an increase of particle dimensions from 150 to 190 nm at 75 °C and from 220 to 240 nm at 90 °C (*Table 5-1*). This effect is consistent with the increase of monomer conversion to polymer (discussed in detail at the end of this Chapter), as reported for the emulsion polymerization kinetics of polystyrene without surfactants.<sup>5</sup> Hearn reported that the polystyrene particle size increases with the time of reaction from 30 to 300 nm. The progressive increase of particle size is also related to the decrease of particle number density at the early stage of polymerization until they reach a constant value and it might reasonably be expected to depend upon the number of oligomer nuclei generated and their stability. Based on this theory, the obtainment of bigger particles corresponds to lower particle number density. The temperature increase provides an effect on the size of the SiO<sub>2</sub>/PI latex particles which grow from 190 to 220 nm at the same reaction time (48 h) (*Table 5-1*). This should be explained by faster kinetic of polymerization at higher temperatures.

The total silica content in the latex composite is quantitatively determined by TGA on the dried samples. *Figure 5-2* shows the thermograms of dry SiO<sub>2</sub> Ludox TM-50 (grey line), commercial poly(1,4-*cis*-isoprene) (IR) (black line) and dried L-SiO<sub>2</sub>/PI.

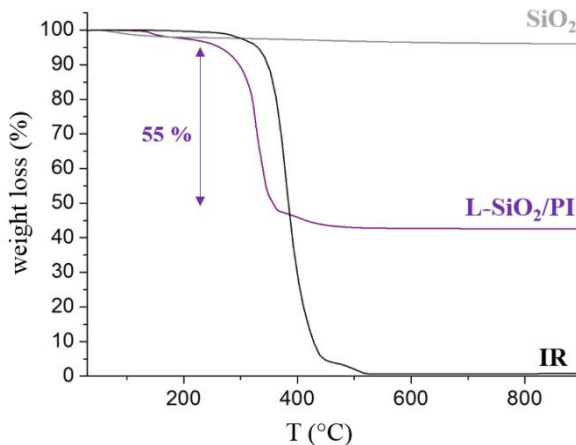


*Figure 5-2. TGA curves of IR (black line), SiO<sub>2</sub> (grey line), L-SiO<sub>2</sub>/PI (purple line).*

The complete degradation of IR is at about 600 °C, while SiO<sub>2</sub> shows only a slight weight loss due to the water physisorbed on silica particles surface. L-SiO<sub>2</sub>/PI sample displays a slight weight loss (~1 %) at 100 °C attributable to physisorbed water, while a major weight loss is detectable from 300 to 500 °C. It is reasonable to assume that the weight loss is associated with the thermo-degradation of the rubber component and the residue undegraded after 1000 °C consists of inorganic silica. Thus, the total silica content of the latex nanocomposite is approximately of 55 % wt.

In addition, an evaluation of the silica tightly linked to the polymer, in latex particle, has been made by TGA analysis of the dried latex composite after removal of the excess silica component by centrifugation. The centrifugation determines the destabilization of the emulsion with the precipitation of free silica on the bottom. The lighter polymer remains floating on the top with the some entrapped silica particles. These silica particles are believed to have a higher contact with the polymer remaining liked also after high speed centrifugation. In detail, *Figure 5-3* shows both silica latex composite L-SiO<sub>2</sub>/PI dried (purple line) and the dried sample after centrifugation (pink line).

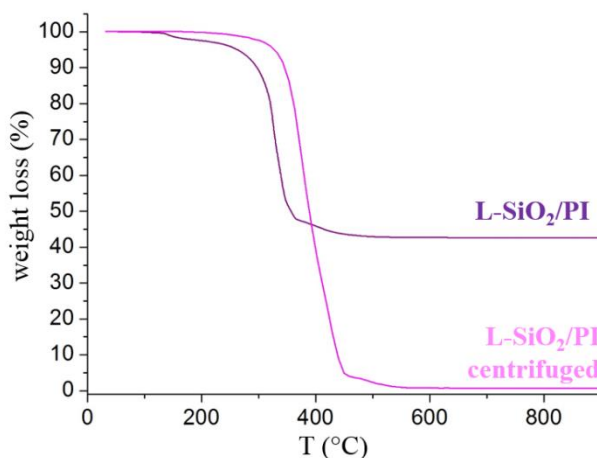


*Figure 5-3. TGA analysis of the L-SiO<sub>2</sub>/PI dried (purple line) and centrifuged (pink line).*

*Table 5-2. Polymer/filler ratio from TGA analysis.*

	Polymer %	Filler %
L-SiO <sub>2</sub> /PI	55.1	43.1
L-SiO <sub>2</sub> /PI after centrifugation	95.4	3.5

By comparing the silica retained from the centrifugation process to the nominal one, the silica inorganic nanoparticles that cover the synthesized polymeric particles can be estimated approximately of 12.3 wt % of the total silica particles present in the latex. Although a large part of silica nanoparticles remain in the continuous phase, the silica content of latex particles prepared via solid-stabilized emulsion polymerization is significant.

After confirming the formation of L-SiO<sub>2</sub>/PI by DLS and TGA, SEM-EDX investigation has been performed. *Figure 5-4* shows the SEM images of L-SiO<sub>2</sub>/PI, obtained at 75 °C during 48 h (similar SEM images have been achieved for samples obtained at different time and temperature). The deposition of a drop of latex on

the SEM stub induces the coagulation process during the evaporation of the solvent. This phenomenon can be explained taking into account the very low  $T_g$  of PI, typically much lower than room temperature,<sup>6</sup> which makes the latex particles very soft. In detail, in the aqueous medium, the inorganic particles around the PI particle form a protective layer, electrostatically charged, and their electrostatic repulsion contributes to the emulsion stabilization. However since the solvent is removed, the collisions between particles result in the coalescence of the latex particles giving rise the coagulated material, i.e. the MB, as shown in *Figure 5-4*.

This does not occur with hard particles of polystyrene or poly(methyl methacrylates), typical polymers selected for the Pickering emulsions. In these cases, the rigid crust of the polymer particles due to high  $T_g$  (100 °C for polystyrene and from 85 to 165 °C for commercial poly(methyl methacrylates)) constitutes a mechanical barrier preventing the coagulation of polystyrene latex particles by steric stabilization.

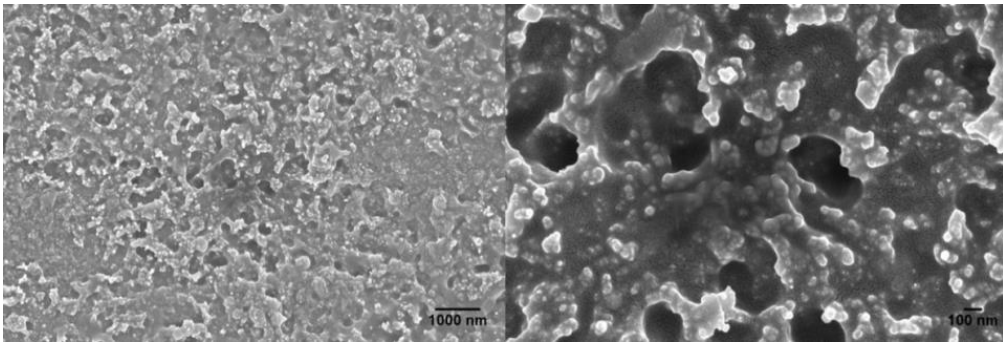


*Figure 5-4. SEM of L-SiO<sub>2</sub>/PI at different magnification.*

Despite the coagulation occurs, the Pickering particles are observed at higher diluted condition. *Figure 5-5* shows spherical PI latex particles with a mean diameter in accordance with DLS around 200 nm and a partial coverage by silica nanoparticles, in line with the TGA analysis.

The adhesion between silica nanoparticles and polymer sphere is evident (*Figure 5-5 a and b*). In any case, the coalesced particles of PI form together with silica a remarkably homogeneous MB (*Figure 5-6*).

To assess the silica dispersion in the rubber matrix of dried L-SiO<sub>2</sub>/PI samples, a silicon atom mapping is performed by EDX analysis. A very homogeneous nanocomposite is visible thanks to the silicon atom spots, assessing good silica distribution in PI (*Figure 5-6*).

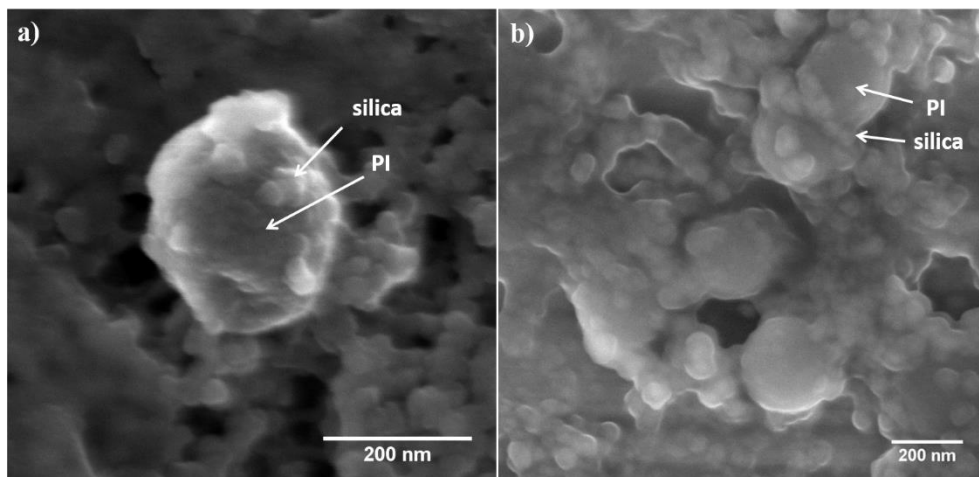


Figure 5-5. a) and b) SEM images of L-SiO<sub>2</sub>/PI at different magnifications in diluted conditions.

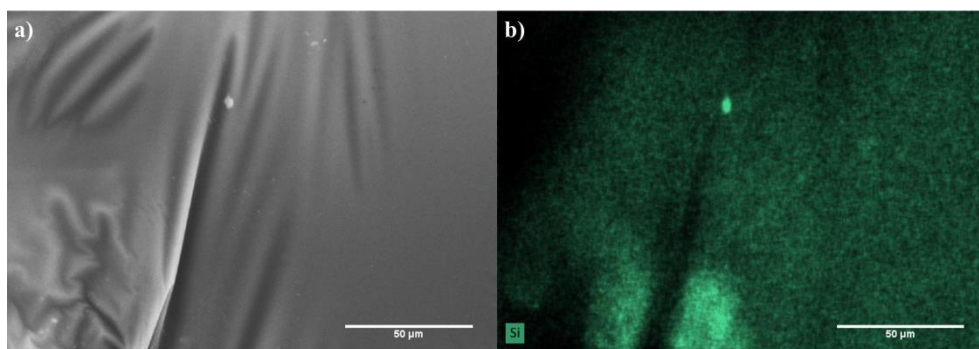


Figure 5-6. SEM micrographs of (a) L-SiO<sub>2</sub>/PI and (b) the corresponding EDX analysis of silicon atom.

To investigate the nature of the interactions between silica surface and PI sphere in latex particles, ATR-FTIR spectra of L-SiO<sub>2</sub>/PI sample are collected and compared to those of pristine silica and commercial IR (Figure 5-7).

The symmetric vibrations of silicon atoms in a siloxane bond occur at  $\sim 800\text{ cm}^{-1}$ . The largest peak observed in a silica spectrum is present at  $\sim 1100\text{ cm}^{-1}$  and is dominated by antisymmetric motion of silicon atoms in siloxane bonds. This broad peak presents a weak absorption at  $950\text{ cm}^{-1}$  due to silanol (Si-OH) stretching vibrations.<sup>7</sup>

ATR-FTIR spectrum of L-SiO<sub>2</sub>/PI sample shows little modifications in the adsorption regions related to silanols region (purple area) which may be related to the formation of new polar interactions. The chemically bound groups, which could interact by H-bond or ionic bounds with silica, may be: i) polymer end groups (e.g., sulfate end groups arising from the persulfate initiator), ii) reaction products of these end groups (e.g., hydroxyl or carboxyl groups), iii) polymer reaction products

(e.g., oxidation to form carboxyl groups). These chemically bound groups remain fixed on the particle surface and could reasonably provide weak interaction between polymer and filler.<sup>8</sup>

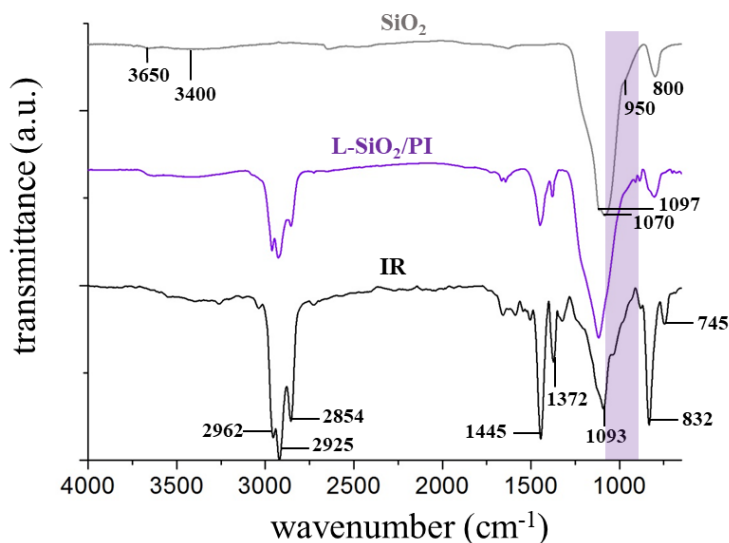
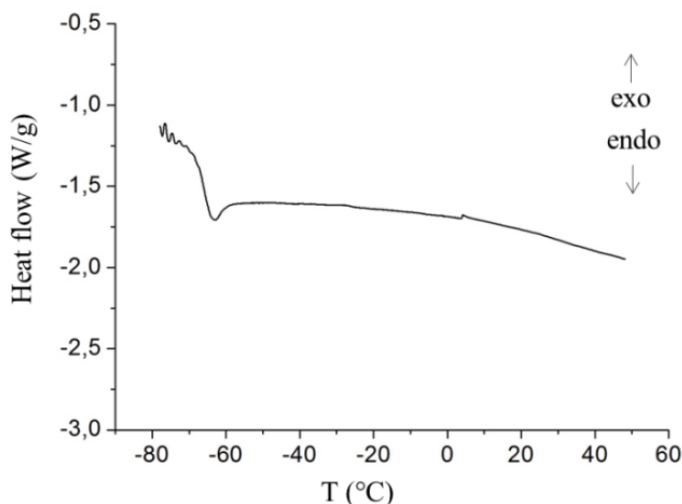


Figure 5-7. FTIR spectra of  $\text{SiO}_2$  (grey line),  $\text{L-SiO}_2/\text{PI}$  (purple line) and IR (black line).

The Pickering polymerization process has been evaluated by the exhaustive analysis of the polymeric component in  $\text{L-SiO}_2/\text{PI}$  sample.

Firstly, DSC analysis has been performed (Figure 5-8). The endothermic peak at  $-66^\circ\text{C}$  is related to the  $T_g$  of the polymer. The  $T_g$  of IR, having stereochemical regularity of 98%, typical of NR, is reported to be  $-69^\circ\text{C}$ .<sup>6</sup> The difference of experimental  $T_g$ , with respect to the reference material, could be attributed to the presence of different isomeric structures, produced during the radical polymerization: 1,2-PI and 3,4-PI.<sup>9</sup> With regards to the relationship between the  $T_g$  and isomer structures, Widmaier *et al.*<sup>10</sup> determined  $T_g$  values for a series of PI samples obtained by anionic polymerization with different isomers. They found  $T_g$  values in the range  $-71$  to  $-36^\circ\text{C}$  for 3,4 units content ranging from 9 to 49%, with a direct dependence  $T_g$  from the 3,4 content. This effect was explained adducing that the steric hindrance, deriving from the sidechain vinyl groups, would lead to stiffening of polymer chains. So, according to the findings reported by Widmaier, PI with a  $T_g$  value of  $-66^\circ\text{C}$ , as in our case, should be expected to have around 90 % of total 1,4 units.

To confirm this, a more in-depth analysis of PI stereochemistry has been performed by  $^1\text{H-NMR}$  spectroscopy to evaluate the amount of 1,4-PI.

Figure 5-8. DSC analysis of L-SiO<sub>2</sub>/PI.Table 5-3. Amount of different isomer structures present in L-SiO<sub>2</sub>/PI obtained via Pickering polymerization.

Isomer	Structure	Amount (%)
<b>cis-1,4-polyisoprene</b>  <b>and</b> <b>trans-1,4-polyisoprene</b>	$\begin{array}{c} \text{-(CH}_2\text{)-CH}_2\text{-} \\   \quad   \\ \text{C}=\text{C} \\   \quad   \\ \text{CH}_3 \quad \text{H} \end{array}$ $\begin{array}{c} \text{-(CH}_2\text{)-} \quad \text{H} \\   \quad   \\ \text{C}=\text{C} \\   \quad   \\ \text{CH}_3 \quad \text{CH}_2\text{-} \end{array}$	89
<b>1,2-PI</b>	$\begin{array}{c} \text{CH}_3 \\   \\ \text{-(CH}_2\text{-C)-} \\   \\ \text{CH=CH}_2 \end{array}$	5,3
<b>3,4-PI</b>	$\begin{array}{c} \text{-(CH}_2\text{-CH)-} \\   \\ \text{CH}_3\text{-C=CH}_2 \end{array}$	5,6

The H<sup>1</sup>-NMR spectrum shows the amount of the isomers obtained by applying Pickering radical polymerization: 89% of conformation 1,4-PI, 5,3% of 1,2-PI and 5,6% of 3,4-PI (Table 5-3).



To evaluate the polymerization yield, the conversion of isoprene monomer into PI, in the presence of silica Ludox TM-50, is estimated by TGA analysis of dried samples obtained at two different temperatures (*Figure 5-9*).

As expected, for a given concentration of monomer, the conversion increases as a function of time. Therefore, the best conversion, corresponding to about 50%, is obtained after 48 h at 90 °C and after 96 h at 75 °C. This effect is coherent with the general rule of the radical polymerization reactions where the polymerization rate strongly increases with the temperature.<sup>11</sup>

In the literature, low yields of emulsion isoprene polymerization have been generally reported (about 20-30%).<sup>12</sup> Cheong *et al.*<sup>13</sup> reported that this low isoprene conversion in emulsion polymerization could be due to its low propagation rate constant. The low constant of isoprene propagation rate would lead to a low propagation rate inside the latex particles as well as to a long aqueous-phase lifetime before particle entry, and hence low entry efficiency, due to termination of isoprene oligomers in the aqueous phase. In our case, even if the polymerization of isoprene shows a slow kinetic of reaction, the Pickering approach reaches isoprene conversion up to 50%, in line with the reported reactions in the presence of surfactants.

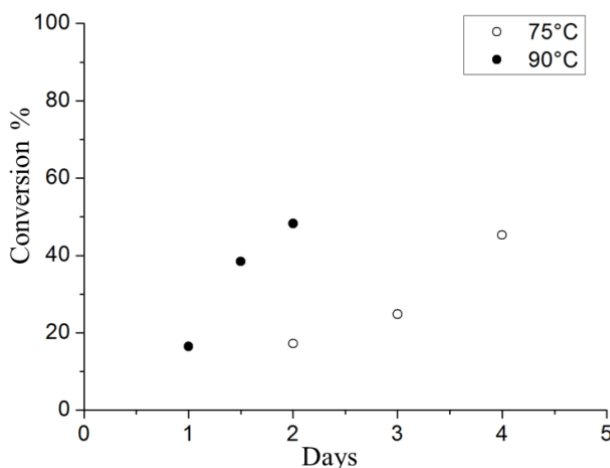


*Figure 5-9. The conversion of isoprene to polymer as a function of polymerization time.*

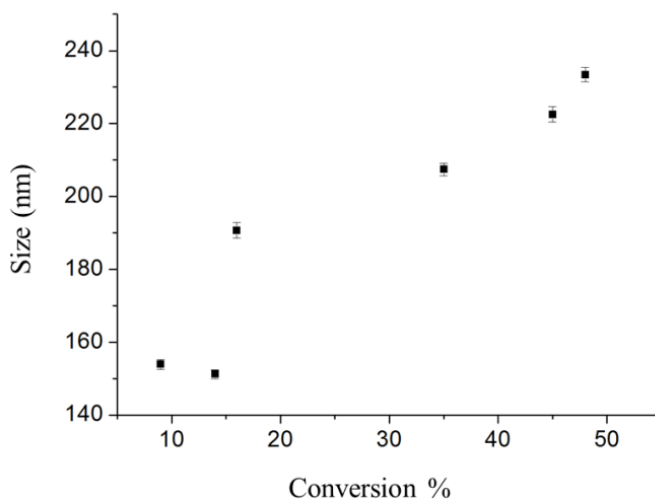
The temperature increase influences not only the conversion value but also the gel content. As shown in *Table 5-4*, the gel content increases by increasing time and temperature. In particular, the higher is the temperature, the greater the effect of the time on the gel content. The higher value of gel content obtained is 30% for the polymerization performed at 90 °C for 98 h.

Probably, the conversion and gel content could be improved by enhancing the concentrations of both initiator and transfer agent.

Table 5-4. Gel content of PI at different synthetic conditions.

Time (h)	Temperature (°C)	Conversion (%)	Gel content (%)
24	90	16	4
48	90	48	31
48	75	17	4
96	75	45	15

Finally, the particle size is analyzed for samples having a different conversion and carried out at different times and temperature. *Figure 5-10* shows an increase of the particle diameter ranging from 150 nm at low conversion to 240 nm at the highest conversion reached. During the reaction, the relatively high monomer availability in the micelles favors the simultaneous nucleation and growing of the particles, which is reflected in the increase in the monomer conversion (*Figure 5-9*) and in a consistent increase of particle size (*Figure 5-10*). This effect is in line with theories invoking a surface phase polymerization mechanism.<sup>5</sup>

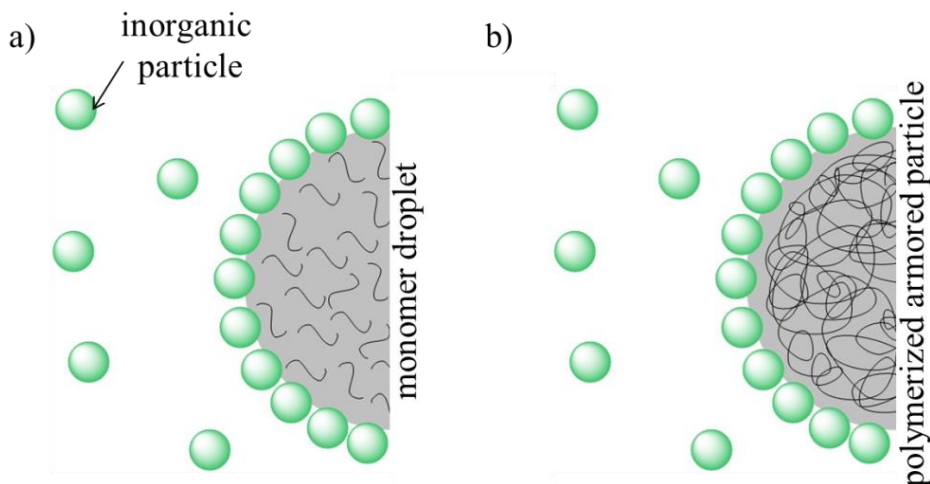
Figure 5-10. L-SiO<sub>2</sub>/PI size versus isoprene conversion.

### 5.2.1 Pickering emulsion polymerization mechanism for L-SiO<sub>2</sub>/PI

On the basis of above reported results, a mechanism for isoprene polymerization in the presence of solid particles is proposed.

The general theory about Pickering emulsion states that by continuous agitation of monomer and inorganic particles in water an emulsion of micrometric size droplets is formed. The solid particles are adsorbed at the oil–water interface to form a particle layer acting as a rigid film and providing a mechanical barrier to

coalescence. When the particle attachment at the oil–water interface is non-reversible, it is obtained a more efficient stabilization than surfactant adsorption. In principle, silica nanoparticles should adsorb at the monomer–water interface forming a Pickering stabilized emulsion (*Scheme 5-1*).



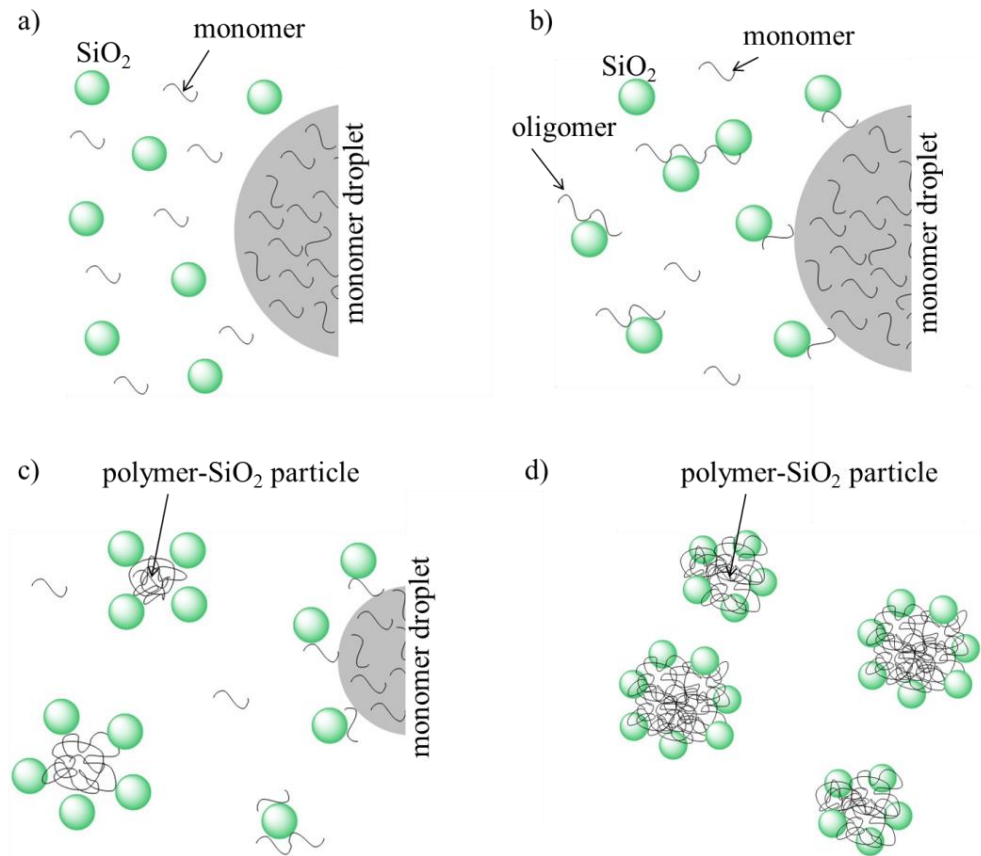
*Scheme 5-1. General mechanism reported for Pickering emulsion polymerization: a) inorganic particles distributes at the oil/water interphase; b) the polymerization forms organic-inorganic armored particles.*

According to this mechanism, there is an optimal pH to favor monomer-filler adhesion and maximize the stability of the monomer/filler composite particles, considering that electrostatic repulsions are controlled by the pH and ionic strength.

At high pH, strong repulsions operate and Pickering emulsions of silica particles are unstable. Indeed, the high pH promotes the dissociation of the silanol groups increasing the electrostatic repulsions that either weaken the adsorption of silica particles, or slow down the adsorption kinetics of silica. The lower the pH the lower the surface charge of silica particles, sensed by a decrease of the  $\zeta$ -potential. The stronger adsorption is obtained at low electrostatic repulsion.<sup>14</sup> Therefore, large electrostatic repulsions cause low density of adsorbed particles with a slow adsorption kinetics. Though, there is no definite proof of such a conjecture, the adsorption kinetics of silica is considered the most relevant mechanism.

On the other hand, in our case, the polymerization of PI in the presence of silica occurs at high pH.<sup>13</sup> This suggest an alternative mechanism respect to the above reported mechanism.

Bon and coworkers<sup>15</sup> reported an interesting mechanism, alternative to the adsorption of a Pickering stabilizer to a latex particle, as shown in *Scheme 5-2*.



*Scheme 5-2. Proposed alternative mechanism: a) the monomer droplets are formed by mixing the monomer and the water silica dispersion; b) the oligomer formed in solution adhere on silica particles; c) silica-oligomer structures coalesce while the monomer droplet are consumed; d) complete polymerization and formation of polymer-silica particles.*

This theory involves the precipitation of a growing polymer chain in the water phase onto a silica nanoparticle, followed by hetero-coagulation with the growing latex particle.

A similar mechanism involving the same hetero-coagulation event was theorized by Sheibat-Othman et al.<sup>16</sup> According to this mechanism, the initiator decomposes under the effect of temperature and pH, reacting with the monomer present in the aqueous phase. The formed oligomer continues growing until it becomes insoluble and adhere on the silica surface. This growing nuclei of silica-oligomer coalesce with one another until they form stable particles. The reaction proceeds with the diffusion of the monomer from the monomer droplets to the newly nucleated silica-polymer particles, as seen in conventional emulsion polymerization. At this stage, a thermodynamic equilibrium is reached by the

monomer distribution between the different phases: aqueous phase, polymer particles, and monomer droplets. As the reaction proceeds the monomer is consumed until the polymerization is complete.

The emulsion polymerization of polyisoprene requires basic pH because at these conditions the thiol is deprotonated to stabilize the formation of radicals, improving the reaction conversion. At pH 9, also the silica silanols are deprotonated, therefore, an adsorption of the silica particles on the monomer surface is unlikely because of poor affinity.

Moreover, the SEM analysis supports this theory because of the observed adhesion of silica particles on the polymer. Our system seems to be more consistent with the model proposed by Bon where the inorganic particles are driven towards the interface as a result of a hetero-coagulation events in the water phase with growing oligoradicals.

### 5.3 SepS9/PI latex nanocomposites

The Pickering emulsion polymerization has also been performed in the presence of anisotropic SepS9 particles.

Until now, clay minerals as colloidal stabilizers have been considered in a limited number of papers,<sup>17–19</sup> though the particles fulfil the required conditions: they are nano-sized; particle size fractions are obtained by sedimentation; they can strongly increase the viscosity of the bulk phase and form three-dimensional networks band-type or cardhouse structures.

In this frame, the synthesis of SepS9/PI latex nanocomposite (named: L-SepS9/PI) is performed to investigate the effect of anisotropic shape in the Pickering emulsion approach. The polymerization is performed at 75 °C for 48 h and 96 h, by using KPS as radical initiator.

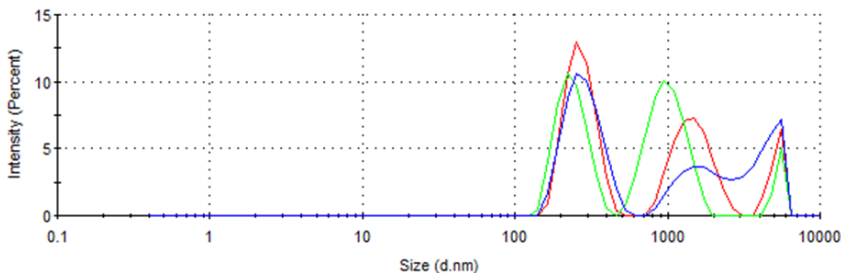


*Figure 5-11. DLS analysis of L-SepS9/PI (red line first record, green line second record, blue line third record).*

DLS analysis of L-SepS9/PI shows a trimodal size distribution. The peaks at 1697 nm can be assigned to clay particles, while the peak at 4333 nm may be due to aggregation of Sep particles. The peak at 284 nm may be associated to the emulsion latex droplet size.

The total content of SepS9 in L-SepS9/PI is quantitatively determined by TGA of dried sample. Since the complete degradation of IR is at about 600 °C, the remaining weight is relative to SepS9. L-SepS9/PI sample displays a small weight loss (~1 %) at 100 °C which belongs to the presence of physisorbed water, while a major weight loss is detectable from 300 to 500 °C. From this weight loss, it is determined the polymer content of 74% and SepS9 content of 24%.

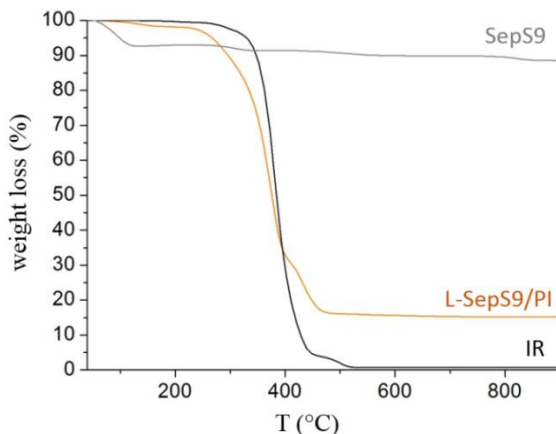


Figure 5-12. TGA curves of IR (black), SepS9 (grey), L-SepS9/PI (orange).

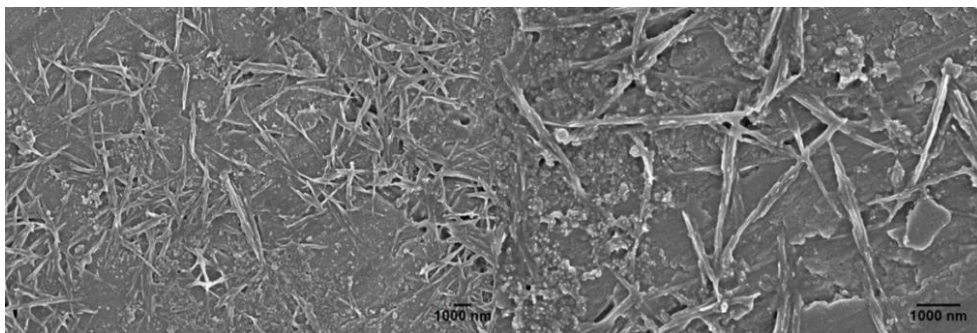


Figure 5-13. SEM of L-SepS9/PI.

SEM analysis performed on the dried L-SepS9/PI shows the formation of a homogeneous dispersion of SepS9 in the polymeric matrix (Figure 5-13) as obtained for L-SiO<sub>2</sub>/PI sample.

Single SepS9 particle looks interestingly covered by a layer of PI and continuously interconnected with the formation of a network.

The assessment of SepS9 dispersion in the rubber matrix of the dried L-SepS9/PI by EDX analysis of silicon atom reveals the formation of a very homogeneous nanocomposite where Sep is finely distributed. The formation of a percolative network is appreciable considering the low presence of voids in the Si map.

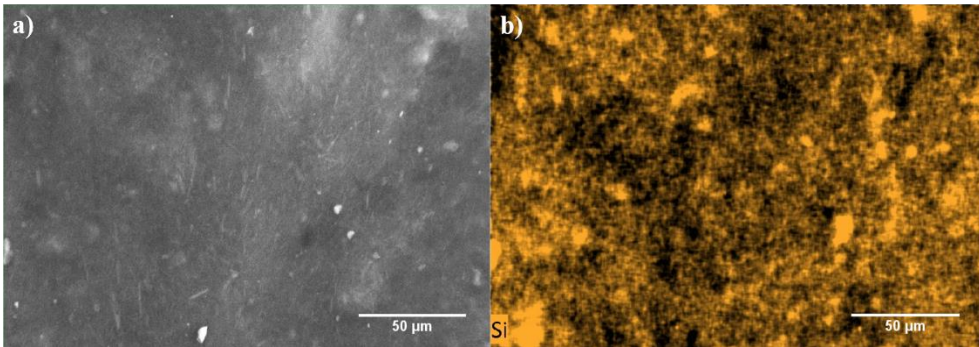


Figure 5-14. SEM micrographs of (a) L-SepS9/PI and (b) the corresponding EDX analysis of silicon atom.

ATR-FTIR spectrum of L-SepS9/PI (Figure 5-15) is compared to those of pristine IR (black line) and SepS9 particles (grey line). The stretching vibration of Si-OH at  $975\text{ cm}^{-1}$  is slightly shifted to higher wavenumbers. This may be an effect due to the formation of new ionic or H-bond between Sep and other products of the emulsion polymerization. As explained for L-SiO<sub>2</sub>/IP, polymer end groups or reaction products of PI, such as carboxyl groups formed by oxidation, may provide polymer filler interaction.

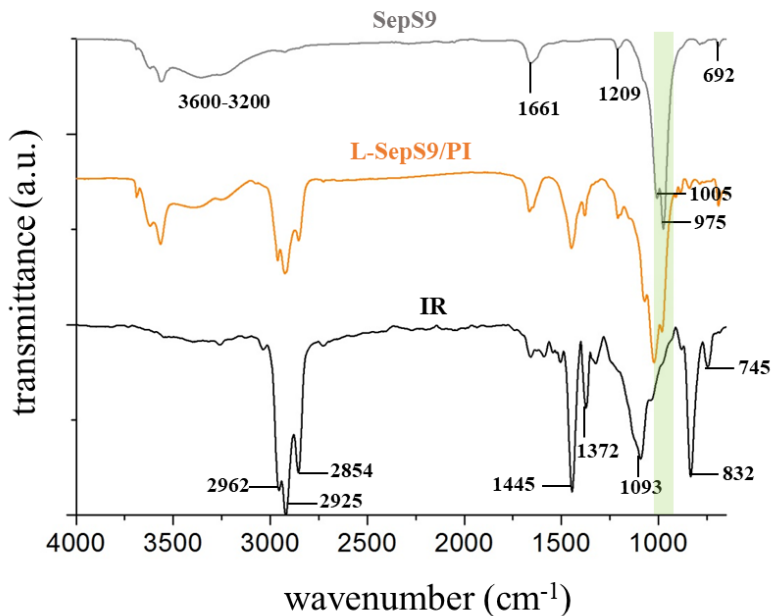


Figure 5-15. FTIR of SepS9 (grey line), L-SepS9/PI particles (orange line) and IR (black line).

The Pickering polymerization process has been evaluated by polymeric component analysis of L-SepS9/PI sample.

DSC analysis of L-SepS9/PI has been performed (Figure 5-16). The endothermic peak at -66 °C is related to the  $T_g$  of PI polymer, which is consistent with  $T_g$  of L-SiO<sub>2</sub>/PI sample. The presence of SepS9 does not seem to impart changes in polymer characteristics. For this, the relative stereochemistry is supposed to be in line with L-SiO<sub>2</sub>/PI. Further investigation is being performed by <sup>1</sup>H-NMR analysis.

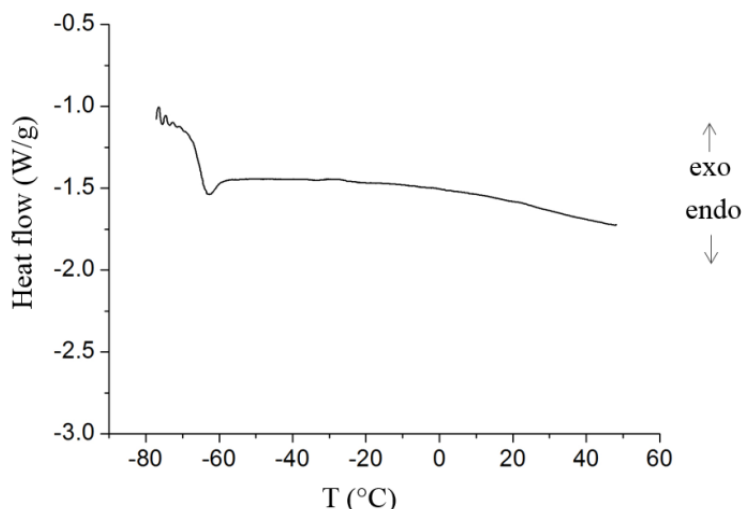


Figure 5-16. DSC analysis of L-SepS9/PI.

The isoprene conversion and gel content are reported in Table 5-5 for different times and temperature.

Similarly to L-SiO<sub>2</sub>/PI, the polymerization kinetic is slow and increases by increasing reaction time from 48 h to 96 h with conversion of 12% and 30% respectively. The gel content also increases along with conversion.

Further analysis are going to be provided for Pickering emulsion polymerization of L-SepS9/PI at 90 °C.

Table 5-5. Conversion % and gel content of PI in L-SepS9/PI.

	Temperature (°C)	Conversion (%)	Gel content (%)
48	75	12,4	7,3
96	75	30,7	11,9

The conversion and gel content values of L-SiO<sub>2</sub>/PI and L-SepS9/PI can be compared in Table 5-6.

In the presence of silica, isoprene conversion improves from 17% during 48 h to 45% during 96 h; instead, in the case of SepS9 conversion improves from 12% to



30%. It seems that the polymerization kinetics in the presence of SepS9 as stabilizer is lower than that carried out in the presence of silica.

After 48 h, L-SepS9/PI presents higher gel content, while after 96 h it is lower than that of L-SiO<sub>2</sub>/PI. Therefore, the formation of crosslinked polymer grows with a different slope for L-SiO<sub>2</sub>/PI and L-SepS9/PI.

The above results suggest that isoprene conversion in the presence of clay Sep has been affected by the lower emulsification efficiency of SepS9 fibers due to their high anisotropic shape. This is also confirmed by the presence of observed sedimentation of SepS9 particles at the end of polymerization. Good and stable dispersion is indeed challenging.

*Table 5-6. Comparison between L-SiO<sub>2</sub>/PI and L-SepS9/PI in terms of conversion and gel content.*

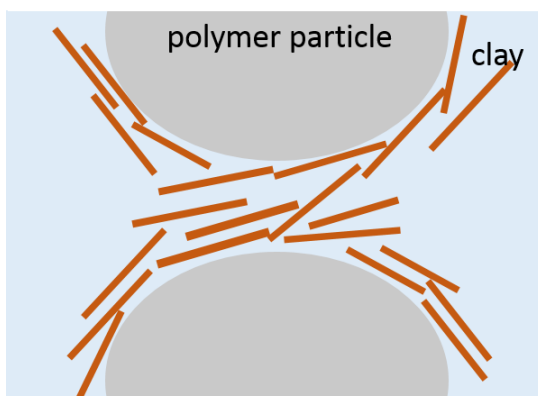
Filler	Time (h)	Temperature (°C)	Conversion (%)	Gel content (%)
SiO <sub>2</sub>	48	75	17,2	3,6
SepS9	48	75	12,4	7,3
SiO <sub>2</sub>	96	75	45,3	14,9
SepS9	96	75	30,7	11,9

### 5.3.1 Pickering emulsion polymerization mechanism for L-SepS9/PI

A specific stabilization mechanism has been proposed for Pickering emulsions stabilized by clay particle.<sup>19</sup> This mechanism is based on particle–particle interactions leading to the formation of a three-dimensional network in the continuous phase. Enhanced stability is obtained through the increase of viscosity. This has been observed particularly in smectite-based systems.

When the particles aggregate and build up a three-dimensional network in the coherent phase, the oil droplets can be trapped in the array of particles. The mechanical stability of the network structure reduces the rate of coalescence. A high elasticity of the network seems to be favorable. Also, the network reduces the mobility of the particles and, in this way, enhances emulsion stability.

The above results for L-SepS9/PI could be consistent with this mechanism, taking into consideration the high AR of SepS9 fibers. Based on this theory, Sep interactions between particles may entrap the oil phase in a colloidal network, where the sites of the polymerization of isoprene are created (*Scheme 5.3*).



*Scheme 5.3. Stabilization of emulsions in the presence of clay particles with formation of three-dimensional network.<sup>19</sup>*

#### 5.4 Conclusions

A preliminary research activity has been performed on Pickering emulsion polymerization approach for preparing silica-based waterborne latexes. The synthesis of latex nanocomposites is based on the polymerization of the isoprene in aqueous emulsion, in the presence of silica and Sep, as emulsion stabilizers.

By SEM and EDX analysis good dispersion and distribution of inorganic particles in PI has been assessed. In particular, it is possible to visualize SiO<sub>2</sub>/PI spherical nanostructures of 200 nm coherently with DLS analysis. Further investigation on the L-SiO<sub>2</sub>/PI and L-SepS9/PI morphology is being performed by means of SAXS analysis.

An evaluation of the characteristics of the polymer are made by means of DSC and <sup>1</sup>H-NMR.

On the basis of our results, we suggest a possible mechanism for emulsion polymerizations stabilized by solid particles. In detail, in the case of silica, the inorganic particles are driven towards the interface as a result of a hetero-coagulation event in the water phase with a growing oligoradical. In the case of Sep fibers, the suggested mechanism is based on particle–particle interactions leading to the formation of a three-dimensional network of particles in the continuous phase.

This approach seem to be an effective way to increase particle dispersion and favor an intimate contact with the waterborne polymer.

Although versatile, Pickering emulsion polymerization do show some limitations, in particular, an excess of solid stabilizers remaining in the continuous phase after polymerization. Future work will be addressed to improve the reaction conditions.

## 5.5 Bibliography

- 1 J. Wu and G. Ma, *Small*, 2016, 4633–4648.
- 2 C. Poochai, P. Pae-on and T. Pongpayoon, *World Acad. Sci. Eng. Technol.*, 2010, **4**, 969–973.
- 3 S. O. Ilyin, V. G. Kulichikhin and A. Y. Malkin, *Colloid Polym. Sci.*, 2015, **293**, 1647–1654.
- 4 J. V. Vanderhoff, *J. Polym. Sci. Polym. Symp.*, 1985, **72**, 161–198.
- 5 J. Hearn, C. D. Establishment, P. Down, S. Wilts and S. P. Ojq, *J. Polym. Sci.*, 1985, **23**, 1869–1883.
- 6 P. Sharma, S. Roy and H. A. Karimi-Varzaneh, *J. Phys. Chem. B*, 2016, **120**, 1367–1379.
- 7 H.-T. Lu, *Colloid J.*, 2013, **75**, 311–318.
- 8 J. W. Vanderhoff, *J. Polym. Sci.*, 1985, **72**, 161–198.
- 9 D. R. Burfield, *October*, 1987, **64**, 1987.
- 10 J. M. Widmaier and G. C. Meyer, *Macromolecules*, 1981, **14**, 450–452.
- 11 E. Princi, *Sintesi di Polimeri*, Rome, Edizioni N., 2012.
- 12 R. G. López, Y. Apolinar, L. F. Ramos, H. Saade and R. Díaz De Len, *J. Nanomater.*, 2010, **2010**, 1–6.
- 13 I. W. Cheong, C. M. Fellows and R. G. Gilbert, *Polymer (Guildf.)*, 2004, **45**, 769–781.
- 14 P. J. Colver, C. A. L. Colard and S. A. F. Bon, *J. Am. Chem. Soc.*, 2008, **130**, 16850–16851.
- 15 R. F. A. Teixeira, H. S. McKenzie, A. A. Boyd and S. A. F. Bon, *Macromolecules*, 2011, **44**, 7415–7422.
- 16 N. Sheibat-Othman and E. Bourgeat-Lami, *Langmuir*, 2009, **25**, 10121–10133.
- 17 N. Negrete-Herrera, J. L. Putaux, L. David and E. Bourgeat-Lami, *Macromolecules*, 2006, **39**, 9177–9184.
- 18 L. Delafresnaye, P. Y. Dugas, P. E. Dufils, I. Chaduc, J. Vinas, M. Lansalot and E. Bourgeat-Lami, *Polym. Chem.*, 2017, **8**, 6217–6232.
- 19 G. Lagaly, M. Reese and S. Abend, *Appl. Clay Sci.*, 1999, **14**, 83–103.



## Conclusions

The research activity of this PhD thesis is focused on the preparation of green elastomeric composites, containing silica-based nanofillers, by using a colloidal approach to increase the dispersion of hydrophilic fillers in line with the new requirements of sustainability.

Two different colloidal strategies have been applied in order to control both filler dispersion and distribution and, thus, tune the mechanical properties of the final materials.

The main part of this study has been related to develop a novel green LCT approach, consisting of blending an aqueous colloidal suspension of both SepS9 and SepB5 fibers in a NRL suspension, resulting in a flocculation process, without using any synthetic flocculation agent, a non-biodegradable chemical, which could negatively affect the properties and performances of the final materials.

The proposed LCT method promotes a homogeneous dispersion of hydrophilic Sep fibers in the rubber matrix, allowing the production of highly-loaded Sep rubber composites.

TEM investigation performed at the early stages of mixing revealed that, when SepB5 fibers bearing alkylammonium salt functionalities are utilized, homo-aggregated NRL micelles embedding some SepB5 fibers are detectable while, in Sep9/NR colloidal system, Sep bundles lay among or in the periphery of the rubber micelles, thus suggesting their poor interactions with NRL.

TEM analysis performed on MBs revealed for SepB5/NR the presence of large and compact filler domains constituted by self-assembled and aligned Sep fibers interconnected by rubber. Conversely, for SepS9/NR poorly tight filler aggregates have been detected in the nanocomposite, indicating the occurrence of weak interactions between the organic and inorganic components.

SAXS analysis supported these outcomes and pointed out that NRL, once in contact with the Sep fibers, unfold leading to the formation of a homogeneous materials.

These results allow us to propose a flocculation mechanism characteristic for both SepB5/NR and SepS9/NR systems, based on electrostatic and depletion attraction forces, respectively, and remarkably connected both to the high content (50 wt.%) and to the peculiar anisotropy of Sep fibers. Our results strengthen the idea that

high AR rods are affected by depletion forces and are suitable materials for the generation of soft matters.

The uniform Sep distribution in the rubber matrix, characteristic of the proposed LCT approach, and the percolative filler network formed give rise to comparable mechanical properties for MB-SepX/NR samples, in comparison to those of analogous materials prepared by conventional melt mixing technique.

Furthermore, by combining latex compounding and melt mixing, environmental friendly composites materials have been produced. This combined approach takes advantage of the good filler distribution and the production of highly-loaded filler rubber composites and also prevents dust from floating in the air during processing, in line with the increasing legislative restrictions about emissions.

Compounds containing silica MBs show the best interactions with the sulfur-based vulcanization compounds, leading to good reinforcement and low energy dissipation.

By employing a controlled drying process to avoid eventual oxidation processes, composite materials containing Sep MBs show mechanical properties in line with the reference materials prepared directly by melt mixing. Therefore, this combined LCT and melt mixing technique can be considered as a suitable approach to prepare rubber nanocomposites with environmental benefits and without affecting the final material properties.

Furthermore, a preliminary activity has been performed on Pickering emulsion polymerization of PI in the presence of inorganic nanoparticles. In such approach, the preparation of silica-based latex nanocomposites is based on the polymerization of the organic isoprene monomer in aqueous emulsion, in the presence of silica-based inorganic colloidal particles, such as silica and Sep, as emulsion stabilizers. This method has been considered as an innovative way for the incorporation of inorganic nanofillers into polymers, with the aim of increasing particle dispersion and favor an intimate contact with the waterborne polymer and an orientation of the colloidal components. By Pickering emulsion polymerization, both *IP*(core)-silica(shell) and *IP*(core)-SepS9(shell) structured composite particles have been synthesized.

On the basis of our results, we suggest a possible mechanism for emulsion polymerizations stabilized by solid particles. In detail, in the case of silica, the inorganic particles are driven towards the interface as a result of a hetero-coagulation event in the water phase with a growing oligoradical. In the case of Sep fibers, the suggested mechanism is based on particle–particle interactions leading to the formation of a three-dimensional network of particles in the continuous phase.

Although versatile, our Pickering emulsion polymerization do show some limitations, in particular, an excess of solid stabilizers remains in the continuous phase after polymerization.

## Conclusions

In summary, latex compounding and *in situ* polymerization show to be effective and promising approaches for the obtainment of highly loaded rubber nanocomposites, suitable for the application in the tyre field. In particular, Sep has been found to be especially appropriate in producing nanocomposites by LCT because of the obtainment of more eco-friendly materials having low hysteresis and high reinforcement, with a reduced environmental impact of the compounding approach.

This work highlights the possibility of exploiting the chemistry of colloids to design innovative materials synthesized by eco-friendly methods. Although it focuses on PI nanocomposites, we expect that the developed sustainable synthetic strategy may be potentially extended to the production of highly-loaded rubber nanocomposites.





A. Appendix

## Appendix

## A.1 Attenuated Total Reflectance Fourier Transform Infrared Spectroscopy (ATR-FTIR)

The infrared spectroscopy instrument used for this characterization is Perkin Elmer Spectrum 100 instrument.

The interaction between matter and infrared radiation determines changes in the vibration modes of the chemical bonds between atoms which give us information on the nature of the sample analysed. Through ATR spectroscopy, the phenomenon of total internal reflection in a crystal is exploited. The radiation undergoes a total internal reflection when the angle of incidence at the interface between the crystal and the material is greater than the critical angle.<sup>1</sup>

The interferometer, moreover, allows a better resolution thanks to the introduction of a mobile mirror which generates interferences (*Figure A-1*). Through the Fourier transform the interferogram, which is detected as a function of intensity, is turned as a function of the frequency.

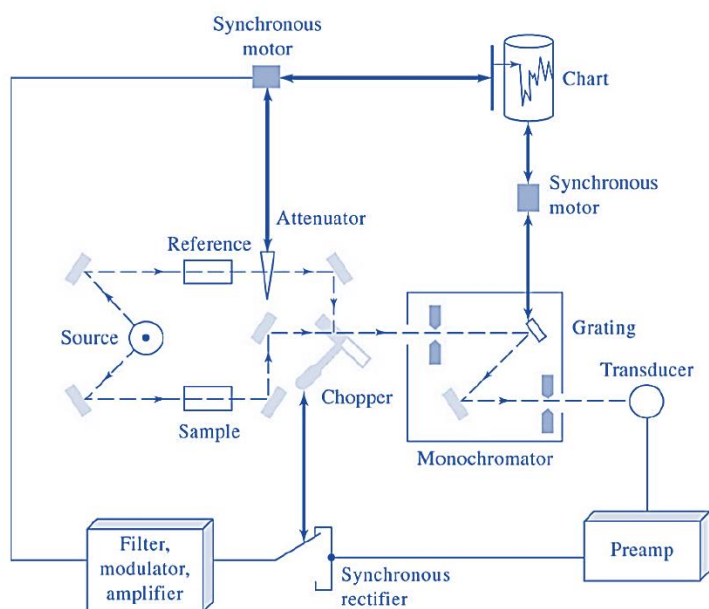


*Figure A-1. Schematic representation of Infrared Spectroscopy.*

The ATR-FTIR ( $4000\text{-}650\text{ cm}^{-1}$ ,  $4\text{ cm}^{-1}$  resolution, 16 scan) has been used to detect vibrational changes in the chemical bonds of atoms belonging to filler, rubber and filler-rubber nanocomposites, assuming them as proofs of interactions between organic and inorganic species.

## A.2 Thermogravimetric analysis (TGA)

The analysis has been carried out by Thermo Gravimetric Analysis (TGA) on Mettler Toledo TGA/DSC1 Star System. TGA is a technique which detects the sample changes of weight as a function of the temperature. Increasing the temperature, it is possible to determine a gradual decomposition of the sample. Every species has a specific region of decomposition where it is possible to appreciate a weight loss. A special optical sensor controls the position of the pan which moves for each mass sample loss. The light horizontal arm (balance) moves inducing an electric current which is recorded as a signal by the machine (*Figure A-2*).<sup>2</sup>

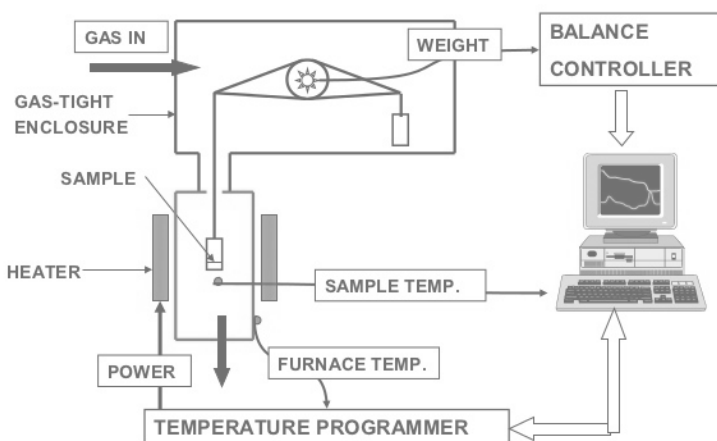


*Figure A-2. Schematic representation of Thermogravimetric Analysis*

TGA has been used to assess the rubber-filler ratio in the MBs and thus the efficiency of the flocculation process. The samples are heated in air from 30 to 1000°C (10° C/min).

## A.3 Gel Fraction Quantification

The determination of the gel fraction is made through an extraction with chloroform of the silica/polyisoprene samples. A comparison is made between the TGA profiles before and after the extraction. It has been assumed that the remaining polymer fraction after the extraction is entirely made of crosslinked polymer.

The procedure of extraction is the following: 50 mg of silica/polymer samples are soaked into chloroform for 20 minutes for three times. Then dried in a ventilated oven at 60 °C overnight.

#### A.4 Differential Scanning Calorimetry (DSC)

DSC is a thermo-analytical technique where the amount of heat is detected as a function of temperature. In particular, it detects the difference in the amount of heat required to increase the temperature of sample and reference. The reference has a well-defined heat capacity over the range of temperatures to be scanned. The sample, under a continuous increment of temperature, undergoes physical transformations such as phase transitions (*Figure A-3*).<sup>2</sup>

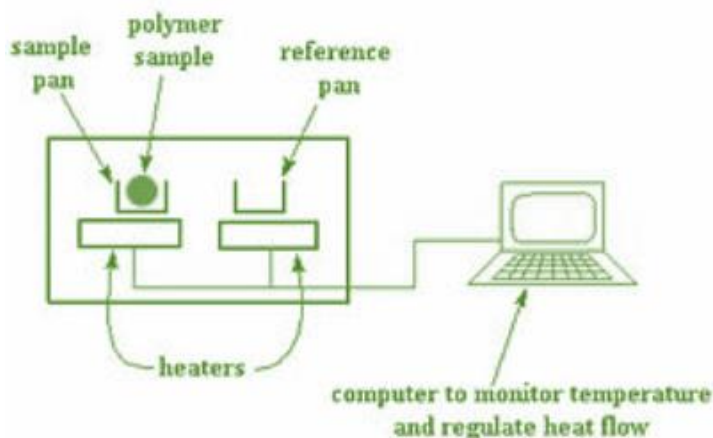


*Figure A-3. Schematic representation of Differential Scanning Calorimetry*

This technique has been used to detect the glass transition temperature ( $T_g$ ) of PI and also to analyse oxidation processes in rubber. The samples were cooled from 25 °C to -80 °C (5 °C/min) and reheated to 25 °C. To determine the presence of oxidation phenomena the samples are heated to 200 °C (10 °C/min).

#### A.5 Dynamic light scattering (DLS)

The instrument used is Malvern Zetasizer Nano Series ZS90.

The dynamic light scattering analysis allows detecting the dimensional distribution of small particles suspended in a solvent. A laser light source hits the sample and the fluctuation of the intensity of the scattered light is analyzed by a detector that is placed perpendicular to the laser light (*Figure A-4*).

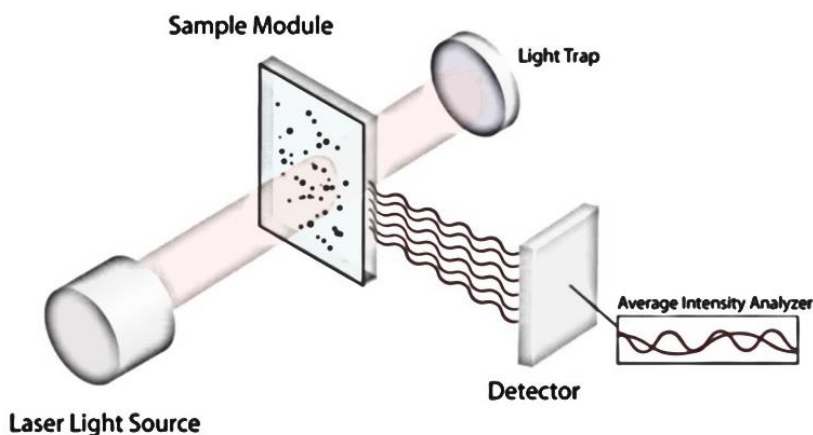


Figure A-4 Schematic representation of the dynamic light scattering

The scattering provided by the particles in the sample is the result of the constructive and destructive interferences which give an average intensity. This intensity is related to the speed of the particles which are moving in the solvent because of the Brownian motions. Through the Stokes-Einstein equation we can calculate the hydrodynamic diameter of the particles.<sup>3</sup>

$$D_z = K_B T / 3\pi \eta \Phi_n \quad (\text{Eq.1})$$

$D_z$  = diffusion coefficient

$K_B$  = Boltzmann constant

T = temperature

$\eta$  = dynamic viscosity of the medium

$\Phi_n$  = hydrodynamic diameter

The hydrodynamic diameter obtained by DLS measurement is indicative of the apparent size of the hydrated/solvated particle. So, the hydrodynamic diameter is the value that we obtain adding the real diameter of the particle to the thickness of the solvated shell. If the particles are not spherical, the measure of the hydrodynamic diameter is given by the diameter of the theoretical rounded particle whose diameter is the real particle length. If the particles are aggregated the DLS analysis will measure the diameter of the aggregates.

The analysis has been used to determine the size of the polymer-silica Pickering emulsion particles. The analysis is carried out with a dilution of 0.1 g/L.

## A.6 Z-metry

The analysis of the  $\zeta$ -potential have been performed with the instrument Malvern Zetasizer Nano Series ZS90.

The application of an electric field to charged particles placed in a liquid generates the mobility of such particles. This mobility can be quantified through an electrophoresis technique. The Z-Metry detects through microscopy the movements of suspended particles under an electric field. The electrophoretic mobility is related to the  $\zeta$ -potential. The  $\zeta$ -potential (*Figure A-5*) is the potential generated by the formation of the electric bilayer, responsible of the particles stability in suspension.<sup>4</sup>

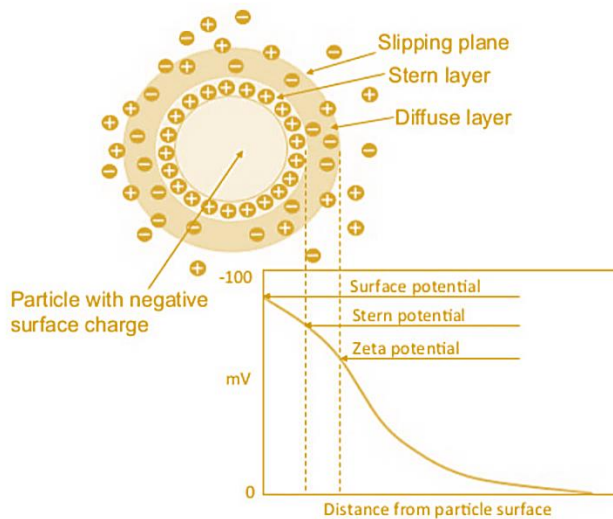


Figure A-5. Representation of the  $\zeta$ -potential

The equation of Smoluchowski relates the electrophoretic mobility with the  $\zeta$ -potential:

$$\mu_E = (4 \pi \epsilon_0) D \Phi_\xi / 4 \pi \eta = \epsilon \Phi_\xi \eta \quad (\text{Eq.2})$$

$\mu_E$  = electrophoretic mobility

$\epsilon_0$  = permittivity of vacuum

$\epsilon$  = permittivity of the medium

$D$  = dielectric constant

$\eta$  = viscosity of the medium

$\Phi_\xi$  =  $\zeta$ -potential

The  $\zeta$ -potential of the NRL particles is determined to investigate the colloid stability. The NRL sample is diluted with deionized water until the pH value is approximately that of Milli-Q water (pH = 6.5).

The  $\zeta$ -potential measurement on pristine NRL is performed at 25 °C at different pH by adding a suitable amount of HCl or NH<sub>4</sub>OH solution to NRL.  $\zeta$ -potential measurements are carried out also on 0,1 gL<sup>-1</sup> Sep dispersions. In detail, SepB5 aqueous dispersion is stirred for 10 min and sonicated for other 10 min, while SepS9 is stirred at different times (10 min, 40 min, 3 h, 24 h) before sonication. In such conditions, the SepS9 suspension after 10 min reached a pH = 8, which remains almost constant reaching the equilibrium (pH = 8.41) after 24 h.

#### A.7 Transmission Electron Microscopy (TEM)

In this work, Zeiss EM 900 microscope and Jeol 3010 High Resolution TEM (High Resolution-TEM) has been used.

The TEM is based on the detection of the electrons transmitted when a focalized electron beam interacts with the sample. An electron gun (source of the electrons) with a narrow energy distribution in high vacuum is focused through magnetic fields to the material to detect. The sample is displaced in a thin layer on an appropriate grid. The electrons which are transmitted from the sample arrive to a fluorescent screen where the energy of the electrons is turned into visible light. Thus, it is possible to obtain live images of the samples and take pictures of it. The sample holder is a copper grid covered with a thin film of carbon that let the electrons pass through it (*Figure A-6*).<sup>5</sup>

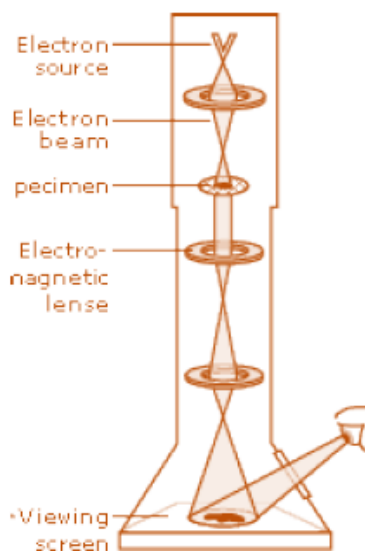


*Figure A-6. Schematic representation of Transmission Electron Microscopy*



The first stages of the flocculation process in Sep/NR systems, are studied by a Jeol 3010 High Resolution TEM (HR-TEM) operating at 300 kV with a high-resolution pole piece (0.17 nm point to point resolution) and equipped with a Gatan slow-scan 794 CCD camera. To visualize Sep/NRL interactions, 10  $\mu\text{L}$  of the Sep/NRL mixture are taken from the flocculation system with the same concentration used in the Sep/NR composite preparation. Then, 1 mL aliquot of the flocculating dispersion is diluted to  $0.1 \text{ gL}^{-1}$ , deposited on a carbon coated TEM grid, to monitor the evolution of the flocculation process.

The morphological investigation of composites is carried out by TEM using a Zeiss EM 900 microscope operating at 80 kV. Ultrathin sections (about 50 nm thick) of Sep/NR nanocomposites previously embedded in an epoxy resin (70 °C, 24 h) are obtained with a Leica EM FCS cryo-ultramicrotome, equipped with a diamond knife, by keeping the samples at -130 °C.

## A.8 Scanning Electron Microscopy (SEM)

SEM has been performed by a Vega TS5136 XM Tescan microscope.

SEM produces images by scanning the surface with a focused beam of electrons (Figure A-7). The principle of operation requires that the electrons generated from a source hit and interact with atoms of the sample, producing signals that contain information about the surface morphology and composition of the sample. The detector collects low energy secondary electrons (SE) and higher energy backscattered electrons (BSE). SE are produced when an energetic electron knocks out a loosely bound outer shell electron in the species, while BSE are beam electrons that are deflected by the interaction with the species and have a wider range of energy.<sup>6</sup>

In our work, the electron beam excitation is 30 kV at a beam current of 25 pA, and a working distance of 12 mm. In this configuration, the beam spot is 38 nm sized. Prior to SEM analysis, samples have been gold-sputtered. ImageJ processing program (Image Processing and Analysis in Java) is utilized to measure manually the Sep fibers dimensions.

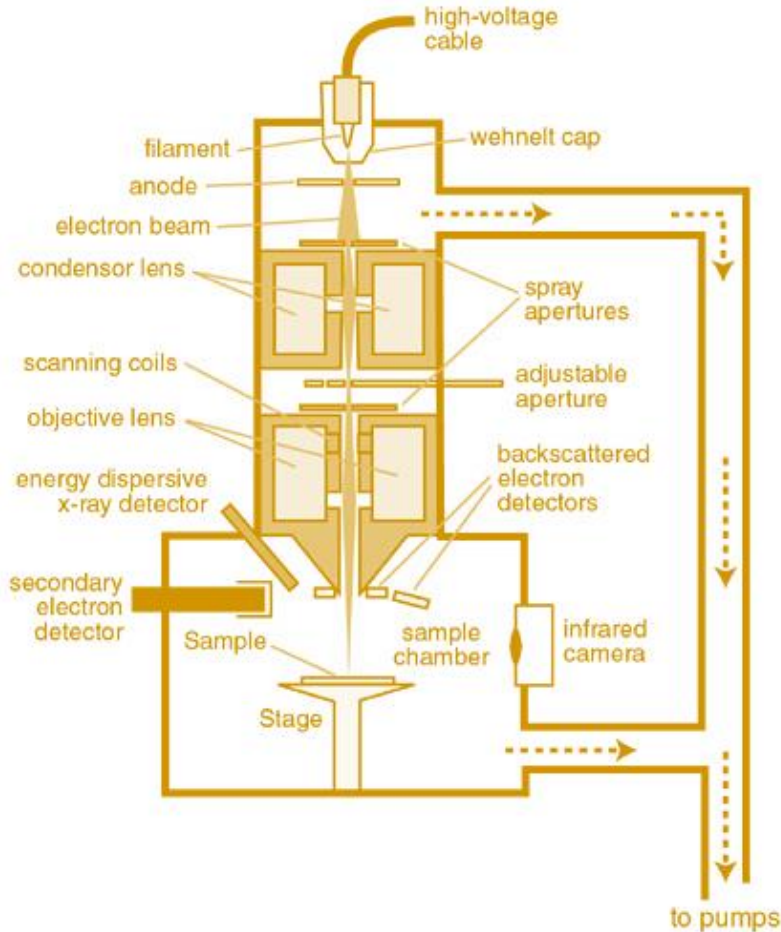


Figure A-7. Schematic representation of Scanning Electron Microscopy

#### A.9 SEM-Energy Dispersive X-ray Spectroscopy (EDX)

To assess the Sep distribution in Sep/NR nanocomposites, SEM-EDX analysis has been performed by A Vega TS5136 XM Tescan microscope operating at 30 kV (25 pA beam current, 12 mm working distance, 38 nm beam spot). Samples are deposited onto a carbon adhesive disc and carbon-sputtered. A map of principal elements of Sep, such as Si, Al and Mg, is detected to visualize the filler dispersion within the rubber matrix.

## A.10 Standard Nessler Reagent Method

The concentration of the ammonium ions, in the aqueous phase containing SepS9, has been analyzed using the standard Nessler reagent method, employing a Varian Cary 4000 Spectrophotometer.

The magnitude of the adsorption/ion exchange of ammonium ions on SepS9 has been studied by using the Nessler method.<sup>7</sup> 10 g of SepS9 are dispersed in water (200 mL) under mechanic stirrer at 200 rpm for 60 min, successively sonicated for 10 min and mixed again for 10 min. In a second vessel, 0.1 g of dried  $\text{NH}_4\text{Cl}$  (drying at 150 °C for 2h) are dissolved in 50 mL of distilled water. The resultant  $\text{NH}_4\text{Cl}$  solution is added to the SepS9 dispersion and stirred at a constant temperature ( $25 \pm 2$  °C). The pH of all solutions is adjusted by adding HCl 37% until pH is in the 6-8 range.

The analyses are performed under the following conditions: 300–600 nm wavelength range, 600 nm  $\text{min}^{-1}$  scan rate, 0.1 s time response, and 2 nm spectral band. 20 mL of sample aliquots are withdrawn at intervals of 3, 15, 30, 60, 120 min and separated by centrifugation. Then, the ammonium content in 0.1 mL of supernatant is analyzed after adding 2.5 mL of distilled water and potassium sodium tartrate tetrahydrate to avoid the magnesium and calcium interference with the Nessler reagent.

## A.11 Inductively Coupled Plasma-Optical Emission Spectrometry (ICP-OES)

The instrument used is the ICP-OES Optima 7000 DV Perkin Elmer. The ICP analysis has been applied to determine possible leaks of  $\text{Mg}^{2+}$  from Sep which might affect the stability of the NRL emulsion.

The instrument is constituted by a quartz tube where a constant flux of Ar 20 L/min transports the vaporized sample to a plasma source. *Figure A-8* shows the extremity of the torch which is a coil generating radiofrequency (40 MHz) that ionizes the Ar with the production of a plasma at a temperature 8000 K.

The detector is a Charged Coupled Device (CCD) camera which measures the intensity of the radiation and converts it in electric signal through a photomultiplier.<sup>8</sup>

A dispersion of 50  $\text{gL}^{-1}$  of SepS9 in Milli-Q water is mixed for 30 min and sonicated for 10 min. Then, the dispersion is filtered and the supernatant centrifuged for 30 min at 9000 rpm to eliminate any residual of SepS9 nanoparticles. The amount of  $\text{Mg}^{2+}$  in the supernatant is analyzed by ICP-OES.

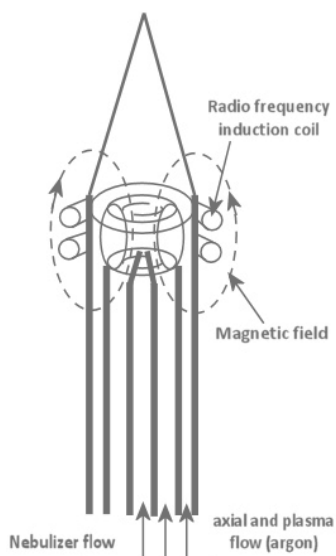


Figure A-8. Schematic representation of the ICP torch

#### A.12 Capillary Electrophoresis (CE)

The experiments for the determination of  $Mg^{2+}$  through Capillary Electrophoresis have been performed using a P/ACE MDQ Capillary Electrophoresis System (Beckman, Fullerton, CA, USA) equipped with UV detector.

CE is an electrokinetic separation method performed in submillimeter diameter capillaries. The working principle of the instrument is the migration of the charged analytes initiated by an electric field that is applied between the source and destination vials. All ions, positive or negative, are pulled through the capillary in the same direction by electroosmotic flow. The analytes separate as they migrate due to their electrophoretic mobility and are detected near the outlet end of the capillary. The output of the detector is sent to a data output and handling device such as an integrator or a computer.<sup>9</sup>

Fused-silica capillaries (75  $\mu m$  I.D., 50 cm effective length, Beckman) have been employed. The analyses have been performed by using indirect UV detection at wavelength of 214 nm. Electrophoresis separations are performed in a running buffer constituted of 6 mM HIBA, 5 mM 18-crown-6 ether and 5 mM imidazole adjusted to pH 4.5 with acetic acid. Analyses are performed by applying a constant voltage of 500  $Vcm^{-1}$  at 25 °C with a resulting current of about 18  $\mu A$ . The separations take place at 25 kV during 6 min. The solutions are injected at the anodic end of the capillary for 10 s at 0.5 psi. Before injection, samples have been diluted 1:5 (v/v) with water containing  $BaCl_2$  (IS) at a concentration of 40  $\mu g mL^{-1}$ .

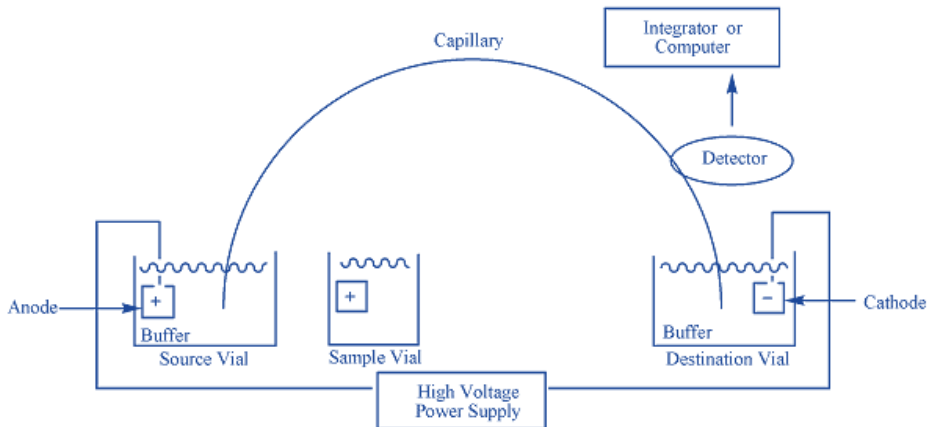


Figure A-9. schematic representation of Capillary Electrophoresis

### A.13 X-ray diffraction (XRD)

The instrument used is the powder diffractometer PANalytical X'Pert Pro in Bragg-Brentano geometry, using Cu K- $\alpha$  source with 1.54 Å wavelength.

The technique of the XRD analysis is based on the elastic coherent diffusion (scattering) of the X-rays from atoms present in the solid structure. The electronic clouds of the atoms act as scattering centres on the radiations. The atoms of a crystalline material are displaced in a fixed regular geometry, proper of the crystal. The distances which exist between the atoms are of the same order of the wavelength  $\lambda$  of the X-rays, therefore, constructive and destructive interferences take place when the incident radiation interacts with the sample according to the Bragg's law (Figure A-10):<sup>10</sup>

$$2 d \sin\theta = n \lambda \quad (\text{Eq.3})$$

$n$  = order of diffraction

$\lambda$  = wavelength of the incident radiation

$d$  = interplanar distance

$\theta$  = incident angle made by the direction of the incoming radiation and by the plans of the crystal lattice

This analysis has been applied to assess the effective incorporation of the filler in the polymeric matrix and to confirm the maintenance of the crystalline structure of sepiolite after the flocculation process.

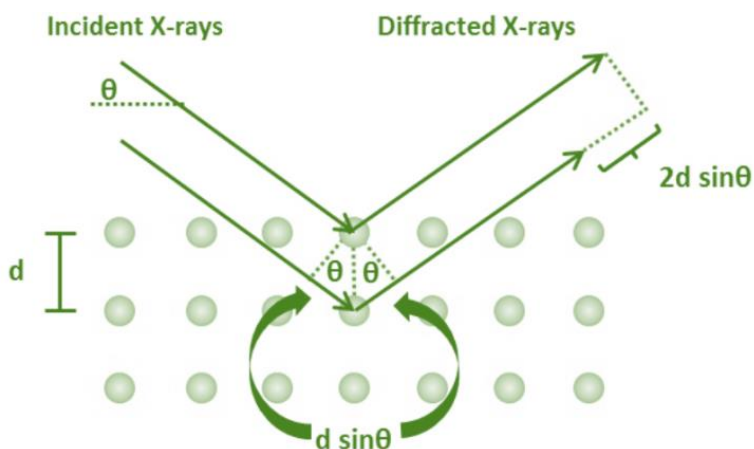


Figure A-10. Geometric representation of the Bragg's law

#### A.14 Small-angle X-ray scattering (SAXS)

Small-angle X-ray scattering (SAXS) has been performed on beamline ID2 at the European Synchrotron Radiation Facility (ESRF, Grenoble FR).

SAXS is a technique which allows to determine the structure of particle systems in terms of averaged particle sizes or shapes. Like XRD, X-rays are sent to the sample and the scattered energy resultant from the interaction between the X-ray and the sample is determined by the averaged structure of all illuminated particles (Figure A-11). The use of small incident angles of X-rays allows the investigation of structures of intermediate scale, ranging between the atomic/molecular resolution of X-ray diffraction and the resolution of an optical microscope.<sup>11</sup>

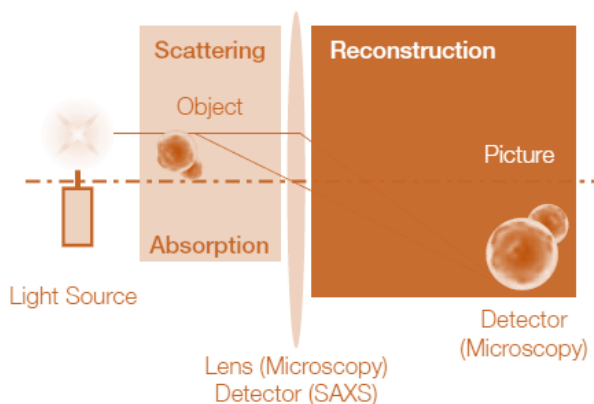


Figure A-11. Schematic representation of Small-angle X-ray scattering

The analysis has been carried out at a wavelength of 1 Å, with a sample to detector distance of 2.5 m, yielding a total q-range from 0.001 to 0.15 Å<sup>-1</sup>. The scattering cross section per unit sample volume dΣ/dΩ (in cm<sup>-1</sup>) (scattered intensity I(q)) is obtained by using standard procedures including background subtraction and calibration given by ESRF. The Debye approximation<sup>12</sup> and the Guinier approach have been adopted for the analysis of the NR and MBs, respectively. The scattering intensity I(q) in the Debye model is given by the following equation:

$$I(q) = I_0 \frac{1}{[1 + (q\xi)^2]^2} \quad (\text{Eq. 4})$$

where ξ is the correlation length of the scattering bodies, in this case associated with the crystalline domains. As particulate systems, the scattering of the Sep rods in the NR can be analyzed using the Guinier approach<sup>13</sup> to get information on the radius of the inorganic fibers and therefore on their dispersion degree. For one dimensional systems the scattering in the intermediate region of the curve can be approximated to:

$$I(q) = \frac{I_0}{q} \exp\left(-\frac{q^2 R_g^2}{2}\right) \quad (\text{Eq. 5})$$

$$R_g^2 = R^2/2 \quad (\text{Eq. 6})$$

where R<sub>g</sub> and R are the radius of gyration and the radius of the fiber, respectively. These parameters are obtained from the linearity dependency of the so called Guinier plot ln(qI) vs. q<sup>2</sup>.

### A.15 X-ray Fluorescence (XRF)

ARL™ 9900 Simultaneous-Sequential XRF Series (Thermo Scientific™) has been used for XRF analysis.

XRF is an analytical technique used for the determination the chemical composition of samples based on emission of fluorescence generated by excitation of secondary electrons by bombarding the sample with X-rays.<sup>14</sup> Each element has electronic orbitals of characteristic energy which can be detected following the removal of an inner electron by an energetic photon like X-rays which determines the drop of an electron from an outer shell. This effect cause a fluorescence emission with a characteristic energy, which is correlated to the element. The intensity of each characteristic radiation is directly related to the amount of each element in the material.

The calibration of the instrument is of the type, so the analysis is to be considered semi-quantitative.

## A.16 Oscillating Dish Rheometry (ODR)

ODR measurements of the uncured MB-Sep/NR and of the cured and uncured model nanocomposites have been performed by Rubber Process Analyzer (RPA 2000, Alpha Technologies) by applying strain sweep tests.

The testing chamber is made of a top cone geometry moving part (rotor) and a plate geometry bottom part. The torque acting on the rotor during oscillation is converted into a value of modulus and divided into a real and an imaginary part. The Storage Modulus  $G'$  is associated with an elastic response, while the Loss Modulus  $G''$  with a viscous response. The ratio between  $G''$  and  $G'$  ( $\tan\delta$ ) is a predictive number of the energy dissipated from the tyre during usage.<sup>15</sup>



*Figure A-12. Rubber Process Analyzer (RPA 2000, Alpha Technologies)*

Strain sweep experiments are carried out on the uncured MBs from 0.1 to 60 % of strain at 100°C and 10 Hz.

The compounded nanocomposites undergo a strain sweep test before and after vulcanization. The strain sweep performed before the vulcanization are carried out from 0.1 to 10 % of strain at 70°C and 10 Hz and from 0.1 to 100 % of strain after the vulcanization. The vulcanization process is performed for 10 minutes at 170°C. Samples are cut by using a Constant Volume Rubber Sample Cutter (CUTTER 2000, Alpha Technologies); the dimensions are 3.5 cm of diameter and  $\approx 0,2$  cm of thickness, for an average weight of  $5\pm 1$  g.



## A.17 Nuclear Magnetic Resonance (NMR)

$^1\text{H}$  NMR represents the most important spectroscopy for the interpretation and the determination of a structure. The main information on the chemical structure of a molecule in a  $^1\text{H}$  NMR spectra are given by the integrals of peaks, by the chemical shifts and by the J-coupling. Through the integration of the peaks (intensity) we define the number of hydrogens. The chemical shift is related to the type of atom that surround the hydrogen considered, since the nuclei are affected by a magnetic field which is modified by the presence of electrons.

The J-coupling describes the indirect interaction between two nuclear spins which arises from hyperfine interactions between the nuclei and local electrons. J-coupling contains information about bond distances, angles and on the connectivity of molecules.

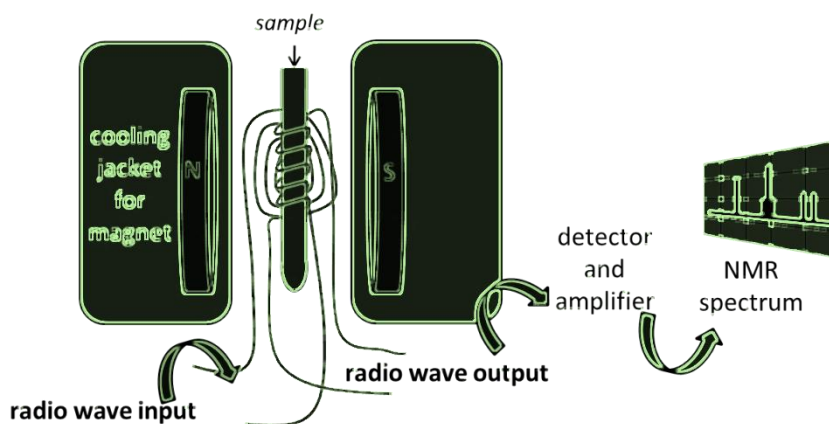


Figure A-13. Schematic representation of NMR.

$^1\text{H}$  NMR spectra have been recorded with Varian 1500 NMR at 500 MHz on samples dissolved in  $\text{CDCl}_3$ (1:10 vol:vol). Chemical shifts are determined relative to the residual solvent peak ( $\text{CDCl}_3$ ,  $\delta$  7.26 ppm).

## A.18 Bibliography

- 1 H. W. Siesler, Y. Ozaki, S. Kawata and H. M. Heise, *Near-infrared spectroscopy: principles, instruments, applications*, John Wiley & Sons, Weinheim, 2008.
- 2 P. Gabbott, *Principles and applications of thermal analysis*, John Wiley & Sons, Oxford, 2008.
- 3 R. Pecora, *Dynamic light scattering: applications of photon correlation spectroscopy*, Springer Science & Business Media, New York, 2013.
- 4 R. J. Hunter, *Foundations of colloid science*, Oxford University Press, Oxford, 2001.
- 5 D. B. Williams and C. B. Carter, in *Transmission electron microscopy*, Springer, 1996, pp. 3–17.
- 6 J. I. Goldstein, D. E. Newbury, J. R. Michael, N. W. M. Ritchie, J. H. J. Scott and D. C. Joy, *Scanning electron microscopy and X-ray microanalysis*, Springer, New York, 2017.
- 7 M. S. Çelik, B. Özdemir, M. Turan, I. Koyuncu, G. Atesok and H. Z. Sarikaya, *Water Sci. Technol. Water Supply*, 1998, **1**, 81–88.
- 8 M. Thompson, *Handbook of inductively coupled plasma spectrometry*, Springer Science & Business Media, 2012.
- 9 J. P. Landers, *Handbook of capillary electrophoresis*, CRC press, 1996.
- 10 R. Jenkins and R. L. Snyder, *Introduction to X-ray Powder Diffraction*, Wiley Online Library, Hoboken, 1996.
- 11 H. Schnablegger and Y. Singh, *The SAXS guide: getting acquainted with the principles*, Anton Paar GmbH, 2013.
- 12 S. Toki, C. Burger, B. S. Hsiao, S. Amnuaypornsrri, J. Sakdapipanich and Y. Tanaka, *J. Polym. Sci. Part B Polym. Phys.*, 2008, **46**, 2456–2464.
- 13 I. Dékány, L. Turi, A. Fonseca and J. B. Nagy, *Appl. Clay Sci.*, 1999, **14**, 141–160.
- 14 R. Jenkins, *X-ray fluorescence spectrometry*, Wiley Online Library, 1999.
- 15 T. Richards, *Am. Lab.*, 2001, **33**, 38–39.





## PROFILE



BIRTH DATE

18/05/1991

Verona

NATIONALITY

Italian



RESIDENCE

Via Corfù 12

37126, Verona, Italy



DOMICIL

Via Falloppio 11

20126, Milano, Italy

## CONTACTS



EMAIL

[irene.tagliaro@unimib.it](mailto:irene.tagliaro@unimib.it)

[i.tagliaro@campus.unimib.it](mailto:i.tagliaro@campus.unimib.it)



+39 3477857579

+1 6178526875

DRIVING LICENCE: B

# Irene Tagliaro

Doctor in Chemical Science and Technology

## WORK EXPERIENCE

**PhD Candidate in Nanotechnologies and Material Science (XXXI cycle)**

**November 2015 – Present (end in November 2018)**

Milano Bicocca University in collaboration with Pirelli & C. Società per Azioni

**During the PhD:**

- **Internship at Harvard University, (MA) United States**

**January 2018 – July 2018**

- **Tutoring:**

**November 2015–December 2017**

Laboratory assistance in the course of General and Inorganic Chemistry  
Didactic tutor of General Chemistry for a student with DSA

**Stage at the CNRS of Bordeaux, France (ERASMUS+ for traineeship)**

**February 2015 – July 2015**

Institute ICMCB (Institut de Chimie de la Matière Condensée de Bordeaux),  
Bordeaux, France

## EDUCATION AND TRAINING

**PhD Candidate Nanotechnologies and Material Science (XXXI cycle)**

**November 2015 – Present (end in November 2018)**

University of Milano Bicocca, Milan Italy

**The project:**

**Novel colloidal approach to prepare highly-loaded silica-based elastomeric nanocomposites**

This PhD thesis is focused on the preparation of eco-friendly silica-based nanocomposites by using a colloidal approach to increase the dispersion of hydrophilic fillers in line with the new requirements of sustainability from the EU policies. Two different colloidal approaches were applied: i) latex compounding technique (LCT) and ii) in situ emulsion polymerization to prepare high-loaded nanocomposite rubber materials containing silica-based fillers, silica and sepiolite (Sep) clay, considered a promising filler candidate for the polymer strengthening due to its fibrous structure and high particle aspect ratio (AR).

## Master's Degree of Science in Chemical Science and Technologies

**110 with honor (min 66 – max 110)**

**November 2013–October 2015**

University of Milano Bicocca, Milan Italy

### Title of master thesis:

Metal oxide nanoparticles for radiotherapy

### General features of the thesis:

Synthesis of inorganic nanoparticles for application in Magnetic Resonance Imaging (MRI) and Radiotherapy.  $\text{TiO}_2$  and  $\text{HfO}_2$  NPs are synthesized by hydrothermal methods. To be detected as contrast agent in MRI they have been doped with rare earth. The radiotherapeutic effect of two different elements with different photoelectric cross section have been compared.

## Secondary School Diploma

**90 (min 60 – max 100)**

**September 2005 – July 2010**

Liceo Scientifico Fracastoro, Verona, Italy

Senior high school specializing in scientific studies

## Bachelor Degree of Science in Chemical Science and Technologies

**100 (min 66 – max 110)**

**October 2010 – October 2013**

University of Milano Bicocca, Milan Italy

### Title of bachelor thesis:

$\text{SiO}_2/\text{ZnO}$  nanocomposites for reinforcing and vulcanization of rubber

### General features of the thesis:

The subject of the thesis was the synthesis of  $\text{SiO}_2/\text{ZnO}$  nanoparticles to produce nanocomposites with styrene butadiene rubber (SBR). The filler was introduced to reinforce the elastomeric matrix and activate the process of vulcanization. The project led to the production of ZnO nanoparticles of 2-3 nm spread on  $\text{SiO}_2$  surfaces (15-20 nm). Additional aim of this work was to increase the dispersion of nanoparticles and the interaction of ZnO with rubber and in this way to increase the rate and the homogeneity of vulcanization, in order to reduce the amounts of ZnO used in industrial processes.

## LANGAGES



- English
- French in improvement
- Italian (mother tongue)

## COMMUNICATION SKILLS



## ORGANISATIONAL / MANAGERIAL SKILLS



## JOB-RELATED SKILLS



## COMPUTER SKILLS

## OTHER SKILLS

## PERSONAL SKILLS

- Accustomed to living and working in multicultural environments, a skill acquired especially during the months of Erasmus experience in Bordeaux and in the United States.
- Self-awareness in managing intercultural relations, capacity reached through the international experience as Erasmus student and at the university of Harvard, facing and working with people from different countries.
- Ability to collaborate and to exchange ideas and competences with a team of work, gained during the internships and during the PhD. Attitude and skills to team work were developed also from a 10 year practice of modern and contemporary dance (hobby).
- Excellent expression and communication skills gained at the high school.
- Ability in participating and, in several occasions, organizing and coordinating study groups and work groups acquired during the laboratory trainings at university and during the two periods of internship.
- Independency and capacity of taking over responsibilities and taking decisions. Skills developed during the PhD leading trainee for bachelor and master thesis.
- Proactive and hands-on attitudes. Interest and eagerness to learn and to bring in new ideas, due to a character marked by curiosity.
- Experience in **inorganic chemistry, polymer synthesis and formulations, nanocomposites and nanomaterials**
- Good at using technological instrumentation, based on formation and training at university and experience during the above mentioned works (non exhaustive list): FTIR (good), UV-Vis (good), ICP (base), TGA (good), DSC (good), SEM (excellent), TEM (base), Raman (base), H-NMR (base), XRD (base), SAXS (base), DLS and Z-merty (good), mechanical characterization: RPA(good)
- Operating system: Windows (good), Linux (base)  
Office Package: Microsoft Word, Microsoft Power Point, Microsoft Excel
- Very good talent in writing: winner of the poetry competition "Premio Montano: La memoria è tesoro e custode di tutte le cose" edition 2009-2010
- Interest and skills in theatre and ballet, gained in years of modern-jazz and contemporary dance training
- Passion for several hand made goods spacing from jewellery to renovation of furniture
- Desire of travelling around the world also for working aims

## PATENT

Tadiello, L; Cipolletti, VR; Giannini, L; Hanel, T; Galimberti, M; Scotti, R; Di Credico, B; Morazzoni, F; D'Arienzo, M; Tagliaro, I, Elastomeric compositions comprising silicate fibers with needle-shaped morphology of nanometric size and tires for vehicles that comprise them, From PCT Int. Appl. (2018), WO 2018116125 A1 20180628

## Publications

B. Di Credico, I. Tagliaro, E. Cobani, L. Conzatti, M. D'Arienzo, L. Giannini, S. Mascotto, R. Scotti, P. Stagnaro and L. Tadiello, A Green Approach for Preparing High-Loaded Sepiolite/Polymer Biocomposites, *Nanomaterials*, 2019, **9**, 46

## Awards

Knowledge and Innovation Community (KIC) European Institute of Innovation & Technology (EIT) Raw Materials labelled IDS-FunMat-INNO



## Conferences and schools

### Oral presentations

“Colloidal approach to prepare new elastomeric nanocomposites”, Complex Fluids, Massachusetts Institute of Technology, Cambridge, (MA) United States, June 15<sup>th</sup> 2018

“Silica based nanofiller-latex composites for green tires compounds”, Workshop CORIMAV, Pirelli Milano June 7<sup>th</sup> 2016, June 20<sup>th</sup> 2017, April 17<sup>th</sup> 2018

### Schools

International Doctoral School in Functional Materials (IDS-FunMat-INNO):

- Training School on Technology Intelligence (Bordeaux), October 22<sup>nd</sup> -26<sup>th</sup> 2018
- Material Selection and Processing & Scientific Communication (Hirschegg / Kleinwalsertal), April 8<sup>th</sup> -14<sup>th</sup> 2018
- Research and Innovation. Life cycle of materials & Project and risk management (Lisbon), April 23<sup>rd</sup> -29<sup>th</sup> 2017
- Entrepreneurship and innovation (Bilbao), September 18<sup>th</sup> -22<sup>nd</sup> 2017

XXXVII Convegno-Scuola AIM “Mario Farina”, Caratterizzazione di materiali polimerici: tecniche per polimeri fusi e allo stato solido, Gargnano (BS), May 2<sup>nd</sup> -6<sup>th</sup> 2016

---

I allow the use and processing of my personal data according to the Dlgs 196/2003 concerning the handling of personal data.